TECHNISCHE UNIVERSITÄT MÜNCHEN

II. Medizinische Klinik und Poliklinik

Klinikum rechts der Isar

Preclinical evaluation of an oral MEK1/2 inhibitor as a therapeutic strategy for GEMM-based Pancreatic ductal adenocarcinoma (PDAC)

Nicole Teichmann

Vollständiger Abdruck der von der Fakultät für Medizin der Technischen Universität München zur Erlangung des akademischen Grades eines

Doktors der Naturwissenschaften

genehmigten Dissertation.

Vorsitzende: Prof. Dr. Radu Roland Rad

Prüfer der Dissertation: 1. Prof. Dr. Dieter Saur

2. Prof. Angelika Schnieke, Ph.D.

Die Dissertation wurde am 02.10.2018 bei der Technischen Universität München eingereicht und durch die Fakultät für Medizin am 02.01.2019 angenommen.

“Everything should be made as simple as possible, but not simpler.”

Albert Einstein

to my grandmother and myself

für meine Omi und mich

Zusammenfassung

Für das duktale Adenokarzinom des Pankreas (PDAC) fehlen heutzutage immer noch kurative Therapieansätze trotz intensiver akademischer Forschung und enormen Bemühungen der Industrie in den vergangenen Jahrzehnten und somit bleibt es eine der tödlichsten Krebserkrankungen der westlichen Welt mit einer durchschnittlichen Überlebenszeit von weniger als sechs Monaten nach Diagnosestellung. PDAC zeichnet sich grundlegend durch die konstitutive Aktivierung des *KRAS*-Onkogens aus, welches weitgehend als nicht therapierbar betrachtet wird, sowie die damit einhergehende Hyperaktivierung einer Vielzahl nachgeschalteter Signalkaskaden, wie beispielsweise des RAS-RAF-MEK-ERK oder MAPK Signalweges, die nicht nur Proliferation und Überleben regulieren, sondern auch eine wichtige Rolle bei der pankreatischen Tumorentwicklung und Tumorerhaltung spielen. Innerhalb der MAPK Signalkaskade nimmt das Enzym MEK1/2 eine bedeutende Schlüsselposition ein, in dem es sein einziges bekanntes Substrat ERK1/2 phosphoryliert. Diese begrenzte Substratspezifität sowie die einzigartige hydrophobe Enzymtasche, die die Bindung von selektiven allosterischen Inhibitoren ermöglicht, führten zur Entwicklung gezielter therapeutischer Strategien, um MEK1/2 und somit den hyperaktivierten RAS-RAF-MEK-ERK Signalweg in verschiedenen Tumorentitäten zu blockieren. Das Ziel der vorliegenden Arbeit bestand insbesondere in der präklinischen Evaluierung des neuen allosterischen MEK1/2 Inhibitors Refametinib als potentiellen Therapieansatz für das duktale Adenokarzinom des Pankreas mit Hilfe genetisch veränderter Mausmodelle (GEMMs).

Zunächst wurden ERK1 und ERK2 als therapeutische Zielstrukturen im PDAC validiert. Hierbei wurde mittels *Kras*^{G12D}-basierter GEMMs und muriner PDAC Zellen gezeigt, dass beide Proteine in ihrer aktiven phosphorylierten (p) Form während der Progression von murinen präneoplastischen Läsionen (mPanINs) zu invasivem PDAC hochreguliert werden. Zusätzlich wurden erhöhte pERK1/2-Proteinlevel in humanen Tumorproben und humanen PDAC Zelllinien nachgewiesen, wobei nur wenige Exemplare pERK1/2-negativ waren. Diese Ergebnisse deuten auch auf eine wichtige Rolle von ERK1/2 während der humanen Pankreas-Tumorgenese hin. Folglich scheint aktives pERK1/2 ein idealer Kandidat für die zielgerichtete Therapie des PDAC zu sein.

Im Weiteren wurden die *in vitro* und *in vivo* Wirkung des hoch selektiven MEK1/2 Inhibitors Refametinib sowie die zugrundeliegenden molekularen Mechanismen der MEK1/2-Inhibierung untersucht. Refametinib blockiert effektiv die Phosphorylierung von ERK1/2 *in*

vitro in humanen und murinen primären PDAC Zelllinien sowie *in vivo* in *Kras*^{G12D};*p53*$^{\Delta/\Delta}$ Mäusen. Demzufolge wurden auch ERK1/2 Substrate herunterreguliert, wie beispielsweise das pro-apoptotische Protein BIM. Dies führte zu einer zeit- und dosisabhängigen Reduktion der Lebensfähigkeit aller getesteten humanen und murinen PDAC Zellen, welche auf die Auslösung des programmierten Zelltodes zurückzuführen ist. Die ausgeprägte zytotoxische Wirkung war auch für die massive Schrumpfung der Pankreastumore verantwortlich, die in allen Refametinib-behandelten *Kras*^{G12D};*p53*$^{\Delta/\Delta}$ Mäusen 1-2 Wochen nach Therapiebeginn mittels Magnetresonanztomographie (MRT) beobachtet wurde. Der ausgelöste Zelltod war sowohl CASPASE 3/7-abhängig als auch mit gespaltenem PARP verbunden. Ferner führte die dauerhafte ERK1/2 Inhibierung in Kombination mit der eindrucksvollen Tumorregression zu einem signifikanten medianen Überlebensvorteil von 26 Tagen im Vergleich zu Placebo-behandelten Kontroll-Mäusen. Im Gegensatz dazu konnte der derzeitige Behandlungsstandard, die Kombination von Gemcitabin mit Erlotinib, die PDAC Progression nicht verhindern. Gemcitabin- und Erlotinib-behandelte Mäuse zeigten keine Verringerung der Tumorlast und keine Zunahme der Lebenserwartung. Somit unterstützen diese präklinischen Daten die Ansicht, dass Refametinib ein neues vielversprechendes Chemotherapeutikum für die Behandlung des PDAC darstellt.

Trotz kontinuierlicher Refametinib-Therapie wurde ein Wiederauftreten der Pankreas-Tumore in allen Tieren circa drei Wochen nach Behandlungsbeginn beobachtet. Die Tumorrezidive wuchsen sukzessive bis zum Tod der Mäuse und waren teilweise mit einer Änderung des PDAC-Subtyps verbunden. 20 % der Refametinib-behandelten Tumore zeigten mesenchymale Eigenschaften einschließlich der Herunterregulierung von E-Cadherin und der Hochregulierung von N-Cadherin und wurden histologisch als sarcomatoid eingestuft. Außerdem zeichnen sich Refametinib-resistente Tumorrezidive mit einem EMT-Phänotyp durch ein anhaltend aktives KRAS aus, welches folglich zu einer kompensatorischen Aktivierung der nachgeschalteten PI3K-AKT-mTOR Signalkaskade führt. Schließlich wurde nachgewiesen, dass sowohl die Induktion eines mesenchymalen Phänotyps, als auch die Verstärkung des KRAS-Signalweges, jedoch ohne zugrundeliegende Amplifikation des *KRAS*-Onkogens selbst, und RAS Effektor-Signalkaskaden tatsächlich erworbene Resistenzmechanismen gegen Refametinib sind und diese Refametinib-Resistenz teilweise durch Rapamycin, einen Inhibitor der mTOR Kinase, *in vitro* überwunden werden kann. Rapamycin verzögert auch das Wachstum der Tumorrezidive *in vivo* unter Anwendung eines sequentiellen Ansatzes nach Refametinib-Behandlung, konnte aber im Vergleich zur Refametinib-Monotherapie das Gesamtüberleben von *Kras*^{G12D};*p53*$^{\Delta/\Delta}$ Mäusen nicht verlängern.

Zusammenfassend geben die Ergebnisse der gegenwärtigen Arbeit nicht nur ein tieferes Verständnis darüber, wie die pharmakologische Inhibierung des MAPK Signalweges die PDAC Progression einschränkt, sondern sind auch von großem Nutzen für die weitere Verbesserung bestehender Behandlungsstrategien, die auf dieses kolossale Signalnetzwerk abzielen, um die Lebensqualität von Patienten mit duktalem Adenokarzinom des Pankreas zu verbessern.

Parts of this thesis were submitted and accepted for publication:

Ardito, C. M., Grüner, B. M., Takeuchi, K. K., Lubeseder-Martellato, C., **Teichmann, N.**, Mazur, P. K., Delgiorno, K. E., Carpenter, E. S., Halbrook, C. J., Hall, J. C., Pal, D., Briel, T., Herner, A., Trajkovic-Arsic, M., Sipos, B., Liou, G. Y., Storz, P., Murray, N. R., Threadgill, D. W., Sibilia, M., Washington, M. K., Wilson, C. L., Schmid, R. M., Raines, E. W., Crawford, H. C., and Siveke, J. T. (2012). EGF receptor is required for KRAS-induced pancreatic tumorigenesis. Cancer Cell *22*, 304-317
(**DOI:** 10.1016/j.ccr.2012.07.024)

Barbara M. Grüner, Isabel Winkelmann, Annette Feuchtinger, Na Sun, Benjamin Balluff, **Nicole Teichmann**, Alexander Herner, Evdokia Kalideris, Katja Steiger, Rickmer Braren, Michaela Aichler, Irene Esposito, Roland M. Schmid, Axel Walch and Jens T. Siveke (2016). Modeling Therapy Response and Spatial Tissue Distribution of Erlotinib in Pancreatic Cancer. Molecular Cancer Therapeutics 15(5), 1145-1152
(DOI: 10.1158/1535-7163.MCT-15-0165)

M. Trajkovic-Arsic, I. Heid, K. Steiger, A. Gupta, A. Fingerle, C. Wörner, **N. Teichmann**, S. Sengkwawoh-Lueong, P. Wenzel, A. J. Beer, I. Esposito, R. Braren & J. T. Siveke (2017). Apparent Diffusion Coefficient (ADC) predicts therapy response in pancreatic ductal adenocarcinoma. Scientific Reports 7: 17038
(**DOI:**10.1038/s41598-017-16826-z)

Parts of this thesis were presented and discussed at international and national conferences:

Presentations:

12/2012 "A promising therapy strategy for PDAC: MEK1/2 inhibition with the novel chemotherapeutic drug BAY 86-9766"

5th Annual Meeting of NGFN-Plus and NGFN-Transfer in the Program of Medical Genome Research
Heidelberg, Germany

10/2012 "MEK1/2 inhibition – a promising treatment strategy for Pancreatic Ductal Adenocarcinoma (PDAC)"

United European Gastroenterology Week
Amsterdam, Netherlands
Prize: National Scholar Award

09/2012 "Präklinische Therapiestudie mit dem neuen allosterischen MEK-Inhibitor BAY 86–9766 in genetisch veränderten Mäusen mit endogenem Pankreaskarzinom"

Viszeralmedizin 2012 - Jahrestagung der Deutschen Gesellschaft für Verdauungs- und Stoffwechselkrankheiten (DGVS)
Hamburg, Germany
Z Gastroenterol 2012; 50 - K131 (DOI: 10.1055/s-0032-1324066)

03/2012 "MEK1/2 inhibition in pancreatic ductal adenocarcinoma (PDAC)"

Interact 2012
Munich, Germany

11/2011 "MEK1/2 inhibition in pancreatic ductal adenocarcinoma (PDAC)"

3rd AIO-Symposium: Academic Drug Development in Oncology - Translating Basic Science Research into Innovative Treatments
Berlin, Germany

Poster presentations:

10/2013 "Sequential combination of the novel allosteric MEK1/2 inhibitor BAY 86-9766 (RDEA119) with the mTOR inhibitor rapamycin decelerates relapse of pancreatic tumors"

AACR-NCI-EORTC International Conference on Molecular Targets and Cancer Therapeutics
Boston, Massachusetts, USA

03/2013 "A promising therapy strategy for PDAC: MEK1/2 inhibition with the novel chemotherapeutic drug BAY 86-9766"

2nd International Meeting on Molecular-Based Treatment of GI Cancer
Göttingen, Germany

06/2012 "MEK 1/2 inhibition with the novel chemotherapeutic agent BAY 86-9766 (RDEA119) – a promising treatment strategy for pancreatic cancer"

AACR conference: Pancreatic Cancer – Progress and Challenges
Lake Tahoe, Nevada, USA

Press Release: Novel Chemotherapy Agent Appears to be a Promising Pancreatic Cancer Treatment (http://www.aacr.org/home/public--media/aacr-in-the-news.aspx?d=2825)

03/2012 "The novel MEK1/2 inhibitor BAY 86-9766 (RDEA119), a promising therapeutic agent for the treatment of pancreatic cancer"

Interact 2012
Munich, Germany

11/2011 "The novel MEK1/2 inhibitor BAY 86-9766 (RDEA119), a promising therapeutic agent for the treatment of pancreatic cancer"

3rd AIO-Symposium: Academic Drug Development in Oncology - Translating Basic Science Research into Innovative Treatments
Berlin, Germany

Table of contents

1. Introduction

1.1 The Pancreas

1.1.1 Pancreas anatomy and physiology

The pancreas is a mixed exocrine and endocrine gland that was first described by the Greek anatomist and surgeon Herophilus around 300 BC (Bay and Bay, 2010). It is located in the abdominal cavity (Figure 1.1A and 1.1B) and is composed of two separate functional units that regulate nutrient digestion and glucose metabolism. The exocrine pancreatic compartment comprises acinar, ductal, and centroacinar cells, and correspond to > 90 % of the pancreatic cell population in the adult (Figure 1.1C and 1.1D). Acinar cells are organized in grape-like structures that synthesize and secrete digestive enzymes, such as trypsin, chymotrypsin, lipases, and nucleases, released to the duodenum via the ductal cells. Ductal cells are variously sized tubules forming a branched tree network that ends in the main duct, allowing the flow of digestive enzymes into the main duct and duodenum (Bardeesy and DePinho, 2002; Edlund, 2002; Hezel et al., 2006). Centroacinar cells are positioned within the center of acini at the duct terminus and play an important role in maintaining the ionic content of the ductal lumen and keep it open for fluid flow (Beer *et al.*, 2016). The endocrine pancreatic compartment makes up only a small percentage of the entire pancreas and consists of five specialized cell types forming the Islets of Langerhans: glucagon-producing α-cells, insulin-producing ß-cells, somatostatin-producing δ-cells, pancreatic polypeptides-producing PP-cells, and ghrelin-producing ε-cells. Hormones are released into the blood stream via intermingled blood vessels (Figure 1.1D), thereby assuring the regulation of metabolism and glucose homeostasis (Bardeesy and DePinho, 2002; Edlund, 2002; Hezel *et al.*, 2006).

1.1.2 Pancreas development

During embryogenesis, the pancreas originates from distinct dorsal and ventral buds in the foregut endoderm. In mice, the dorsal pancreatic bud first emerges at embryonic day (E) 9.5. The ventral bud appears later at E 10.25-10.5 (Kim and Hebrok, 2001). These two pancreatic lineages proliferate, form branched tubular structures and, as a result of gut rotation, eventually fuse into one single organ by E 12.5 containing almost entirely undifferentiated multipotent progenitor cells (MCPs) that are characterized by a strong

expression of the homeodomain transcription factors *Hlxb9* and *Pdx1* as well as of the basic helix-loop-helix-protein PTF1-p48 (also known as Ptf1a and p48; hereafter, Ptf1a) (Apelqvist *et al.*, 1999; Hart *et al.*, 2003; Norgaard *et al.*, 2003). After this early phase of pancreatic development, pancreatic epithelium continues to expand and branch into a complex highly ordered tubular network starting from E 12.5 until birth. This secondary transition involves the differentiation of MPCs into acinar, ductal, and endocrine cells (Gu *et al.*, 2003; Zhou *et al.*, 2007) through the segregation of tip and trunk domains finally resulting in the lineage restriction of tip progenitors to an acinar fate and of trunk progenitors to an endocrine and ductal fate (reviewed by Shih *et al.*, 2013).

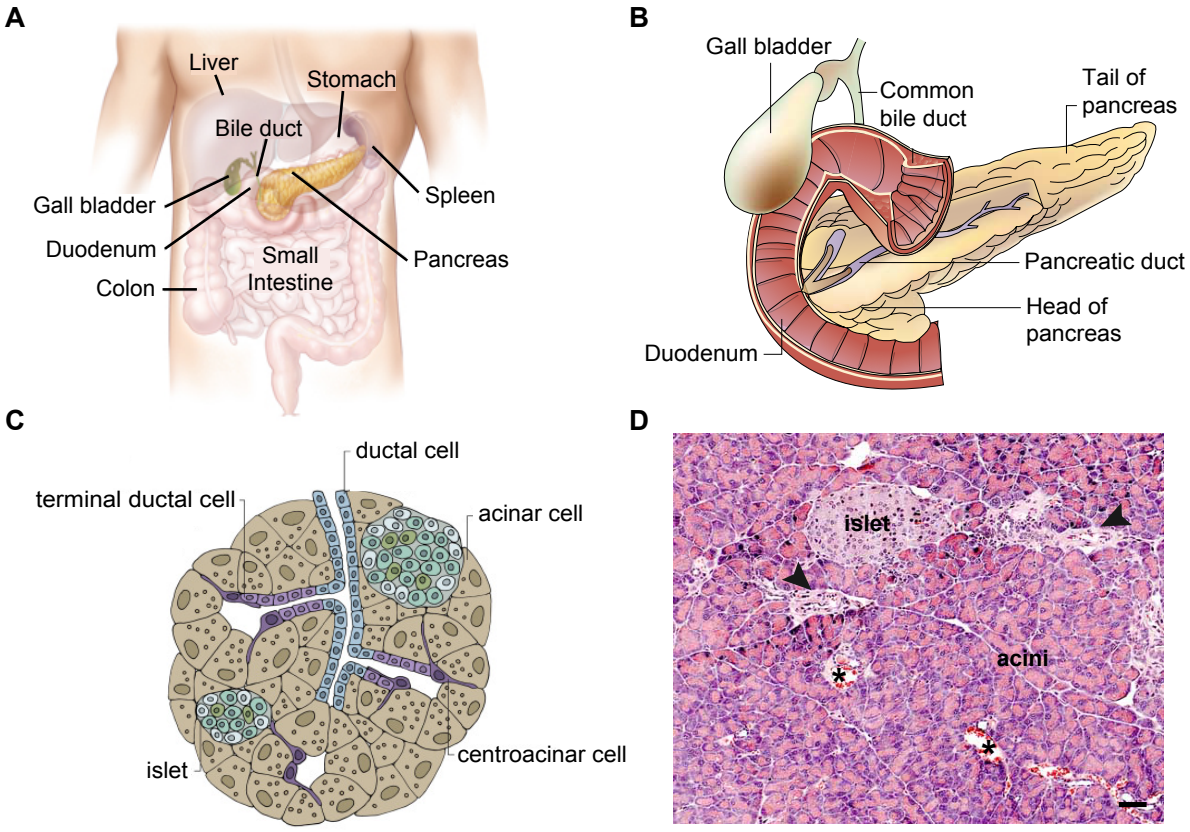

Figure 1.1 Anatomy of the adult pancreas. (A) Localization of the pancreas in the human body. The pancreas lies behind the liver and the stomach in the abdomen (Winslow, 2010). (B) Gross anatomy of the pancreas. The head of pancreas is attached to the duodenum (the most anterior part of the small intestine), whereas the tail of pancreas is situated adjacent to the spleen (Bardeesy and DePinho, 2002). (C) Illustration of a portion of adult mouse pancreas containing acinar cells (brown), centroacinar cells (dark purple), terminal ductal cells (light purple), ductal cells (blue) and islets (Beer *et al.*, 2016). (D) The major components of the pancreatic parenchyma on a histological level (murine wild-type pancreas). Murine islets of Langerhans display a higher variation in size and distribution compared to humans and usually an interlobular localization. Therefore, murine pancreatic islets are found in the vicinity of interlobular ducts (black arrowheads) and blood vessels (black asterisks). Scale bar represent 50 µm.

In the mature pancreas, acinar, ductal, and endocrine islet cells are characterized by different expression patterns of various transcription factors, which are nowadays used to

study the contribution of distinct cell populations to fatal pancreatic diseases, such as pancreatic cancer (described in chapter 1.2). *Ptf1a* expression is thereby restricted to acinar cells (Adell *et al.*, 2000; Kawaguchi *et al.*, 2002; Krapp *et al.*, 1996; Krapp *et al.*, 1998), whereas PDX1 is present in islet ß-cells and at a lower level in acinar cells. Ductal cells exclusively express many of the same transcription factors that segregate to the trunk domain during tip/trunk separation, for example *Sox9*, *Tcf2*, *Onecut-1*, *Hes1*, *Prox1*, and *Glis3*, and that are later excluded from the endocrine compartment (reviewed by Shih *et al.*, 2013).

1.2 Pancreatic ductal adenocarcinoma (PDAC)

1.2.1 Epidemiology of PDAC

Pancreatic ductal adenocarcinoma (PDAC), also known as pancreatic cancer or infiltrating ductal adenocarcinoma, currently represents the fourth leading cause of cancer-related death in men and women in both Europe and the USA and is anticipated to become the second within the next decade (Rahib *et al.*, 2014). This most aggressive disease predominantly affects elderly population (Siegel *et al.*, 2013). Besides increasing age, there are other established risk factors, including tobacco smoking (relative risk = 2), diets high in meats and fat, low serum folate levels, obesity, long-standing diabetes mellitus (type II), chronic pancreatitis and hereditary pancreatitis as well as a family history of the disease (reviewed in Brune and Klein, 2008; Ghaneh *et al.*, 2007; Lowenfels and Maisonneuve, 2006; Maitra and Hruban, 2008).

Whereas death rates for most cancer types (lung, colorectum, breast, and prostate) decline, this does not hold true for PDAC (Siegel *et al.*, 2013). The median survival after diagnosis is below six months and the overall 5-year survival rate is 3 %-5 % (Li *et al.*, 2004). This poorest prognosis amongst all solid tumors is mainly attributed to the inability to diagnose pancreatic cancer at an early resectable stage due to late occurrence of symptoms as well as a lack of reliable biomarker for detection. Other reasons include the early dissemination to distant organs, the tumor genetic heterogeneity and the high intrinsic resistance to any therapeutic intervention including chemo- and targeted therapy as well as ionizing radiation.

1.2.2 Pathology of PDAC

PDAC is the most common malignancy of the pancreas, accounting for more than 85 % of all pancreatic epithelial neoplasms (Klimstra *et al.*, 2009). The vast majority of PDACs

locate in the head of the pancreas (65 %) and tend to present earlier with obstructive jaundice or acute pancreatitis, abdominal pain, and weight loss. In contrast, tumors located in the tail (10 %) or body (15 %) region of the pancreas tend to present late and are associated with a worse prognosis. 10 % of all pancreatic cancers even present as multifocal (Ghaneh *et al.*, 2007). Although the putative cell of origin for pancreatic cancer remains elusive, the disease recapitulates normal duct characteristics that are gland or tubule formation and mucin production (Ghaneh *et al.*, 2007). In addition, PDAC is primarily characterized by an extensive stromal compartment, termed desmoplasia, consisting of proliferating myofibroblasts (pancreatic stellate cells), and deposition of type I collagen, hyaluronic acid, and other extracellular matrix components, as well as multiple types of inflammatory cells, including macrophages, mast cells, lymphocytes, and plasma cells (Maitra and Hruban, 2008). This abundant dense non-neoplastic stroma has been shown to be biologically critical in PDAC with both tumor-inhibiting effects under normal conditions and tumor-promoting effects due to strong tumor-stroma interactions (Bulle *et al.*, 2017; Moffitt *et al.*, 2015). Moreover, main tumors harbor a remarkable affinity for perineural, (close to 80 % of cases) and vascular invasion, the latter being responsible for early infiltration into surrounding tissues and for the metastatic spread (Maitra and Hruban, 2008). Invasive PDAC also manifests a high degree of intratumoral cellular and morphological heterogeneity, which is reflected in the frequent mixture of glandular and non-glandular (anaplastic) patterns as well as in the unusual degree of numerical and structural chromosomal instability (reviewed by Hansel *et al.*, 2003).

1.2.3 Evolving neoplastic precursor lesions and implicated molecular signaling pathways in PDAC

It is thought that PDAC arises from distinct non-invasive precursor lesions: the most common and best characterized pancreatic intraepithelial neoplasia (PanIN), less frequently observed mucinous cystic neoplasm (MCN) and intraductal papillary mucinous neoplasm (IPMN) (Hruban *et al.*, 2001; Hruban *et al.*, 2004), as well as the recently identified atypical flat lesions (AFLs) (Aichler *et al.*, 2012). In contrast to the macroscopic, cystic MCNs and IMPNs, PanINs typically progress through defined histological and molecular stages subclassified into PanIN-1A, PanIN-1B, PanIN2, and PanIN-3. This morphological PanIN progression from typical columnar, mucinous epithelium of PanIN-1 to increasing nuclear atypia and architectural disorganization of PanIN-3 correlates with genetic and epigenetic alterations that are crucially involved in the malignant transformation to PDAC (Figure 1.2). Activating point mutations of the proto-oncogene *KRAS2*, mostly at codon 12, 13 or 61, are one of the earliest genetic alterations in PanIN-1A and PanIN-1B

lesions and are also found in >90 % of invasive PDAC (Caldas and Kern, 1995; Klimstra and Longnecker, 1994). Telomere shortening and the overexpression of the epidermal growth factor receptor (EGFR) as well as of ERBB2 also occur in low-grade PanIN-1 (Bardeesy and DePinho, 2002; Salomon *et al.*, 1995). Loss of $p16^{INK4A}$ function, through either mutation, deletion or promotor hypermethylation, is generally seen in moderately advanced PanIN-2 lesions and with a frequency of 80-95 % in PDAC cases (Rozenblum *et al.*, 1997; Schneider and Schmid, 2003).

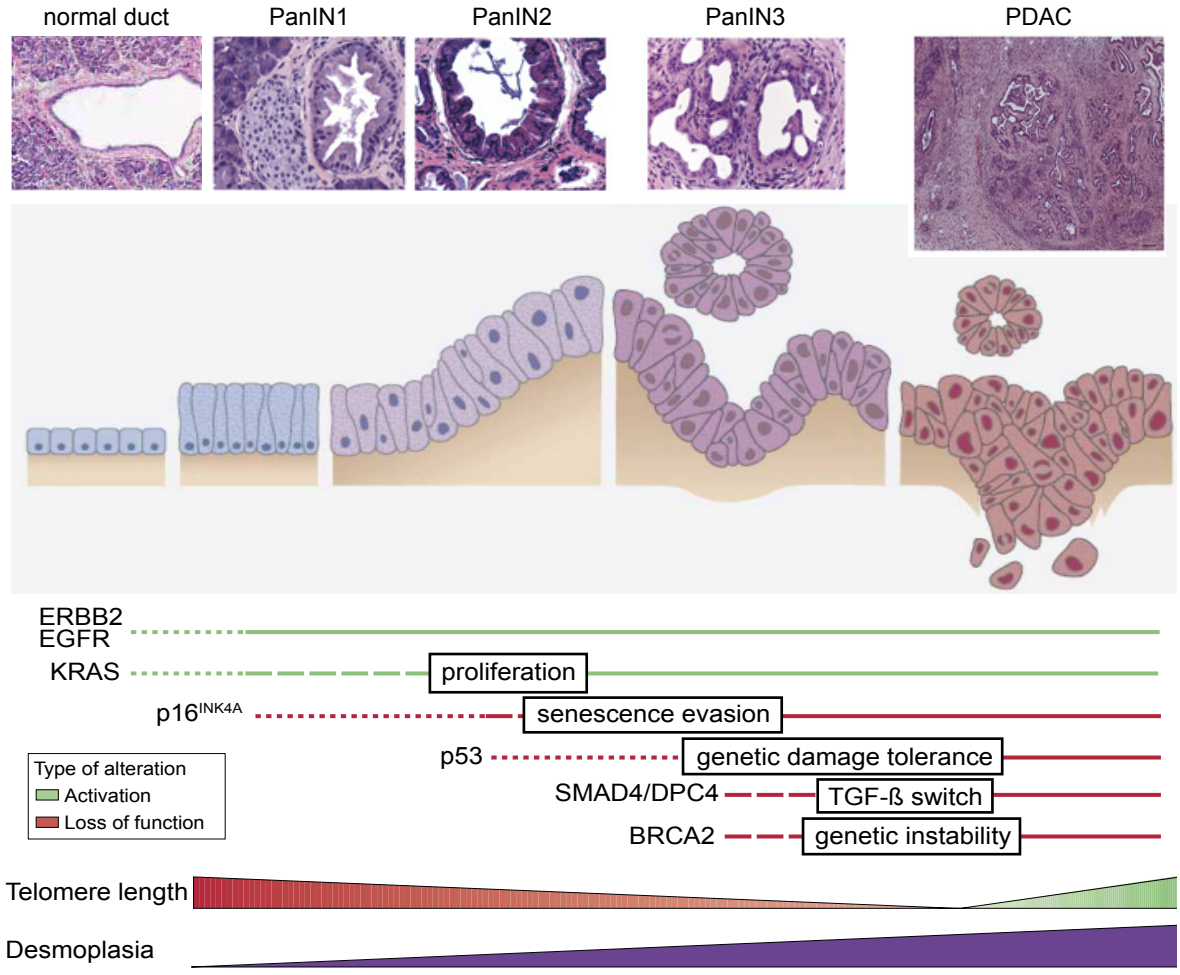

Figure 1.2 Model of PanIN progression to invasive PDAC. The transition of the normal ductal epithelium (far left) through the graded PanIN stages (1–3) to invasive PDAC (far right) is illustrated on a histological level and as a schematic. Morphologically, the normal ductal epithelium consists of cuboidal to low-columnar cells with amphophilic cytoplasm, whereas PanINs are lined by columnar mucinous epithelium: PanIN-1 lesions show hyperplasia without dysplasia, PanIN-2 are variable dysplastic and PanIN-3 correspond to high-grade dysplasia or *frank carcinoma in situ* including loss of nuclear polarity, cribiforming, the “budding off” of small clusters of epithelial cells into the lumen, combined with luminal necrosis, dystrophic goblet cells, abnormal mitosis, and prominent (macro) nucleoli (Hruban *et al.*, 2001; Hruban *et al.*, 2004). The progression from low-grade PanINs to invasive PDAC is associated with an increasing accumulation of genetic changes, ultimately resulting in the rampant genomic instability and profound aneuploidy seen in PDAC. Lines represent the stage of onset of these alterations, whereas the thickness of the line indicates the frequency of the alteration. Moreover, the physiological consequences of each genetic alteration is highlighted (adapted from Bardeesy and DePinho, 2002; Hezel *et al.*, 2006; Mazur and Siveke, 2012).

Inactivation of the tumorsuppressor-genes *TP53*, *SMAD4/DPC4* and *BRCA2* is considered as relative late genetic event during pancreatic tumorigenesis and hence mostly occur at the PanIN-3 stage (Bardeesy and DePinho, 2002; Hezel *et al.*, 2006; Rozenblum *et al.*, 1997). Approximately 50 % of PDACs harbor SMAD4/DPC4 loss through either homozygous deletion or by intragenic mutations and loss of the second allele (Hahn *et al*., 1996; Luttges *et al*., 2001), whereas mutations in the *Tp53* tumor suppressor gene on chromosome 17p mostly by a missense alteration of the DNA-binding domain on one allele coupled with loss of the second allele can be found in 50-75 % of PDACs (Redston *et al*., 1994; Rozenblum *et al*., 1997). IPMNs manifest similar genetic alterations with increasing cytoarchitectural atypia as PanINs including activating *KRAS2* mutations, but mostly at codon 12 (Wu *et al*., 2011), *TP53* mutations and loss of $p16^{Ink4A}$ (Biankin *et al*., 2003). In contrast to PanINs, abrogation of *SMAD4*/*DPC4* is rare in IPMNs, but biallelic inactivation of *STK11/LKB1*, the gene associated with Peutz-Jeghers syndrome, and mutation of the *PIK3CA* gene are quite frequently observed (Iacobuzio-Donahue *et al*., 2000; Schonleben *et al*., 2006; Su *et al*., 1999). Highly proliferative AFLs accumulate the same genetic changes as PanIN lesions and IPMNs that are fundamentally contributing to PDAC development and evolution like *KRAS* activation, $p16^{Ink4A}$ ablation, and p53 dysregulation, but additionally show loss of *PDX1* expression (Aichler *et al*., 2012; Esposito *et al*., 2012; Esposito *et al*., 2014). Given the fact that the well-known genetic alterations documented in all precursor lesions were also identified in PDAC underpins the current neoplastic precursor lesion-to-PDAC progression models (Aichler *et al*., 2012; Esposito *et al*., 2014; Hruban *et al*., 2008; Jones *et al*., 2008; Matthaei *et al*., 2011).

Recent genomic analyses of human pancreatic cancer confirmed not only the four most prominent mutations belonging to the genetic fingerprint of PDAC (*KRAS2*, *TP53*, *SMAD4/DPC4* and *CDKN2A*), but also a more complex and heterogeneous mutational landscape that nevertheless aggregates only into a few affected core signaling pathways including KRAS, transforming growth factor β (TGF-β), Hedgehog, Wingless-related integration site (WNT), Notch signaling, apoptosis, chromatin modification, DNA damage repair, RNA processing, cell cycle regulation and axonal guidance (Bailey *et al*., 2016; Biankin *et al*., 2012; Jones *et al*., 2008; Waddell *et al*., 2015). Not all of the analyzed pancreatic cancers harbor alterations in all pathways, and the key mutations in each pathway vary widely from one tumor to another, thus emphasizing the importance of genetic heterogeneity of human PDAC (Jones *et al*., 2008). The identification of diverse molecular subtypes further underpins the extremely complex and heterogeneous nature of the disease (Bailey *et al*., 2016; Collisson *et al*., 2011; Moffitt *et al*., 2015). Oncogenic KRAS, however, still remains as one of the PDAC key drivers. The *KRAS* proto-oncogene encodes two ~ 21 kDa small, membrane-bound GTPases, KRASA and KRASB, which

represent alternative splice variants. Both proteins operate as binary switches between a GDP-bound inactive and a GTP-bound active state. Upon stimulatory signals from upstream growth factors and their corresponding receptor tyrosine kinases, so-called guanine nucleotide exchange factors (GEFs) trigger the exchange of GDP to GTP, thus placing KRAS in its active, signaling configuration. Inactivation of KRAS is then mediated by GTP hydrolysis involving both the intrinsic GTPase activity of KRAS itself and GTPase-activating proteins (GAPs). Activating mutations of *KRAS* found in human PDAC (point mutations at codon G12 (98 % of all *KRAS* mutations in PDAC), G13 and Q61) block the interaction between KRAS and GAPs, which in turn results in the pronounced attenuation of GTP hydrolysis and a constitutive active KRAS in the absence of extracellular stimuli (Pylayeva-Gupta *et al.*, 2011). As a consequence, a multitude of downstream signaling cascades, such as the mitogen activated protein kinase (MAPK, see also chapter 1.5.1), the phosphoinositide-3-kinase (PI3K), and the RalGDS pathways, are persistently stimulated (Figure 1.3) driving a variety of cancer hallmarks: sustained proliferation, suppression of apoptosis, metabolic reprogramming, remodeling of the tumor microenvironment, evasion of the immune response as well as cell migration and metastasis (Parada and Weinberg, 1983; Pylayeva-Gupta *et al.*, 2011).

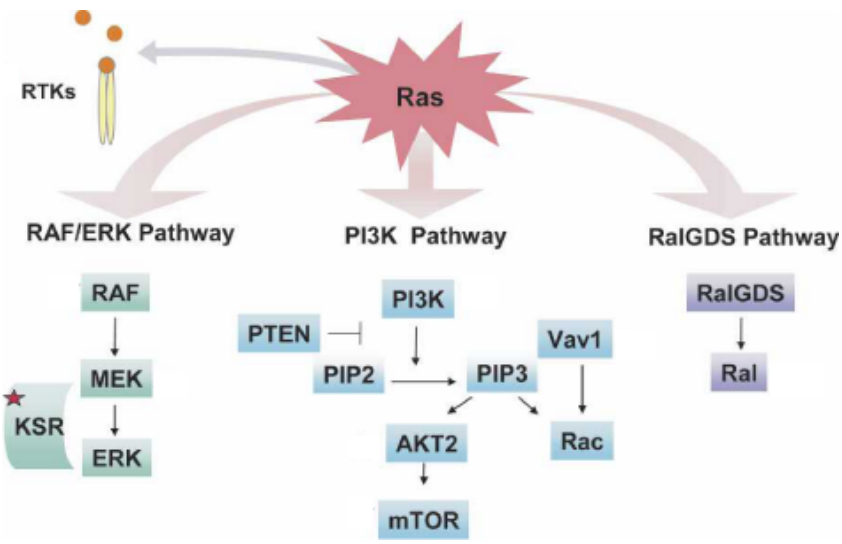

Figure 1.3 The RAS signaling network. Depicted are the three major signaling pathways that have been implicated in PDAC: the mitogen activated protein kinase (MAPK) pathway, the phosphoinositide-3-kinase (PI3K) pathway, and the RalGDS pathway (adapted from Hezel *et al.*, 2006).

The thorough understanding of the disease course and the molecular biology of PDAC have helped to develop new diagnostic approaches and several mechanistic based treatment regimens. However, disease prognosis is still extremely poor due to its silent course and explosive fatal nature with so far no available curative approaches in hand. The

current established therapeutic strategies for patients diagnosed with pancreatic cancer will be presented in the next chapter (see 1.3).

1.3 Current therapeutic options for PDAC

Today, the only potential curative approach for patients with pancreatic cancer is a radical resection of the localized tumor. However, only a minority of patients (10-20 %) are present with local disease at the time of diagnosis and can undergo potentially curative surgery (Jemal, *et al*., 2010; Lahat *et al*., 2011). Standard surgical procedures are (1) the classic "Kausch-Whipple" pancreaticoduodenectomy including a distal gastrectomy and (2) the pylorus-preserving pancreaticoduodenectomy preserving antral and pyloric function, respectively. Both surgical strategies are equally effective for the removal of tumors in the head and neck of the pancreas, but the 5-year overall survival rates after successful surgery are still only about 20 % due to fast post-operative relapses (Tran *et al*., 2004; Wagner *et al*., 2004).

The main contraindications for pancreatic resection are the presence of local or distant metastases, mainly to the liver, the lungs, the abdomen, and regional lymph nodes (Maitra and Hruban, 2008), and tumor infiltration of local vessels, including the celiac artery, superior mesenteric artery and vein, portal vein, and hepatic artery. Almost 80 % of patients are diagnosed with locally advanced and metastasized pancreatic cancer, thus having only palliative treatment options with the objective of relieving disease-related symptoms and prolonging survival. Since 1997, the reference first-line therapy for those patients is infusional gemcitabine, a fluorine substituted deoxycytidine analog and inhibitor of nucleic acid synthesis. Gemcitabine functions as an antimetabolite, arresting cells at the G1/S interphase. This strongly hydrophilic drug requires facilitated uptake into the cell via nucleoside transporters, and following uptake, must be phosphorylated to its active metabolites gemcitabine diphosphate and gemcitabine triphosphate to exert its cytotoxicity (Spratlin and Mackey, 2010). Gemcitabine not only alleviates disease-related symptoms, but also improves significantly the median survival compared to 5-fluorouracil (5-FU) treatment (5.65 months versus 4.41 months) (Burris *et al*., 1997). Thus, single-agent gemcitabine provides a modest survival benefit for only a minority of PDAC patients, and its efficiency needs to be urgently improved.

To date, the only approved targeted therapy for advanced, unresectable pancreatic cancer is the combination of gemcitabine with erlotinib, an orally available EGFR inhibitor, which extend patients survival by two more weeks compared to gemcitabine alone (6.24 months versus 5.91 months). Interestingly, a subgroup of patients that develop skin rash grade 2 or

higher as a side effect has a significant better median survival rate of 10.5 months (Moore *et al*., 2007). Erlotinib (Tarceva®) was approved by the U.S. Food and Drug Administration (FDA) in 2005, but European registration is restricted to patients with metastatic disease and does not include those with locally advanced pancreatic cancer.
In 2011, new hope was given to an aggressive treatment regimen called FOLFIRINOX. This multidrug combination of oxaliplatin, irinotecan, 5-FU, and leucovorin showed superiority over gemcitabine monotherapy in all efficacy parameter, including the median overall survival (11.1 months versus 6.8 months) and the progression-free survival (6.4 months versus 3.3 months). Unfortunately, patients treated with FOLFIRINOX had a definitive degradation of life quality and developed more adverse events, such as neutropenia, febrile neutropenia, thrombocytopenia, and diarrhea (Conroy *et al*., 2011). A similar increased toxicity profile (neutropenia, febrile neutropenia, peripheral neuropathy, fatigue) was observed in a clinical trial comparing gemcitabine plus albumin-bound paclitaxel particles (nab-paclitaxel, Abraxane) with gemcitabine alone. The combination treatment significantly prolonged the median overall survival (8.5 months versus 6.7 months) as well as the progression-free survival (5.5 months versus 3.7 months) of metastatic pancreatic cancer patients (Von Hoff *et al*., 2013). Despite their considerable toxicity, the increase in patients survival rates at all time points was a base for FDA approval and the establishment of both FOLFIRINOX and Abraxane plus gemcitabine as new first-line therapeutic options for metastatic pancreatic cancer replacing the current standard-of-care therapy with gemcitabine (Adamska *et al*., 2017). However, novel effective treatment strategies with less toxicity are still desperately needed.

Oncology drug development relies heavily on suitable models for efficacy testing of new therapeutic agents, which should faithfully recapitulate various aspects of the corresponding human disease. The different, currently available preclinical models for PDAC will be described and discussed in the next chapter (see chapter 1.4).

1.4 Preclinical models of PDAC for oncologic drug development

As a first step in the evaluation process of novel therapeutics, pancreatic cancer cells derived from primary human pancreatic adenocarcinomas and their metastases are widely used to perform *in vitro* proliferation and cytotoxicity screens. Although these cultured cell lines typically display molecular alterations observed in primary pancreatic tumors, their interaction with their *in vivo* milieu has been changed or even lost at both the cellular and molecular levels through the isolation, purification, and maintenance process (Melstrom and Grippo, 2008). Indeed, it is well documented that the complex tissue milieu, especially the desmoplasia seen in PDAC, dramatically influences cancer growth and its response to treatment. As a consequence, more reliable *in vivo* mouse models were developed, such as xenograft transplantations of either cultured pancreatic cancer cells (often termed 'indirect xenograft') or patient-derived tissue subcutaneously or orthotopically into immunocompromised mice. Especially cultured PDAC xenografts subcutaneously inoculated served as a major preclinical screening method in oncology drug development for the last several years due to its low cost, easy generation, and well-defined tumor measurements (Mazur *et al*., 2015b). However, the lack of a host environment including the absence of a functional immune system, homogenous cell composition, and long-term selection of cells in culture media are just a few suggested reasons for the inconsistent efficacy prediction of novel therapeutics often seen in PDAC and other cancers when using indirect xenograft models models (Garber, 2009; Van Cutsem *et al*., 2004; Voskoglou-Nomikos *et al*., 2003).

With the developed ability to target the endogenous locus by homologous recombination in embryonic stem cells and to spatially, and even temporally, restrict gene expression, using *Cre/loxP* or *Flp/FRT* technologies for example (Branda and Dymecki, 2004; Sauer, 1998), as well as with the identification of the early genetic initiator alterations in pancreatic precursor lesions (see chapter 1.2.3) a new generation of mouse models evolved, which more faithfully mimic sporadic tumor formation or carcinogenesis (Jonkers and Berns, 2002). The major breakthrough in recapitulating human pancreatic carcinogenesis was then achieved by Hingorani and colleagues, who generated mice with conditional *Cre/loxP*-based activation of endogenous oncogenic $Kras^{+/LSL\text{-}G12D}$ triggered by either transgenic *Pdx1-Cre* or by the *Cre* knock-in at the *Ptf1a/p48* locus to target the pancreatic progenitor cell population (Hingorani *et al*., 2003); see also chapter 2.1.1). These genetically engineered mouse models (GEMMs) faithfully mimic all three postulated stages of non-invasive PanIN precursor lesions (PanIN1-3) as well as their gradual, age-dependent progression to invasive and metastatic PDAC, both in morphological and in genetical features (see also chapter 1.2.3). These models are better suited for studying early

detection of pre-invasive disease and of potential chemopreventive agents. However, the fact that the so-called mouse PanINs or mPanINs only occasionally progressed to invasive cancer in mice older than 12-15 months limits the use of both models for translational therapeutic approaches and survival studies. Additionally, Obata *et al*. observed notable expression of *Ptf1a* also in the dorsal part of the neural tube, which develops to the cerebellum, the medulla oblongata, and the spinal cord (Obata *et al*., 2001). *Pdx1*, on the other hand, is expressed in the developing foregut (stomach and duodenum) as well as in the epidermis (Mazur *et al*., 2010). Thus, it has to be considered that tumor development in both *Ptf1a*$^{+/Cre}$ mice and *Pdx1-Cre* animals may occur in extrapancreatic organs, potentially affecting pancreatic carcinogenesis and responses to therapeutic approaches as well as the lifespan of respective mice (Mazur and Siveke, 2012).

To circumvent the long latency and hard predictability of tumor development in the *Pdx1-Cre;Kras*$^{+/LSL\text{-}G12D}$ or *Ptf1a*$^{+/Cre}$*;Kras*$^{+/LSL\text{-}G12D}$ models, a plethora of pancreatic cancer mouse models has been generated by introducing additional conditional heterozygous or homozygous mutations, mainly in known tumor suppressor genes, such as *Ink4a/Arf*, *Tp53* and *Smad4/Dpc4* (reviewed by Mazur and Siveke, 2012). However, only a few of these mouse models are useful tools for the validation of therapeutic strategies, namely *Pdx1-Cre;Kras*$^{+/LSL\text{-}G12D}$*;Trp53*$^{R172H/+}$ (Cook *et al*., 2012; Hingorani *et al*., 2005) and *Ptf1a*$^{+/Cre}$*;Kras*$^{+/LSL\text{-}G12D}$*;Trp53*$^{loxP/loxP}$ mice (Bardeesy *et al*., 2006). Concomitant expression of *Kras*$^{+/LSL\text{-}G12D}$ and dominant-negative mutated *Trp53*$^{R172H/+}$ results in much accelerated PDAC (median survival approximately five months) with highly glandular, well-differentiated tumors, occurring primarily at the head of the pancreas, and widespread metastases to the liver and lung (Hingorani *et al*., 2005). In contrast, when *Kras*$^{+/LSL\text{-}G12D}$ activation is combined with biallelic conditional loss of p53, the development of gross metastases is not prominent in these mice due to the rapid disease progression, yielding already lethal tumors by eight weeks of age (Bardeesy *et al*., 2006).

Taken together, GEMMs provide another important tool for studying novel, potential therapies for pancreatic cancer as these models not only take into account the inflammatory response at the tumor side and the vascular network, but also reflect more the intratumoral genetic heterogeneity and the strong desmoplastic reaction, both hallmark characteristics of PDAC. Thus, GEMMs have the potential for a greater predictive clinical value than xenograft models (Singh *et al*., 2010). Surprisingly, relatively few studies of cytotoxic agents have been reported to date in such models (Ardito *et al*., 2012; Frese *et al*., 2012; Heid *et al*., 2017; Mazur *et al*., 2015a; Morton *et al*., 2010; Olive *et al*., 2009; Singh *et al*., 2010).

1.5 The MEK1/2 dual-specificity protein kinases

1.5.1 The RAS-RAF-MEK-ERK or MAPK signaling pathway

The RAS-RAF-MEK-ERK signal transduction pathway, which is also denoted as mitogen-activated protein kinase (MAPK) signaling pathway, is one of the best-characterized kinase cascades in cancer cell biology and is involved in regulating a multitude of biological processes, including proliferation and cell cycle progression, apoptosis, cell growth, cell migration and adhesion, differentiation, metabolism, and angiogenesis. Binding of extracellular ligands, such as growth factors (e.g. epidermal growth factor (EGF)), hormones or cytokines, to their respective cell-surface receptor tyrosine kinases (e.g. EGFR) triggers dimerization of the receptor and autophosphorylation of specific tyrosine residues in the C-terminal region of the receptor (Figure 1.4). This generates binding sites for specific adaptor proteins containing either Src-homology 2 or phospho-tyrosine binding (PBT) domains, like growth factor receptor-bound protein 2 or SHC, which then recruit the guanine nucleotide exchange factor Son-of-sevenless (SOS) at the plasma membrane (Figure 1.4). SOS activates the membrane-bound RAS by catalyzing the replacement of GDP with GTP (Figure 1.4). In its GTP-bound active form, RAS recruits rapidly accelerated fibrosarcoma (RAF) serine/threonine kinases (A-RAF, B-RAF, and C-RAF, which was originally discovered as RAF-1) to the plasma membrane, where they become activated through a multi-stage process of protein-protein interactions, phosphorylation, dephosphorylation, and conformational changes (Wellbrock *et al*., 2004). RAF, aka MAP kinase kinase kinase (MAPKKK), has restricted substrate specificity and phosphorylates the MAPK and extracellular signal-regulated kinase (ERK) kinases MEK1 and MEK2. All three RAF isoforms can phosphorylate the two serine residues in the MEK activation loop, although B-RAF is much more effective at doing so than C-RAF, which is better than A-RAF. Thus, B-RAF is considered the predominant activator of the MEK1/2 enzyme, which in turn catalyzes the activation of the effector MAP kinases ERK1/2 (Figure 1.4; for more details, see also chapter 1.5.2). Once activated, ERK1/2 phosphorylates more than 160 known nuclear and cytosolic substrates that include various transcription factors, cytoskeletal proteins, signaling proteins and receptors (for a detailed review, see Yoon and Seger, 2006).

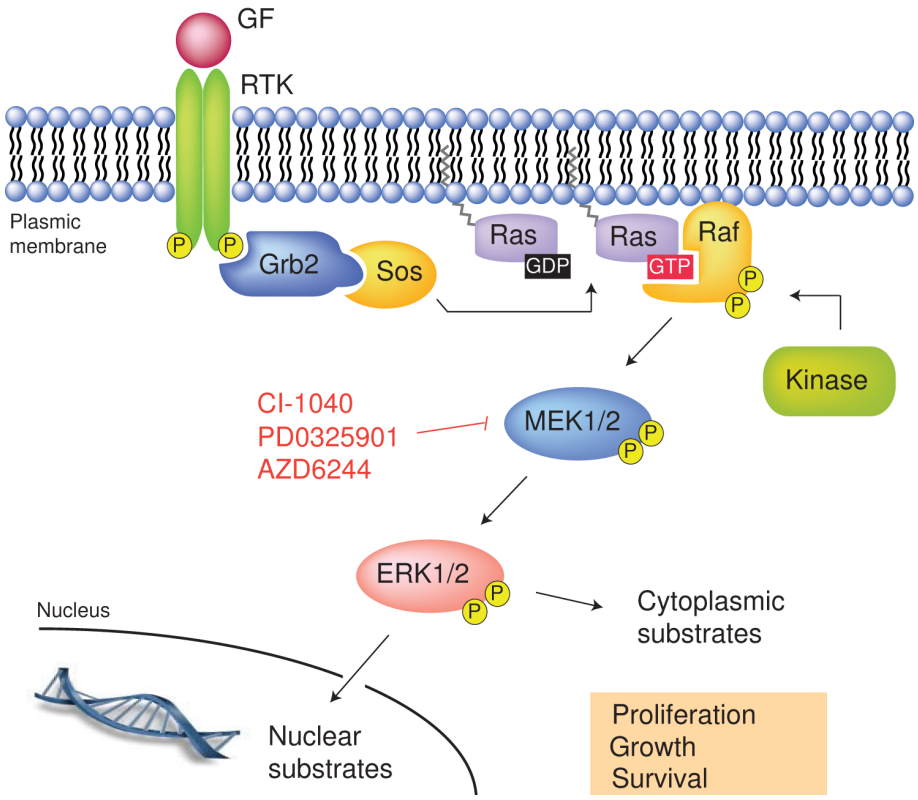

Figure 1.4 The RAS-RAF-MEK-ERK signaling pathway. Growth factor (GF) binding to receptor tyrosine kinases (RTKs) triggers MAPK signaling leading to the activation of dozens of cytosolic and nuclear substrates involved in regulating cell proliferation, cell growth, and cell survival. The organization in a three-tiered kinase module provides the cell with a high potential for signal amplification, and the strength of the response increases as the signal proceeds down the pathway (Harding and Hancock, 2008). Protein phosphorylation, dephosphorylation, and the association with scaffold and/or adaptor proteins, such as kinase suppressor of RAS (KSR), provide temporal and spatial regulation of the MAPK pathway (reviewed by Kolch *et al.*, 2005). Additionally, the presence of negative-phosphorylation sites on the individual kinases allows both fine-tuning and termination of the signal via regulatory feedback loops acting at multiple levels (Orton *et al.*, 2005).

1.5.2 Structure, function, and regulation of MEK1/2

MEK1/2 (also termed MAPKK1/2) belong to the small family of related MAP kinase kinases (MAPKKs, also known as MEKs or MKKs), which are dual specificity enzymes catalyzing the phosphorylation and thus activation of their MAP kinase substrates (ERK1/2 is the only substrate of MEK1/2). In human, two highly homologous genes, *MAP2K1* on chromosome 15 (chromosome 9 in mice) and *MAP2K2* on chromosome 19 (chromosome 10 in mice), encode the 43.5 kDa MEK1 and 44.5 kDa MEK2 proteins, respectively (Brott *et al.*, 1993; Crews *et al.*, 1992; Wu *et al.*, 1993). The two isoforms are known to form homodimers (Figure 1.5A) and are structurally similar: MEK2 bears a 90 % sequence similarity to MEK1 and an 81.5 % sequence identity. The major divergence between both MEK1 and MEK2 sequences are the first 30 amino acids at the N-terminus, and an approximately 50 amino acid insert between the conserved kinase domains IX and X within the proline-rich region (Figure 1.5B). Furthermore, Brott and colleagues were able to show that *Mek2* expression

levels are highest in the intestine and spleen, and lowest in the brain and heart of adult mice (Brott *et al*., 1993). In contrast, *Mek1* is expressed abundantly in murine brain tissue (Crews *et al*., 1992). More recently, functional redundancy of MEK1 and MEK2 has been addressed in the mouse. *Mek1* deficient mice die between E 8.5 (Catalanotti *et al*., 2009) and E 10.5 (Giroux *et al*., 1999). This embryonic lethality results from defects in placental vascularization implicating an important role of MEK1 in placental development. However, *Mek2* knockout mice are viable and fertile with no morphological alteration, indicating that MEK1 can compensate for MEK2 ablation and that MEK2 is dispensable for embryonic growth and development (Belanger *et al*., 2003). Besides these observations it was found that MEK1 and MEK2 are functionally redundant in the epidermis with loss of either protein showing no obvious phenotype (Scholl *et al*., 2007).

As an essential component of the MAPK pathway MEK1/2 is involved in fundamental cellular processes through activation of its only physiologically known substrate ERK1/2. MEK1/2 initially catalyzes the phosphorylation of Tyr204/187 in the ERK1/2 activation loops. After dissociation of tyrosine-phosphorylated ERK from the MEK enzyme and reassociation with the same or another active MEK, phosphorylation of the respective threonine residue (Thr202/185) takes place (Ferrell and Bhatt, 1997). Phosphorylation of either single residue is not sufficient to fully activate ERK1/2; indeed, ERK1/2 kinase activity requires phosphorylation of both tyrosyl and threonyl residues within the Thr-Xaa-Tyr motif (Anderson *et al*., 1990). MEK1 and MEK2 are both equally competent to phosphorylate ERK substrates and additionally, functions as cytoplasmatic anchors for ERKs (Fukuda *et al*., 1997b; Ohren *et al*., 2004; Rubinfeld *et al*., 1999). Moreover, MEKs were found to also play a role in the nuclear export of ERKs and other proteins (Adachi *et al*., 2000).

Several phosphorylation and dephosphorylation processes strictly regulate MEK1/2 activity (reviewed in Roskoski, 2012; Figure 1.5B). It is worth to mention that full catalytic activity of the human enzyme requires phosphorylation of two serin residues in the activation loop (Ser218 and Ser222 in MEK1; Ser222 and Ser226 in MEK2; Figure 1.5B) located within a Ser-Xaa-Ala-Xaa-Ser/Thr motif by upstream RAF kinases. The scaffolding protein kinase suppressor of RAS (KSR) promotes this stimulatory RAF phosphorylation of MEK (Brennan *et al*., 2011). Unlike other signaling molecules, MEK1 and MEK2 do not seem to be regulated by proteinase degradation or changes in transcription and translation levels (Bendetz-Nezer and Seger, 2005).

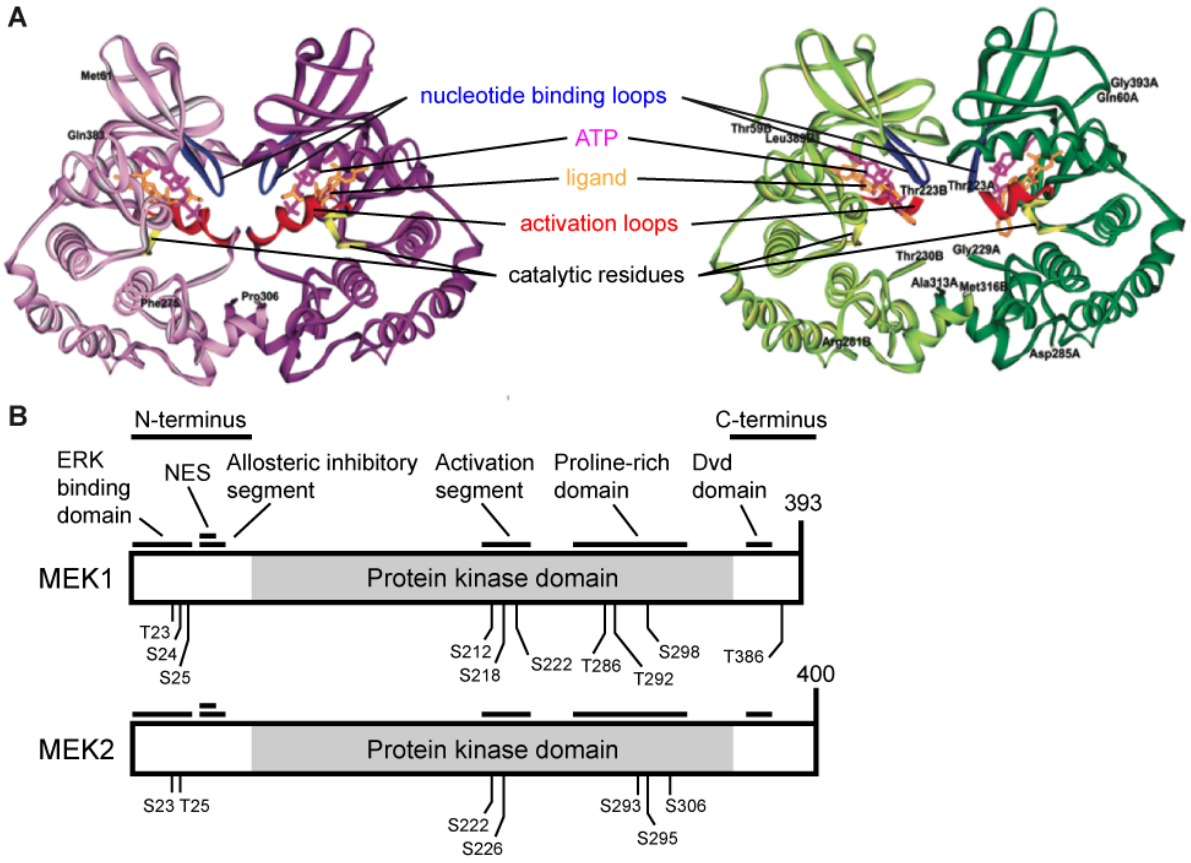

Figure 1.5 Structures of MEK1 and MEK2. (A) Ribbon-style representation comparing the MEK1 (different shades of purple) and MEK2 (different shades of green) homodimer structures. The nucleotide-binding loops are depicted in blue, the catalytic residues are gold, the activation loops are colored in red, ATP is pink, and the ligand is orange. (B) Schematic representation of human MAPKK1 (MEK1) and MAPKK2 (MEK2). MAPKKs in general are composed of a kinase catalytic domain flanked by N- and C-terminus extensions of varying length. The ERK1/2 binding site is located at the N-terminal region as well as the strong leucin-rich nuclear export signal (NES), which is an exclusive feature not found in other MAPKK family members and necessary for the cytosolic location and nuclear exclusion of MEK1/2 during signal transmission (Fukuda *et al*., 1997a). Essential phosphorylation sites for the regulation of MEK1/2 activity are also depicted, e.g. Ser298, which is phosphorylated by p21-activated kinase-1 (PAK1) for the enhanced association of MEK with ERK, and the negative-phosphorylation sites including Thr292, Thr286, Thr386, and Ser212 that are targeted by either ERK, CDK5, both ERK and CDK5, or a so far unknown protein kinase, respectively, for attenuation of MEK1/2 signaling (adapted from Ohren *et al*., 2004; Roskoski, 2012).

1.5.3 MEK1/2 signaling in pancreatic cancer and targeted chemotherapy

The MAPK pathway is usually constitutively activated not only in pancreatic cancer but also in a significant proportion of other human tumors via several mechanisms. The mutational landscape in PDAC involves almost universally gain-of-function mutations in the *KRAS2* proto-oncogene, mostly through a substitution of G12 (see also chapter 1.2.3). In several recent animal models it has been confirmed that not only KRAS mutations are an initiating step in pancreatic carcinogenesis, but also accompanied constitutive KRAS downstream signaling is crucial for both PDAC progression and maintenance (Eser *et al*., 2014; Parada

and Weinberg, 1983). EGFR overexpression is also reported in 50-70 % of human pancreatic tumors, with or without associated gene amplifications, leading to aberrant MEK-ERK signaling and a significant shorter survival of patients (Lee *et al*., 2007; Luo *et al*., 2011; Tobita *et al*., 2003; Ueda *et al*., 2004). Unlike in glioblastomas and lung cancer, *EGFR* mutations are uncommon in PDAC. Also no *HRAS*, *ARAF*, and *CRAF* mutations have so far been found in any pancreatic tumor, and *NRAS* and *BRAF* mutations were only infrequently (2 %) detected (Ishimura *et al*., 2003; Neuzillet *et al*., 2013). *MEK* mutations were identified with a low prevalence (~ 1 %) in carcinomas of the lung and the colon as well as in melanoma, but not in PDAC (Emery *et al*., 2009; Marks *et al*., 2008; Murugan *et al*., 2009). No mutation in the *MAPK3* and *MAPK1 g*enes, encoding ERK1 and ERK2, respectively, has been reported to date in any tumor entity, indicating that multiple upstream events are sufficient to drive inappropriate activation of MEK1/2 and their effector MAP kinases in cancer. The hyperactivated MEK-ERK signaling promotes basically the same cellular processes as it does in its normal biological function, especially cell survival and proliferation, thereby supporting the cellular transformation to a neoplastic phenotype. As a result, enforced cell proliferation, non-regulated tumor growth, and survival can be observed in PDAC.

Conventional chemotherapy has only limited effect in pancreatic cancer (Conroy *et al*., 2011; Moore *et al*., 2007; Von Hoff *et al*., 2013). Thus, targeted therapies might be a new treatment option and the MAPK pathway represents a good pool of new targets for therapeutic intervention. Efforts to pharmacologically target KRAS with farnesyl- and geranyl-transferase inhibitors interfering with the membrane-association and subcellular localization of this oncoprotein have failed so far in the clinic (Berndt *et al*., 2011). Recently, direct RAS binding small molecules have been discovered, challenging the perception that KRAS is an “undruggable” protein (reviewed by Zeitouni *et al*., 2016). However, none of these anti-RAS drugs has yet reached the clinic. Consequently, the development of downstream kinase inhibitors, such as RAF and MEK inhibitors, was reinforced. RAF inhibitors, e.g. vemurafenib and dabrafenib, have shown striking clinical results in *BRAF* mutated tumors like melanoma (Falchook *et al*., 2012; Flaherty *et al*., 2010). However, when these RAF inhibitors were used in RAS-mutant cancers, activation rather than inactivation of ERK was unexpectedly observed (Hatzivassiliou *et al*., 2010; Heidorn *et al*., 2010; Poulikakos *et al*., 2010). This is due to the propensity of these first-generation RAF inhibitors to induce RAF dimerization, which causes activation of CRAF (Samatar and Poulikakos, 2014). Furthermore, the facts that these agents exclusively target mutant B-RAF and that these mutations being infrequently observed in PDAC already exclude them as favorable new therapeutic options for pancreatic cancer patients. Therefore, MEK inhibitors remain one of the potential strategies for KRAS driven cancers, such as PDAC.

Given the pivotal position that MEK1/2 occupies within this signal transduction cascade, its narrow substrate specificity to only native ERK1/2 proteins and its unique hydrophobic pocket that allows for the interaction of selective allosteric inhibitors, targeting the MEK molecule has become an attractive approach of blocking the hyperactivated RAS-RAF-MEK-ERK pathway in different tumor entities. In 1995, the first synthetic small-molecule inhibitor of MEK1 and MEK2 kinase activity, PD98059, was discovered that however only served as valuable research tool to underpin the knowledge of ERK1/2 biology (Dudley *et al*., 1995). CI-1040 (PD 0184352; Pfizer) was then the first potent and selective allosteric MEK1/2 inhibitor to enter clinical oncology trials. A phase I study undertaken in 77 patients with advanced cancers demonstrated that this orally administered benzhydroxamate derivative was well tolerated at doses resulting in a median 73 % inhibition of pERK1/2 (range 43 % to 100 %) in tumor biopsies. Interestingly, one patient with pancreatic cancer achieved a partial response with significant symptomatic improvement in pain, anorexia, and fatigue that lasted 12 months (Lorusso *et al*., 2005). However, in a subsequent multitumor phase II study in non–small-cell lung, breast, colon and pancreatic cancers, CI-1040 did not provide sufficient antitumor activity to be taken forward (Rinehart *et al*., 2004). Two 2nd generation MEK1/2 inhibitors with an increased oral bioviability and greater potency have then been clinically developed: the CI-1040 analogue PD0325901 (Pfizer) and the benzimidazole derivative AZD6244 (Selumetinib, ARRY-142886; Array BioPharma/ AstraZeneca). For both small molecule inhibitors half-maximal inhibitory concentration (IC_{50}) values at nanomolar concentrations against purified MEK1 and MEK2 were reported as well as significant anti-tumor activity in several *in vitro* and *in vivo* models (Davies *et al*., 2007; Sebolt-Leopold and Herrera, 2004; Solit *et al*., 2006; Yeh *et al*., 2007). Although PD0325901 demonstrated preliminary evidence of clinical activity in a phase I study with melanoma patients, its further clinical development had to be stopped due to retinal vein occlusion and other associated neurotoxicities (LoRusso *et al*., 2010). AZD6244 is the most widely studied MEK1/2 inhibitor in both preclinical settings and in the clinic, but has shown only modest clinical activity as a single agent in all phase I and II solid tumor studies that was not superior over the clinical response of the standard-of-care (Adjei *et al*., 2008; Janne *et al*., 2013; Leijen *et al*., 2011). As a result of these studies, there has not been an advocacy for AZD6244 as a monotherapy. Besides AZD6244, hope for pancreatic cancer also lies on several other MEK1/2 inhibitors, namely GSK1120212 (trametinib), MSC1936369B (pimasertib), BAY 86-9766 (refametinib), and MEK162 (retrieved from clinicaltrials.gov on 01.04.2015) that are currently under investigation in preclinical and/or clinical studies. Of these, refametinib was developed recently by Ardea Biosciences/Bayer and the structural and pharmaceutical properties of this compound will be presented in the next chapter.

1.5.4 Refametinib - a novel MEK1/2 inhibitor for the treatment of cancer

BAY 86-9766/RDEA119 (referred to as refametinib hereafter) represents a substituted cyclopropane-sulfonamide with a molecular weight of 572 g/mol (Figure 1.6A). This orally available small molecule potently inhibits MEK1/2 activity (MEK1 IC_{50} = 19 nM; MEK2 IC_{50} = 47 nM) in a non-ATP-competitive manner through binding to an allosteric pocket adjacent to the Mg-ATP-binding site (Figure 1.6B). Complete suppression of ERK1/2 phosphorylation was not only demonstrated in human tumor cell lines of different tissue origin including A375 (melanoma), Colo205 (colon), MDA-MB-231 (breast) and Bx-Pc3 (pancreas), but also in multiple human tumor xenograft models. ERK1/2 inhibition was accompanied by a highly efficacious inhibition of cell proliferation *in vitro*, and a tumor growth inhibition *in vivo*. Furthermore, tumor regressions were seen in melanoma, colon, epidermal, and hepotacellular carcinoma xenografts (Iverson *et al*., 2009; Schmieder *et al*., 2013). The potent antitumor activity of refametinib in human orthotopic primary pancreatic cancer xenografts was then confirmed by Chang and colleagues (Chang *et al*., 2010). Additionally, Diep *et al*. showed that refametinib is also effective in combination with erlotinib in a subset of pancreatic cancer cells and xenografts harboring wild-type KRAS (Diep *et al*., 2011).

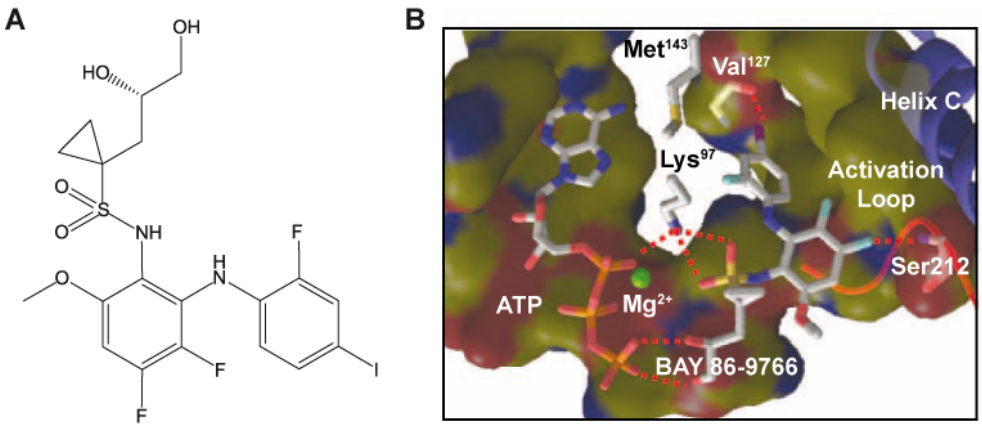

Figure 1.6 Structure of refametinib and its non-ATP-competitive binding to MEK1/2. (A) Chemical structure of (S)-N-(3,4-difluoro-2-(2-fluoro-4-iodophenylamino)-6-methoxyphenyl)-1-(2,3-dihydroxypropyl) cyclopropane-1-sulfonamide (refametinib). (B) Ternary complex of human MEK1 bound to ATP and refametinib. Refametinib interacts extensively with ATP, the activation loop and other surrounding protein residues (i.e. Lys^{97}, Met^{143}, and Ser^{212}) through hydrogen bonding and hydrophobic interactions (red dashed lines). Atoms are colored according to type: carbon in gray, oxygen in red, nitrogen in blue, sulfur in yellow, fluorine in light blue, and iodine in purple (adapted from Iverson *et al*., 2009).

Due to its good selectivity, high potency, and favorable pharmacokinetic profile, refametinib has been selected for clinical development and is now undergoing several phase I and II clinical studies in late-stage cancer patients refractory or intolerant to other anticancer

therapies including one study that evaluates refametinib in combination with gemcitabine in patients with locally advanced inoperable or metastatic pancreatic cancer (retrieved from clinicaltrials.gov on 01.04.2015).

1.6 Aims and significance of this study

The overall goal of this thesis was the preclinical evaluation of the selective MEK1/2 inhibitor refametinib in genetically engineered mouse models (GEMMs) of PDAC as a potential therapeutic strategy for this otherwise fatal disease.

To achieve this goal the following aims were addressed during the present study:

(1) Validation of the ERK1 and ERK2 kinases as a therapeutic target for PDAC.

(2) Evaluation of tumor progression and *in vivo* response to refametinib in comparison to the standard-of-care combination therapy gemcitabine plus erlotinib in a GEMM of pancreatic cancer.

(3) Investigation of the underlying molecular mechanisms upon MEK1/2 inhibition.

As MEK1/2 and its only physiologically known downstream target ERK1/2 have been acknowledged as important players in driving pancreatic tumor development, the results of this thesis will not only contribute to a better understanding of pharmacological intervention of the MAPK pathway in limiting PDAC progression, but also be of benefit for further enhancing existing treatment strategies targeting this colossal signaling network.

2. Materials and Methods

2.1 Animal experiments

2.1.1 Mouse strains

For preclinical studies modern genetically engineered mouse models (GEMMs) were used that are based on the *Cre/loxP*-technology to activate or inactivate genes in a tissue-specific manner. Mice were maintained on a mixed Sv129/C57BL6J background. The following genotypes and abbreviations were applied:

Ptf1a$^{+/Cre}$;*Kras*$^{+/LSL\text{-}G12D}$ *Kras*^{G12D}

Ptf1a$^{+/Cre}$;*Kras*$^{+/LSL\text{-}G12D}$;*Trp53*$^{fl/fl}$ *Kras*^{G12D};*p53*$^{\Delta/\Delta}$.

Littermates without *Ptf1a*$^{+/Cre}$ expression served as wild-type (WT) controls.

All animal experiments were conducted in accordance with the European guidelines for the care and use of laboratory animals as well as the German Federal Animal Protection Laws and approved by the Institutional Animal Care and Use Committees (IACUC) of Technische Universität München and Regierung von Oberbayern.

2.1.1.1 *Ptf1a*$^{+/Cre}$

Dr. H. Nakhai generated this *knock-in* mouse strain in our laboratory (Klinikum rechts der Isar, Munich) by targeting one allele of the *pancreas specific transcription factor 1a* (*Ptf1a*, also known as *Ptf1a-p48)* gene with a vector replacing part of exon 1 with the Cre recombinase (Nakhai *et al.*, 2007).

2.1.1.2 *Kras*$^{+/LSL\text{-}G12D}$

This *knock-in* mouse strain was first generated by Erica L. Jackson (Jackson *et al*., 2001) and kindly provided by Prof. T. Jacks (Massachusetts Institute of Technology, Cambridge, Massachusetts, USA). In *Kras*$^{+/LSL\text{-}G12D}$ mice, one endogenous *Kras* allele is replaced with a construct engineered to contain a glycine (G) to aspartate (D) transition in codon 12 of

exon 1 (Hingorani *et al*., 2003). Silencing of the mutated construct results from an upstream STOP cassette flanked by functional *loxP* sites (*LoxP-Stop-LoxP (LSL)* sequence). Thus, the constitutively active $KRAS^{G12D}$ is only expressed in cells when Cre recombinase has excised the STOP cassette. This system mimics the acquisition of activating point mutations in human malignancies.

2.1.1.3 $p53^{\Delta/\Delta}$

This *knock-in* mouse strain was generated by Silvia Marino (Marino *et al*., 2000) and kindly provided by Prof. T. Jacks (Massachusetts Institute of Technology, Cambridge, Massachusetts, USA). Exons 2-10 of the tumorsuppressor gene *TP53* are flanked by functional *loxP* sites leading to engineered null mutations within the gene after excision by Cre recombinase (Marino *et al*., 2000).

2.1.2 *In vivo* treatment of $Kras^{G12D};p53^{\Delta/\Delta}$ mice

Different treatment protocols for drug efficacy studies were established and $Kras^{G12D};p53^{\Delta/\Delta}$ mice treated accordingly:

- five consecutive days a week (two day break) with refametinib (25 mg/kg bodyweight;) by oral gavage.
- daily with erlotinib (50 mg/kg bodyweight) by oral gavage.
- daily with erlotinib (50 mg/kg bodyweight) by oral gavage plus four intraperitoneal (i.p.) injections of 100 mg/kg gemcitabine every third day.
- five consecutive days a week (two day break) with refametinib (25 mg/kg bodyweight;) by oral gavage plus i.p. injections of 2 mg/kg rapamycin two days a week
- five consecutive days a week (two day break) with refametinib (25 mg/kg bodyweight;) by oral gavage for one or two weeks followed by i.p. injections of 2 mg/kg rapamycin two days a week.

Refametinib (kindly provided by Bayer Schering) was diluted in a 30 % HP-ß-CD-Form1 solution. Erlotinib (Tarceva, Roche) was dissolved in 0.5 % methylcellulose and 0.9 % NaCl. Gemcitabine (kindly provided by Klinikum rechts der Isar, Munich) was received as a 38 mg/ml solution and was further diluted with 0.9 % NaCl before treatment. Rapamycin (Calbiochem, 553210) was prepared as described by Sarbassov and colleagues (Sarbassov *et al*., 2006): 10 mg of rapamycin were dissolved in 200 µl of absolute ethanol,

which was then further diluted with Ringer's saline solution to a final concentration of 1 mg/ml directly before use. Oral gavage was performed with a 22 Gauge feeding needle (straight, 25 mm). For all *in vivo* studies, the body weight of enrolled mice was monitored five days a week during therapy to exclude drug intolerance, and weekly non-invasive MRI (see chapter 2.1.3) was performed to track tumor progression. T2-weighted images (viewed with the OsiriX DICOM Software 3.9.1) were used to measure tumor growth.

2.1.3 Magnetic resonance imaging (MRI)

Imaging of endogenous tumors was performed by non-invasive, T2-weighted MRI on a clinical MRI device (Achieva 1.5 T, Philips Medical Systems, Best, The Netherlands) from four weeks of age onwards. Mice were anesthetized by continuous gaseous infusion of isoflurane (2 % per liter O_2, Abbott, 05260-05) for at least 10 minutes prior to scanning using a veterinary anesthesia System (Vetland Medical Sales and Services). These inhalation anesthetics are better-tolerated than injectable anesthetics (Cook *et al*., 2008). Following anesthesia, animals were placed in prone position on top of a 47-mm microscopy surface coil, which is attached to the divan bed of the MRI scanner. An axial multi-slice T2-weighted turbo spin-echo (TSE) sequence (resolution 0.3 × 0.3 × 0.7 mm^3, minimum 25 slices, TE = 90 milliseconds, TR > 3 seconds) covering the complete mouse abdomen was applied for tumor detection and tumor volume quantification (Heid *et al*., 2017). During the scan, anesthesia was maintained by a gaseous infusion of isoflurane at 2 % using a respiratory mask. Additionally, mice were warmed with a pair of gloves containing hot water to prevent a decline in body temperature, and eye ointment (Bepanthen® Augen- und Nasensalbe, Bayer Vital GmbH) was applied to prevent drying-out of the cornea. After completing the examination, mice were placed back in their appropriate cage and warmed with an infrared heat lamp until they returned to normal social behavior. Upon detection of solid tumors with a minimum size of 5 mm^3 in diameter, mice were enrolled into the intervention studies and monitored by MRI, weekly.

2.1.4 Mouse necropsy and sampling process

Kras^{G12D};*p53*$^{\Delta/\Delta}$ mice were euthanized with isoflurane either at indicated time points (after 4, 7, 12 and 24 hours, 5 days or 2 weeks of vehicle or refametinib treatment) or upon tumor development and notable symptoms of disease, such as raising of hackles, abnormal posture, cachexia, dehydration, and changed social behavior. Blood was taken directly from the heart without opening the thorax and centrifuged at 10,000 rpm for five minutes. Serum was transferred to an Eppendorf reaction tube and frozen at -20 °C. After opening

the thorax, pieces of two different pancreas regions were resected for both RNA extraction (see chapter 2.3.4) and protein isolation (see chapter 2.4.1), snap frozen in liquid nitrogen and stored at -80 °C for further processing. Additionally, the lung and all four liver lobes (typical sites of metastasis for PDAC) as well as the duodenum, spleen, kidneys, and sometimes even the brain were resected.

2.2 Histological analyses

2.2.1 Production of formalin-fixed, paraffin-embedded (FFPE) sections

All resected mouse organs were fixed in 4 % formaldehyde (16 % solution purchased from Electron Microscopy Sciences, 15710; diluted in phosphate buffered saline (PBS, Biochrom AG, L182-50)) for 24 hours and then dehydrated, cleared and infiltrated with paraffin in a Leica S300 tissue processing unit. Finally, all organs were embedded in melted paraffin wax and cooled at a 4 °C cooling plate until the paraffin wax was completely solidified. The formalin-fixed, paraffin-embedded (FFPE) blocks were stored at room temperature. For further histological analyses, sectioning of FFPE-blocks on a microtome (Leica) was performed. 3 µm sections were transferred to a 50 °C water bath for stretching and collected on microscopic glass slides (Thermo scientific, 631-9483). For subsequent staining, the slides were allowed to completely dry overnight.

2.2.2 Hematoxylin and eosin (H&E) staining

FFPE tumor sections of vehicle or refametinib treated *Kras*^{G12D}*;p53*$^{\Delta/\Delta}$ mice were first deparaffinized in two changes xylol (Roti®-Histol, Roth, 6640.4) for five minutes and rehydrated with three times one minute absolute ethanol followed by a short washing step with double distilled water (ddH_2O). Then, a 5-minute staining with Mayer's hemalum solution (Merck, 1.09249.2500) was performed to visualize acidic compounds, e.g. chromatin within the nuclei, in a deep purplish-blue color followed by short rinsing in ddH_2O (three times), in ammonia water, in ddH_2O, in HCl water, in tap water, in ammonia water, in ddH_2O and 70 % ethanol. Afterwards, sections were counterstained with eosin (Chroma, 2C-140; diluted 1:5 in 96 % ethanol) for two minutes to label basophilic structures like the cytoplasm including connective tissue and collagen as well as other extracellular substances in pink, dehydrated in three times absolute ethanol followed by two times xylol for one minute each and finally, mounted with pertex® (Medite, 41-4010-00) and covered with cover slides. After appropriate staining, slides were evaluated under a light microscope

(Axio Imager A1, Zeiss) using the AxioVision Software 4.8.1 (Zeiss). The histopathological examination of H&E stained tumor sections was kindly performed by Prof. Bence Sipos M.D., a pathologist at University Hospital Tübingen with expertise in human and mouse PDAC pathology.

2.2.3 Immunohistochemical staining (IHC)

FFPE tumor sections of vehicle or refametinib treated *Kras^{G12D};p53$^{\Delta/\Delta}$* mice were first deparaffinized with xylol (Roti®-Histol) and rehydrated through a graded series of ethanol (100 % EtOH, 96 % EtOH and 70 % EtOH two times three minutes each) followed by a two times 5-minute washing step with ddH_2O. Then, slides were placed in a black plastic jar containing the citrate-based antigen unmasking solution (Vector, H-3300, pH 6.0) and boiled in a microwave (350 W) for 15 minutes. After the antigen retrieval, endogenous peroxidase quenching was performed in the dark using aqueous 3 % hydrogen peroxide. Then, sections were washed (two times five minutes in ddH_2O, five minutes in PBS, five minutes in PBS-Triton (0.1 %)) and blocked for one hour with 5 % goat serum (Sigma, G9023) in PBS-Tween (0.025 %) in a humidity chamber followed by an overnight incubation with the appropriate primary antibody diluted in SignalStain® Antibody Diluent (Cell Signaling, #8112). All primary antibodies are listed in table 2.1. After rinsing five minutes in PBS, two times five minutes in PBS-Triton (0.1 %) and a one-hour-incubation with the appropriate secondary biotinylated antibody (see table 2.2) diluted in PBS-Triton (0.1 %), sections were stained with ABC (Vector, PK-6100) for 30 minutes at room temperature followed by the DAB brown stain (Vector, SK-4100). Finally, sections were counterstained with hematoxylin solution modified acc. to Gill III (Merck, 1.05174.2500), rinsed in tap water for 10 minutes, dehydrated with an ascending series of ethanol (70 % EtOH, 96 % EtOH and 100 % EtOH two times one minute each) followed by two times xylol for two to three minutes each and mounted with pertex®. After appropriate staining, slides were also evaluated under the Axio Imager A1 light microscope using the AxioVision Software 4.8.1.

Table 2.1 Primary antibodies for IHC.

Antigen	Species	Dilution	Company
E-Cadherin	mouse	1:100	BD Transduction Laboratories (610920)
P-p44/42 MAPK (Thr202/Tyr204)	rabbit	1:100	Cell Signaling (#4376)

Table 2.2 Secondary biotinylated goat antibodies for IHC.

Species	Dilution	Company
rabbit	1:500	Vector (BA-1000)
mouse	1:500	Vector (BA-9200)

2.2.4 TUNEL staining

For staining apoptotic cells with TUNEL (TdT-mediated dUTP-biotin nick end labeling), the In Situ Cell Death Detection Kit, Fluorescein (Roche, 11684795910) was used according to manufacturers protocol. Briefly, FFPE tumor sections of *Kras*^{G12D};*p53*$^{\Delta/\Delta}$ mice treated with vehicle or refametinib for 4, 7 and 24 hours were deparaffinized, rehydrated and washed as described in the procedure for immunohistochemical staining. After the antigen retrieval, sections were washed two times five minutes with PBS and labeled with 50 µl of TUNEL reaction mixture (containing the label solution and enzyme solution) for one hour at 37 °C in a dark humidified atmosphere. Samples serving as positive control were pre-treated with DNase I (Macherey-Nagel, 740963) for 10 minutes to induce DNA strand breaks prior to the labeling procedure. Negative control samples were incubated with the label solution only. Finally, sections were rinsed three times five minutes in PBS, mounted with Fluoromount™ Aqueous Mounting Medium (Sigma, F4680) and directly analyzed under an inverted fluorescence microscope (Axiovert 200M, Zeiss) with the AxioVision Software 4.8.1.

2.3 RNA/DNA analyses

2.3.1 Genotyping of transgenic mice

All offspring were genotyped between three and four weeks of age by polymerase chain reaction (PCR) from genomic DNA isolated from mouse tail clips using the tail and tissue lysis buffer from Peqlab (DirectPCR-Tail, 31-102-T) plus adding 5 % Proteinase K (Roche, 03115887001). Tails were incubated overnight at 56 °C and then, the enzyme was inactivated at 85 °C for 45 minutes. 1 µl of genomic DNA served as template for PCR, which was performed with primers specific for *Ptf1a*$^{+/Cre}$, *Kras*$^{+/LSL\text{-}G12D}$ and *Trp53fl/fl* (see table 2.3) using the REDTaq® ReadyMix (Sigma, R2523). The following PCR conditions were applied: 95 °C for 5 minutes, 35 cycles of 95 °C for 30 seconds, 58 °C for 30 seconds and 72 °C for 1 minute, 72 °C for 10 minutes. Genotyping results were visualized on 2 % agarose gels.

Table 2.3 Genotyping primer sequences (5'-3'; final concentration 10 pM) and indicated band sizes.

Name	Sequences (5'-3')	Band sizes (WT / Lox)
Ptf1a$^{+/Cre}$	ACCAGCCAGCTATCAACTCG / TTACATTGGTCCAGCCACC / CTAGGCCACAGAATTGAAAGATCT / GTAGGTGGAAATTCTAGCATCATCC	324 bp / 199 bp
Kras$^{+/LSL-G12D}$	CACCAGCTTCGGCTTCCTATT / AGCTAATGGCTCTCAAAGGAATGTA / CCATGGCTTGAGTAAGTCTGC	300 bp / 200 bp
Trp53$^{fl/fl}$	CACAAAAACAGGTTAAACCCA / AGCACATAGGAGGCAGAGAC	250 bp / 350 bp

2.3.2 DNA isolation from cultured cells

DNA isolation from cultured cells was performed using the DNeasy® Blood&Tissue Kit (Qiagen) as described by the manufacturer. Afterwards, DNA quality and yield was measured in a spectrophotometer (NanoDrop 2000, Thermo Scientific) at a 260 nm wavelength. In addition, a measurement at a 280 nm wavelength was performed to determine contaminations with proteins, phenols and other aromatic compounds.

2.3.3 *Kras* deleted PCR (loss of heterozygosity (LOH)-PCR)

This PCR detects single *loxP* sites left after removal of the floxed STOP cassette by Cre recombinase. The primers (forward: GGGTAGGTGTTGGGATAGCTG; reverse: TCCGAATTCAGTGACTACAGATGTACAGAG) are specific for intron 1 of the *Kras* gene as well as for the original targeting vector and wild-type Kras (serving as a control). Due to the GC rich nature of the *Kras* gene, the PCR reaction was performed using the Advantage®-GC cDNA PCR Kit (Clontech) according to the manufacturers protocol. 1 µl DNA isolated from cultured cells (see chapter 2.3.2) was used in the PCR mix. The PCR conditions yielding expected PCR products of 285 bp for WT *Kras* and 315 bp for the removed STOP cassette were as follows: 98 °C for 5 minutes, 35 cycles of 98 °C for 30 seconds, 58 °C for 30 seconds and 72 °C for 30 seconds, 72 °C for 10 minutes.

2.3.4 RNA extraction

Cells cultured on a 10 cm cell culture dish were first washed two times with ice cold PBS, then scratched in RA1-buffer (Macherey-Nagel) containing 1 % β-mercaptoethanol and finally, snap frozen in liquid nitrogen. Freshly resected pieces of mouse pancreata were immediately homogenized in RA1-buffer containing 1 % β-mercaptoethanol with an electrical tissue homogenizer (SilentCrusher M, Heidolph Instruments) and also snap frozen in liquid nitrogen.

Total RNA was isolated with the Maxwell® 16 LEV simplyRNA Tissue Kit (Promega) according to the manufacturer's instruction using the Maxwell® 16 machine (Promega). Afterwards, RNA yield was measured in a spectrophotometer (NanoDrop 2000, Thermo Scientific) at a 260 nm wavelength and RNA quality was determined on a 1 % agarose gel.

2.3.5 cDNA synthesis and quantitative real-time-PCR (qRT-PCR)

2 µg of total RNA was reverse transcribed with the SuperScript™ II (SS II, Invitrogen) and Oligo(dT)$_{12-18}$ primer in a total volume of 20 µl for two hours at 42 °C. SS II was inactivated by heating at 70 °C for 15 minutes. Then, cDNA was either diluted tenfold (for the following genes: *Kras*, *Hras*, *Nras*) or twofold (all other genes), and 4 µl were used for each 20 µl PCR using the SYBR GREEN PCR Master Mix (Roche). The Taqman primers were designed using Primer 3 Software (version 0.4.0) and first, efficacy of each primer was determined in a test run. Only primers with an efficacy of at least 80 % were used for further gene expression analysis. Moreover, product specificity was controlled with a 2 % agarose gel. All primer sequences are listed in table 2.4. Real-time PCR was performed in a LightCycler®480 device (Roche). The PCR conditions for all genes were as follows: 95 °C for 5 minutes preincubation, 45 amplification cycles of 95 °C for 20 seconds, 55 °C for 20 seconds and 72 °C for 20 seconds, melting curve analysis 95 °C for 5 seconds and 65 °C for 1 minute, cooling at 37 °C for 30 seconds. For each gene, qRT-PCR was performed in triplicates in three independent experiments using two different batches of total RNA. The *Cyclophilin* and *Gapdh* gene served as an RNA input control. Relative gene expression levels were calculated on the basis of both the standard curve method and the delta-delta-CT method using the following formula: $2^{-[\text{DeltaCT(target gene)} - \text{DeltaCT(Cyclophilin or Gapdh)}]}$.

Table 2.4 Mouse specific primer sequences (5'-3'; final concentration 0.5 µM) used for qRT-PCR.

Name	Sequences (forward / reverse)
mCyclophilin	ATGGTCAACCCCACCGTGT / TTCTGCTGTCTTTGGAACTTTGTC
mE-Cadherin	AGGTTTTCGGGCACCACTTA / TGATGTTGCTGTCCCCAAGT
mGapdh	ATGTTCCAGTATGACTCCACTCACG / GAAGACACCAGTAGACTCCACGACA
mHras	GACACAGCAGGTCAAGAAGA / TGATCTGCTCCCTGTACTGA
mKras	GCGCCTTGACGATACAGCTAA / CCTGCTGTGTCGAGAATATCCA
mN-Cadherin	CATCAACCGGCTTAATGGTG / ACTTTCACACGCAGGA TGGA
mNras	CAGTACATGAGGACAGGCGAAG / CACACGCTTAATTTGCTCCCT
mSnail	AAGATGCACATCCGAAGC / GAGAATGGCTTCTCACCAGT
mVimentin	AGCACCCTGCAGTCATTCAGA / GATTCCACTTTCCGTTCAAGGT

2.3.6 qRT-PCR for *Kras* amplification

qRT-PCR of isolated DNA (see chapter 2.3.2) to test for *Kras* amplification was kindly performed in cooperation with the laboratory of PD Dr. Malte Buchholz in Marburg using SYBR Green MasterMix (Applied Biosystems) and specific primer pairs for *Kras* and *Rplp0* (listed in table 2.5) designed with the PrimerExpresss program (Applied Biosystems). Relative abundance of target sequences was calculated with the delta-delta-CT method using the signal for ribosomal protein, large, P0 (RPLP0) as internal reference: $2^{-[\mathrm{DeltaCT}(Kras) - \mathrm{DeltaCT}(Rplp0)]}$.

Table 2.5 Mouse specific primer sequences (5'-3') used for *Kras* amplification qRT-PCR.

Name	Sequences (forward / reverse)
mRplp0	TGG GCAAGAACACCATGATG / AGTTTCTCCAGAGCTGGGTTGT
mKras	TTGGCCAGGAGTGCATTAAGA / GGCAAGCACCTTGGGAGAA

2.4 Protein biochemistry

2.4.1 Isolation of protein from cells or tissue

Cells grown on a 10 cm cell culture dish to approximately 90 % confluency were harvested by removing the medium, two times washing with ice cold PBS and scratching in 1 ml PBS supplemented with a phosphatase inhibitor cocktail (PhosSTOP Phosphatase Inhibitor Cocktail Tablets, Roche, 04906837001). Cell pellets were collected by centrifuging at 4 °C for 10 minutes at 13,200 rpm and removing the supernatant. For cell lysis, cell pellets were resuspended in 200 µl of RIPA lysis buffer (50 mM Tris HCl pH 8.0, 150 mM NaCl, 1 % NP-40, 0.5 % Sodium deoxycholate, 0.1 % SDS) containing the phosphatase inhibitor cocktail as well as protease inhibitors (cOmplete Protease Inhibitor Cocktail Tablets, Roche, 04693124001).

Resected pieces of mouse pancreata (see chapter 2.1.5) were thawed in non-denaturating lysis buffer (NDLB, 20 mM Tris HCl pH 8.0, 137 mM NaCl, 10 % Glycerol, 1 % NP-40, 2 mM EDTA pH 8.0) containing protease and phosphatase inhibitors and were immediately homogenized with the electrical tissue homogenizer SilentCrusher M (Heidolph Instruments).

After an incubation period of 30 minutes on ice, both types of lysates were sonicated for 30 seconds (Sonopuls, Bandelin) to obtain nuclear extracts and centrifuged at 4 °C for 10 minutes at 13,200 rpm. Supernatants were transferred to new Eppendorf reaction tubes and stored at -80 °C.

2.4.2 Protein quantitation

Protein concentrations of tissue or cell lysates were determined using the Pierce™ BCA Protein Assay Kit (Thermo Scientific) based on bicinchoninic acid (BCA) with included albumin standard as described by the manufacturer. The absorbance is nearly linear with increasing protein concentrations and was measured with a microtiter plate reader (Thermo Scientific Multiskan FC) at a 570 nm wavelength.

2.4.3 SDS polyacrylamide gel electrophoresis (SDS PAGE) and Western blot analysis

60 µg of protein lysate were supplemented with 5x Laemmli buffer (10 % SDS, 300 mM Tris, 0.05 % bromphenol blue, 50 % glycerol and 5 % ß-mercaptoethanol; pH 6.8) and denatured at 95 °C for five minutes. Protein separation was performed on an appropriate SDS polyacrylamide gel (either 8 %, 10 %, 12 % or 15 %, depending on the size of detected proteins) in a Mini-PROTEAN® Tetra Cell Gel System chamber (Bio-Rad) filled with 1x SDS running buffer at 40-80 mA.

Resolving gel (10 ml, 8 %)	
H_2O	4.6 ml
30 % acrylamide mix	2.7 ml
1.5 M Tris (pH 8.8)	2.5 ml
10 % SDS	100 µl
10 % ammonium persulfate	100 µl
TEMED	6 µl

Resolving gel (10 ml, 10 %)
4.0 ml
3.3 ml
2.5 ml
100 µl
100 µl
4 µl

Resolving gel (10 ml, 12 %)	
H_2O	3.3 ml
30 % acrylamide mix	4.0 ml
1.5 M Tris (pH 8.8)	2.5 ml
10 % SDS	100 µl
10 % ammonium persulfate	100 µl
TEMED	6 µl

Resolving gel (10 ml, 15 %)
2.3 ml
5.0 ml
2.5 ml
100 µl
100 µl
4 µl

Stacking gel (10 ml, 5 %)	
H_2O	6.8 ml
30 % acrylamide mix	1.7 ml
1.0 M Tris (pH 6.8)	1.25 ml
10 % SDS	100 µl
10 % ammonium persulfate	100 µl
TEMED	10 µl

10x SDS running buffer
250 mM Tris, 1.92 M glycin and 0.1 % SDS

For transfer of separated proteins to a methanol-activated PDVF membrane (Immobilon-P with a 0.45 µm pore size, Millipore, IPVH00010), the Western blot sandwich was built up as follows: sponge, two Whatman filter papers, membrane, gel, two Whatman filter papers, sponge and subsequently placed into a Mini Trans-Blot® Cell blotting chamber (Bio-Rad) filled with 1x transfer buffer. Then, protein transfer was conducted at 150 mA/gel for one hour up to 2.5 hours (depending on the protein size) in a 4 °C cold storage room.

10x transfer buffer for wet transfer
1,918 M glycin, 1 M Tris HCl pH 8.0

1x transfer buffer for wet transfer
100 ml 10x transfer buffer, 200 ml methanol, 700 ml ddH2O

After western blot transfer, membranes were incubated first with 5 % milk in Tris buffered saline-Tween® 20 (TBS-T) for up to one hour to block unspecific antibody binding sites followed by an overnight incubation with the respective primary antibody diluted in 5 % BSA/TBS-T at 4 °C. All primary antibodies are listed in table 2.6.
To remove unattached antibody, membranes were washed (two times one minute and four times five minutes with TBS-T) and then, incubated with the appropriate horseradish peroxidase (HRP) linked secondary antibody (see table 2.7) diluted in blocking solution for one hour at room temperature. After additional washing steps (two times one minute and four times five minutes with TBS-T, five minutes with TBS), signal detection was performed using either the Amersham ECL Western Blotting Detection Reagent (GE Healthcare, RPN2106) or the Super Signal® West Femto Chemiluminescent Substrate (Thermo Scientific, 34095) for detection of relative low protein amounts combined with high performance chemiluminescence films (GE Healthcare, 28906836).

10x TBS
1,37 M NaCl
260 mM Tris HCl pH 7.6

10x TBS-T
1,37 M NaCl
260 mM Tris HCl pH 7.6
1 % (v/v) Tween® 20 (Roth, 9127.1)

To control accurate loading, membranes were stripped with the Restore™ PLUS Western Blot Stripping Buffer (Thermo Scientific, 46430), afterwards washed (two times one minute and four times five minutes with TBS-T) and again blocked with 5 % milk in TBS-T for up to one hour before overnight incubation with the primary antibody for loading control at 4 °C.

Table 2.6 Primary antibodies for Western blot analysis.

Antigen	Species	Dilution	Company
ß-Actin	mouse	1: 20.000	Sigma (A1978)
AKT1/2	goat	1:200	Santa Cruz (sc-1619)
Bim	rabbit	1:1000	Cell Signaling (#2933)
Cleaved Caspase-3	rabbit	1:500	Cell Signaling (#9661)
Cleaved Caspase-3	rabbit	1:500	Cell Signaling (#9664)
Cleaved PARP	rabbit	1:500	Cell Signaling (#9544)
E-Cadherin	rabbit	1:1000	Cell Signaling (#3195)
N-Cadherin	mouse	1:1000	BD Transduction Laboratories (610181)
ErbB-3/HER-3	mouse	1:1000	Millipore (05-1131)
EGFR	rabbit	1:500	Millipore (06-847)
ERK1	rabbit	1:1000	Santa Cruz (sc-93)
ERK2	rabbit	1:1000	Santa Cruz (sc-154)
GSK-3ß	rabbit	1:1000	Cell Signaling (#9315)
HSP 90 α/β	rabbit	1:500	Santa Cruz (sc-7947)
IGF-1Rß	rabbit	1:500	Cell Signaling (#9750)
IRß	rabbit	1:500	Cell Signaling (#3025)
PCNA	mouse	1:1000	Santa Cruz (sc-56)
P-4E-BP1 (Thr37/46)	rabbit	1:500	Cell Signaling (#2855)
P-AKT (Ser473)	rabbit	1:500	Cell Signaling (#3787)
P-AKT (Thr308)	rabbit	1:500	Cell Signaling (#2965)
P-EGFR (Tyr845)	rabbit	1:500	Cell Signaling (#6963)
P-EGFR (Tyr1068)	rabbit	1:500	Cell Signaling (#3777)
P-GSK-3ß (Ser9)	rabbit	1:500	Cell Signaling (#9336)
P-IGF-1Rß (Tyr1135/1136)/IRß (Tyr1150/1151)	rabbit	1:500	Cell Signaling (#3024)
P-p44/42 MAPK (Thr202/Tyr204)	mouse	1:500	Cell Signaling (#9106)
P-p70 S6 Kinase (Thr389)	rabbit	1:500	Cell Signaling (#9234)
P-S6 Ribosomal Protein (Ser235/236)	rabbit	1:1000	Cell Signaling (#2211)
PTEN	rabbit	1:1000	Cell Signaling (#9559)
p70 S6 Kinase	rabbit	1:500	Cell Signaling (#2708)
Ras	rabbit	1:1000	Epitomics (#1819-1)
Snail	mouse	1:500	Cell Signaling (#3895)
S6 Ribosomal Protein	rabbit	1:1000	Cell Signaling (#2217)
Twist	mouse	1:200	Abcam (ab50887)
Vimentin	mouse	1:500	DakoCytomation (M7020)

Table 2.7 Secondary HRP linked antibodies for Western blot analysis.

Species	Dilution	Company
donkey anti-rabbit	1:8000	GE Healthcare (NA934V)
sheep anti-mouse	1:8000	GE Healthcare (NA931V)
donkey anti-goat	1:8000	Santa Cruz (sc-2020)

2.4.4 Ras activation assay

To determine the amount of active, GTP-bound Ras in a protein cell lysates, GTP-Ras pull-down assay was performed using the Ras Activation Assay Kit (Upstate) as described by the manufacturer. 500 µg protein lysate in Magnesium-containing lysis buffer (MLB, included in the Kit, plus phosphatase and protease inhibitor cocktail was added) were incubated with 10 µl Raf-1 agarose beads, which contain the Ras binding domain (RBD) that specifically binds and precipitate only the GTP-bound Ras in the lysate but not the GDP-bound. After 45 minutes of incubation at 4 °C, beads were collected by centrifuging at 4 °C full speed for 10 seconds and washed three times with MLB to remove unbound protein. Then, agarose beads were resuspended in 5x Laemmli buffer, boiled at 95 °C for five minutes followed by separation with SDS PAGE on a 15 % polyacrylamide gel and detection with standard Western blot analysis (see chapter 2.4.3). For loading control of total Ras amount, a second 15 % polyacrylamide gel was run with 50 µg total protein lysate.

2.5 Cell Culture and drug *in vitro* studies

2.5.1 Isolation and cultivation of primary tumor cell lines from murine PDACs

To isolate and culture primary mouse pancreatic tumor cell lines, small firm pieces of PDACs from *Kras*^{G12D} and *Kras*^{G12D};*p53*$^{\Delta/\Delta}$ mice were immediately resected after sacrificing mice with lethal tumor burden (see chapter 2.1.5) and shortly stored on ice until they were cut into very small fractions on a 10 cm cell culture dish under sterile conditions. Then, cell culture medium was added (Dulbecco's Modified Eagle Medium (DMEM) supplemented with 10 % FCS, 1 % non-essential amino acids and 1 % penicillin/streptomycin, all Gibco®) and cells were incubated at 37 °C in a humidified atmosphere containing 5 % CO_2. After attachment of tumor cells on the plate, medium was changed every two to three days. At a confluence of 90 %, cells were passaged at least three times to ensure no contamination with fibroblasts and then used for further experiments.

2.5.2 Cultivation of adherent human pancreatic tumor cell lines

Human pancreatic cell lines (AsPc1 and DanG were kindly provided by Dieter Sauer, Klinikum rechts der Isar, Munich; all other cell lines were kindly provided by Günther Schneider and Christoph Michalski, Klinikum rechts der Isar, Munich) were propagated in

RPMI medium containing 10 % FCS, 1 % non-essential amino acids and 1 % penicillin/streptomycin (all Gibco®) and incubated at 37 °C in a humidified atmosphere containing 5 % CO_2. Reaching a confluence of 90 %, cells were detached from the bottom of the cell culture flask using 0.05 % Trypsin EDTA (Gibco®) and either reseeded for further cultivation or used for experiments.

2.5.3 Drug *in vitro* studies

The following drugs were studied: refametinib (kindly provided by Bayer Schering), BKM120 (Selleckchem, S2247), BX-912 (Selleckchem, S1275), gemcitabine (kindly provided by Klinikum rechts der Isar), rapamycin (Calbiochem, 553210) and salinomycin (Sigma, S4526). All drugs were dissolved in 100 % dimethylsulfoxide (DMSO, Sigma, D5879) and then further diluted in the appropriate cell culture media for experiments. In all experiments control cells were incubated with DMSO alone. The final DMSO concentration was maintained at 0.1 % without effecting cell viability.

2.5.4 Cytotoxicity Assay

For cell viability analysis, the optimal cell number for each cell line was determined to ensure that each was in growth phase at the end of the assay (≈80 % confluence). Adherent cells were seeded in 96-well plates one day prior to the treatment with escalating concentrations of the drugs (11-point twofold dilution series for all compounds). For combination treatments of refametinib plus gemcitabine, the inhibitory concentration (IC_{20}) of gemcitabine treatment alone was first determined in three independent experiments and then used for the combination assays. After a 72-hour drug exposure, 10 µl MTT (3-[4,5-Dimethylthiazol-2-yl]-2,5-diphenyltetrazolium bromide) reagent (Sigma, M5655; diluted in PBS: 5 mg/ml) was added for four hours followed by an overnight incubation with 100 µl of lysis buffer containing 10 % SDS (99 ml) and 1 N HCl (1 ml). Finally, the plate was spectrophotometrically quantified with a microtiter plate reader (Thermo Scientific Multiskan FC) at a 570 nm wavelength. All experiments were repeated at least three times with three replicates per experiment. The half-maximal inhibitory concentration (IC_{50}) of each cell line was calculated with the GraphPadPrism5 software.

2.5.5 Proliferation Assay

Proliferation was determined using the Cell Proliferation ELISA, BrdU colorimetric (Roche) according to manufacturers instructions. Briefly, cells were exposed to increasing concentrations of refametinib for 48 hours, and then BrdU labeling solution was added for an additional incubation of 24 hours. After cell fixation, treatment with the antibody conjugate and washing, 100 µl substrate solution was added. Finally, this reaction was stopped after 10 minutes with 1 M H_2SO_4 and the absorbance was measured in an ELISA reader (anthos Reader 2001) at 450 nm. All experiments were repeated at least three times with three replicates per experiment.

2.5.6 Apoptosis Assay

Cell Death was measured by using the Caspase-Glo® 3/7 Assay (Promega) as described by the manufacturer. In brief, the optimal cell number of each cell lines was seeded in white-walled 96-well plates and treated with escalating concentrations of refametinib. Staurosporine (LC Laboratories, S-9300) treatment served as positive control. After 4, 12 and 24 hours, 100 µl of Caspase-Glo® 3/7 Reagent was added directly to the cell culture medium and incubated for 30 minutes at room temperature. Finally, luminescence was measured in a plate-reading luminometer (BertholdTech Mithras). All experiments were repeated at least three times with three replicates per experiment.

2.5.7 Colony forming assay

For long-term proliferation analysis, 1×10^3 cells were seeded in 6-well plates and the following day incubated with increasing concentrations of refametinib at 37 °C in a humidified atmosphere. Cell culture medium containing the MEK1/2 inhibitor was changed every three days. When sufficient colonies were visible under control conditions (DMSO treatment), typically after 10 days, cells were washed once with PBS before fixing in -20 °C cold methanol for 15 minutes. After two additional washing steps with PBS, Giemsa stain (diluted in CertiPUR Buffer solution pH 6.88, Merck, 1.07294.1000) was added for 15 minutes. Finally, cells were rinsed in ddH_2O and air-dried. All experiments were repeated at least three times.

2.5.8 Generation of drug-resistant cell lines

Long-term treated, refametinib resistant cell lines were generated using the dose-escalation method as previously described (Corcoran *et al*., 2010; Little *et al*., 2011). Briefly, primary mouse pancreatic *Kras*^{G12D};*p53*$^{\Delta/\Delta}$ cells (called *Kras*^{G12D};*p53*$^{\Delta/\Delta}$ parental cells hereafter) were passaged in their exponential growth phase and initially exposed to 10 nM refametinib. The cultures were maintained and passaged normally with gradually increasing doses of refametinib after every second passage, up to maximal doses of 300 nM, 500 nM or 1 µM for each cell line. The established resistant cell lines were then maintained in medium containing the maximal dose of refametinib to maintain selective pressure for refametinib resistance and named *Kras*^{G12D};*p53*$^{\Delta/\Delta}$ resistant cells.

2.6 Statistical analysis

Graphical depiction, data correlation and statistical analysis were done with GraphPadPrism5 software. Data are presented in arithmetic mean +/- standard deviation of the mean, if not stated otherwise. Survival curves were done by Kaplan-Meier survival analysis. Fractional survival (y-axis) was plotted as a function of time (x-axis). The log-rank (Mantel-Cox) test was used for comparison of different survival curves. For analysis of statistical significance the significance levels error probability p was employed: $p<0.05$ (*), $p<0.005$ (**), $p<0.001$ (***).

3. Results

3.1 MEK1/2 inhibition with refametinib has potent antitumor activity against human and murine PDAC cell lines and against tumors in *Kras^{G12D};p53$^{\Delta/\Delta}$* mice

3.1.1 Active pERK1/2 is upregulated in human PDACs

Phosphorylation status of ERK1/2 was analysed in human PDAC tissue specimens and human PDAC cell lines. Immunohistochemistry (IHC) and Western blot analysis for pERK1/2 (pT202/T204) were performed. In humans, active pERK1/2 could be detected in both epithelial cancer cells and the stromal compartment with different phosphorylation levels varying from low to very high (Figure 3.1A). Only around 6 % of human PDAC samples were found to be pERK1/2 negative (Figure 3.1B). Surprisingly, patients with low pERK1/2 expression in the PDAC did not survive significantly longer than patients with high pERK1/2 levels (Figure 3.1D). Similar to the different human PDAC samples, analysis of 10 human PDAC cell lines demonstrated universal presence of phosphorylated ERK1/2 albeit at different levels (Figure 3.1C). pERK1/2 was most prominent in AsPc-1 and Capan-1 cells, which represent highly aggressive PDAC phenotypes due to their isolation from ascites and liver metastasis, respectively (Figure 3.1C; Melstrom and Grippo, 2008; Moore *et al*., 2001).

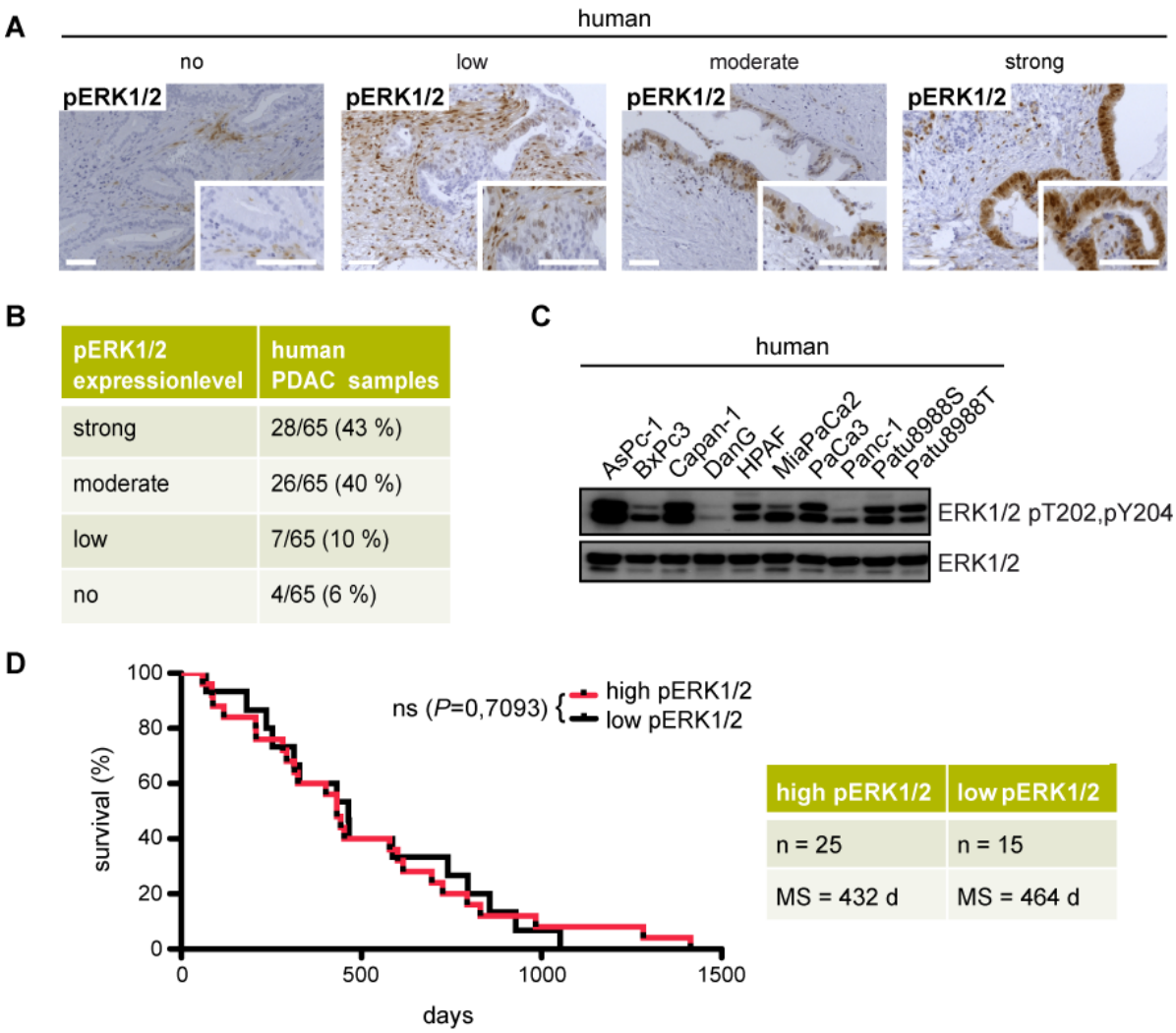

Figure 3.1 pERK1/2 expression levels in human PDAC specimens. (A) IHC* for ERK1/2 pT202,pY204 in different human PDAC specimens. Scale bars 50 µm. (B) Percentage of human pancreatic carcinomas expressing either no, low, moderate, or strong pERK1/2 levels, as calculated from the pERK1/2-IHC stainings*, is shown in tabular form. (C) Western blot analysis for ERK1/2 pT202,pY204 from lysates of murine *Kras*^{G12D} and *Kras*^{G12D};*p53*$^{\Delta/\Delta}$ cell lines. ERK1/2 served as loading control. (D) Kaplan-Meier curves showing survival (in %) of PDAC patients with either a high or low pERK1/2 PDAC status. The statistically not significant (ns) *P* value was determined using the log-rank test. The number (n) of PDAC specimens for each group and the median survival (MS; in days, d) are denoted in the legend **.

* IHC staining of human PDAC specimens for ERK1/2 pT202,pY204 was kindly performed by Prof. Bence Sipos M.D., a pathologist at University Hospital Tübingen with expertise in human and mouse PDAC pathology.

** Prof. Bence Sipos M.D. also provided survival data of PDAC patients to Nicole Teichmann for further analysis.

3.1.2 Active pERK1/2 is upregulated in murine PDACs

Phosphorylation status of ERK1/2 was further analysed in tissue samples of *Ptf1a*$^{+/Cre}$;*Kras*$^{+/LSL\text{-}G12D}$ (referred to as *Kras*^{G12D} hereafter) and the *Ptf1a*$^{+/Cre}$;*Kras*$^{+/LSL\text{-}G12D}$;*Trp53*$^{fl/fl}$ (referred to as *Kras*^{G12D};*p53*$^{\Delta/\Delta}$ hereafter) mouse models and in murine PDAC cells. Immunohistochemistry (IHC) and Western blot analysis for pERK1/2 (pT202/T204) were performed. Normal, healthy pancreatic tissue from wild-type (WT) mice showed only a few pERK1/2-IHC positive acinar cells (Figure 3.2A, white arrowhead) and pERK1/2-IHC negative Langerhans islets (Figure 3.2A, black arrowheads). In contrast, phosphorylated pERK1/2 was detectable in mPanIN lesions of 6-months-old and 1-year-old *Kras*^{G12D} mice as well as in tumors of *Kras*^{G12D};*p53*$^{\Delta/\Delta}$ mice (Figure 3.2A). Moreover, liver metastasis from *Kras*^{G12D} mice (black arrowhead) and lung metastasis from *Kras*^{G12D};*p53*$^{\Delta/+}$ mice (black arrowheads) showed strong pERK1/2 staining in the metastasis (Figure 3.2A). Western blot analysis of pancreatic lysates revealed very low ERK1/2 phosphorylation in WT tissue and higher pERK1/2 protein levels in 6-months-old and 1-year-old *Kras*^{G12D} pancreata as well as in PDAC tissue from *Kras*^{G12D};*p53*$^{\Delta/\Delta}$ mice (Figure 3.2B). Similar to the different murine and human PDAC samples, analysis of 10 murine primary pancreatic cell lines derived from PDACs taken from the endogenous *Kras*^{G12D} and *Kras*^{G12D};*p53*$^{\Delta/\Delta}$ mouse models (referred to as murine *Kras*^{G12D} and *Kras*^{G12D};*p53*$^{\Delta/\Delta}$ cells hereafter) also demonstrated universal presence of phosphorylated ERK1/2 albeit at different levels (Figure 3.2C).

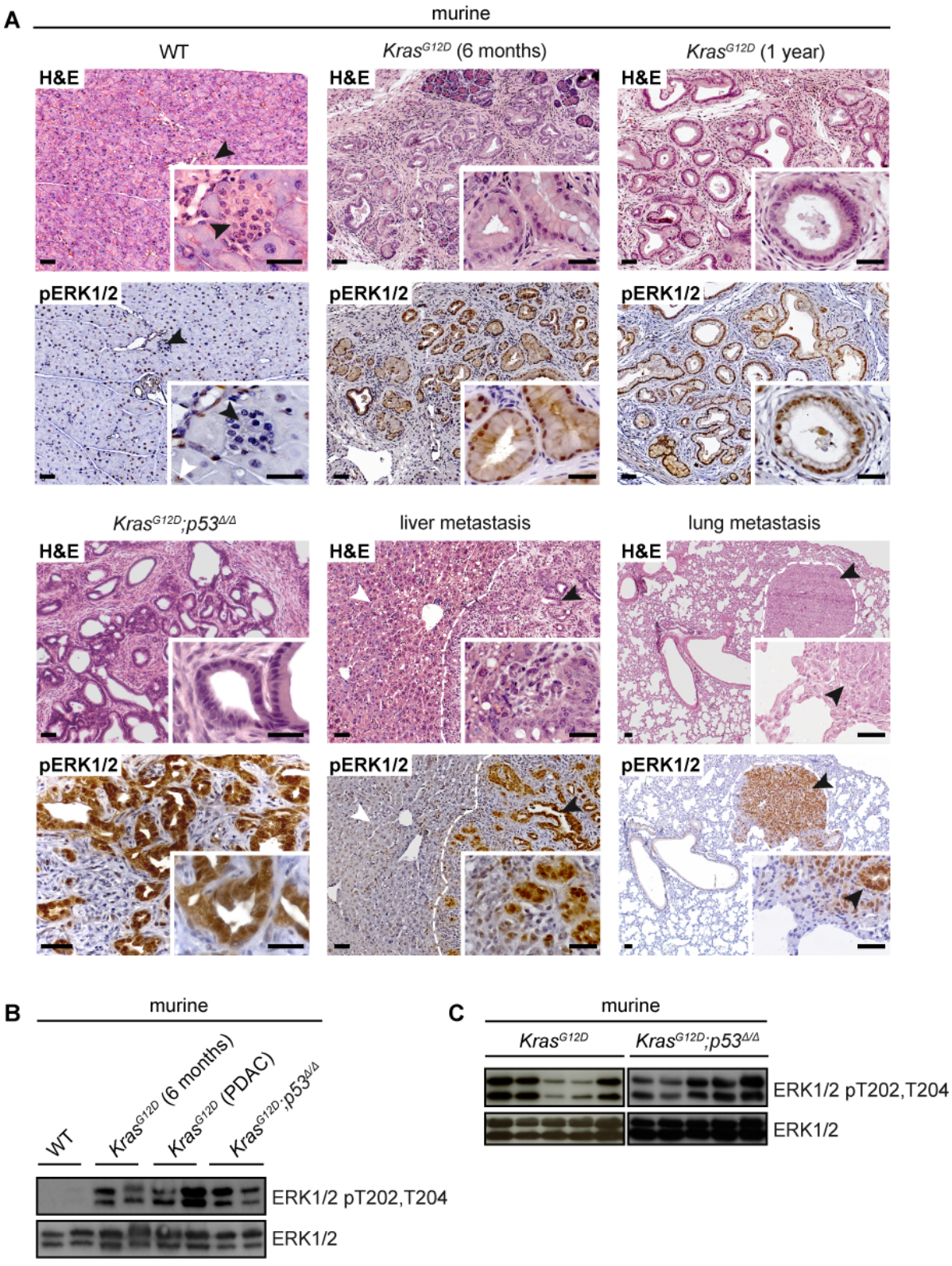

Figure 3.2 Induction of active ERK1/2 during pancreatic tumorigenesis. (A) Hematoxylin and eosin staining (H&E) and IHC for ERK1/2 pT202,pY204 in wild-type (WT), *Kras*^{G12D} (6-months-old and 1-year-old) and *Kras*^{G12D};*p53*$^{\Delta/\Delta}$ pancreata as well as in a liver metastasis from a *Kras*^{G12D} mouse (11-months-old) and in a lung metastasis from a *Kras*^{G12D};*p53*$^{\Delta/+}$ mouse (5-months-old). Scale bars represent 50 µm. (B) Western blot analysis of pancreatic lysates for ERK1/2 pT202,pY204 from wild-type (WT), *Kras*^{G12D} (6-months-old and 1-year-old) and *Kras*^{G12D};*p53*$^{\Delta/\Delta}$ mice. ERK1/2 served as loading control. (C) Western blot analysis for ERK1/2 pT202,pY204 from lysates of murine *Kras*^{G12D} and *Kras*^{G12D};*p53*$^{\Delta/\Delta}$ cell lines. ERK1/2 served as loading control.

3.1.3 Refametinib treatment efficiently blocks phosphorylation of ERK1/2 *in vitro* and *in vivo*

In first experiments, refametinib was evaluated for its efficacy to inhibit MEK1/2 activity in several human and murine *Kras*^{G12D};*p53*$^{\Delta/\Delta}$ pancreatic tumor cell lines. ERK1 and ERK2 are the so far only physiologically known substrates of the MEK1/2 kinase and thus represent a suitable measurement of MEK1/2 inhibitors efficacy (Neuzillet *et al*., 2013). Cells were treated with escalating concentrations of refametinib for 72 hours. The Western blot analysis revealed a dose-dependent inhibition of MEK1/2 kinase activity with concentrations between 10 to 300 nM required for complete ERK1/2 inhibition (Figure 3.3A). Additionally, all tested cell lines independent of their basal pERK1/2 status showed a remarkable reduction of pERK1/2 after a 72-hour exposure to 300 nM refametinib (Figure 3.3B).

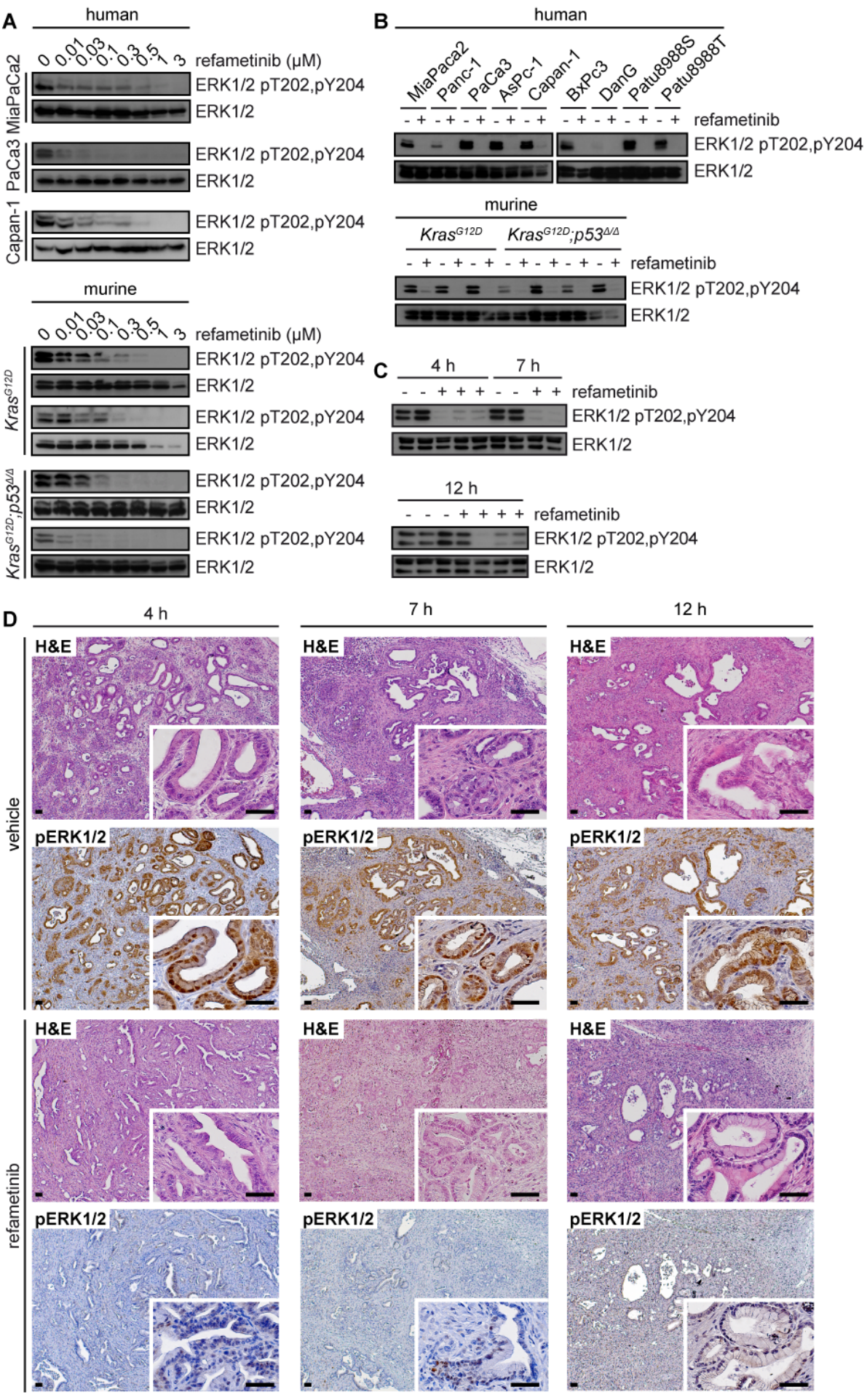
A
human
0 0.01 0.03 0.1 0.3 0.5 1 3 refametinib (μM)
MiaPaCa2
ERK1/2 pT202,pY204
ERK1/2
PaCa3
ERK1/2 pT202,pY204
ERK1/2
Capan-1
ERK1/2 pT202,pY204
ERK1/2
murine
0 0.01 0.03 0.1 0.3 0.5 1 3 refametinib (μM)
KrasG12D
ERK1/2 pT202,pY204
ERK1/2
KrasG12D;p53Δ/Δ
ERK1/2 pT202,pY204
ERK1/2
B
human
MiaPaca2 Panc-1 PaCa3 AsPc-1 Capan-1 BxPc3 DanG Patu8988S Patu8988T
refametinib
ERK1/2 pT202,pY204
ERK1/2
murine
KrasG12D KrasG12D;p53Δ/Δ
refametinib
ERK1/2 pT202,pY204
ERK1/2
C
4 h 7 h
refametinib
ERK1/2 pT202,pY204
ERK1/2
12 h
refametinib
ERK1/2 pT202,pY204
ERK1/2
D
4 h 7 h 12 h
vehicle
refametinib
H&E
pERK1/2

Figure 3.3 Refametinib efficiently decreases ERK1/2 phosphorylation *in vitro* and *in vivo*. (A, B) Western blot analysis for ERK1/2 pT202,pY204 from lysates of human and murine *Kras*^{G12D} and *Kras*^{G12D};*p53*$^{\Delta/\Delta}$ cell lines after treatment with increasing concentrations of refametinib (A) or 300 nM refametinib (B) for 72 hours. ERK1/2 served as loading control. (C) Western blot analysis of whole pancreatic lysates for ERK1/2 pT202,pY204 in *Kras*^{G12D};*p53*$^{\Delta/\Delta}$ mice after treatment with refametinib (25 mg/kg bodyweight) or vehicle for the indicated time points (2-4 animals per group). ERK1/2 served as loading control. (D) H&E staining and IHC for ERK1/2 pT202,pY204 in *Kras*^{G12D};*p53*$^{\Delta/\Delta}$ pancreata after treatment with one single dose of refametinib (25 mg/kg bodyweight) or vehicle solution consisting of 30 % HP-ß-CD-Form1 by oral gavage for 4, 7, and 12 hours. Scale bars represent 50 µm.

Generating *Kras*^{G12D};*p53*$^{\Delta/\Delta}$ mice by introducing p53 nullizygosity (*p53*$^{\Delta/\Delta}$) into the *Kras*^{G12D}-GEMM caused a more rapid progression to invasive PDAC compared to *Kras*^{G12D} mice (Hingorani *et al*., 2003) or *Kras*^{G12D};*Trp53*$^{R172H/+}$ *mice* (Hingorani *et al*., 2005), yielding in lethal tumors by around eight weeks of age (Bardeesy *et al*., 2006). These locally advanced tumors exhibit a typical human-like morphology with abundant desmoplasia and moderate to poor epithelial differentiation. Gross metastases (e.g. to the liver and lungs) are usually not prominent in *Kras*^{G12D};*p53*$^{\Delta/\Delta}$ mice due to the fast clinical course of the disease (Bardeesy *et al*., 2006; Mazur and Siveke, 2012). To investigate whether the MEK1/2 inhibitor refametinib is inhibiting MEK activity in endogenous tumors in this PDAC mouse model, *Kras*^{G12D};*p53*$^{\Delta/\Delta}$ mice were treated with one single dose of refametinib (25 mg/kg bodyweight) and euthanized after 4, 7, and 12 hours of administration. A profound and durable reduction of active pERK1/2 was detected by both Western blot analysis and IHC (Figures 3.3C and 3.3D), indicating indeed a good bioavailability of this MEK1/2 inhibitor to PDAC tissue.

3.1.4 EGFR inhibition with erlotinib does not limit PDAC progression in *Kras*^{G12D};*p53*$^{\Delta/\Delta}$ mice

To validate robustness of our *Kras*^{G12D};*p53*$^{\Delta/\Delta}$ mouse model for preclinical studies and to test if it reflects the clinical data, a randomized, parallel-group survival study was conducted comparing erlotinib and the standard-of-care combination therapy of gemcitabine plus erlotinib. Mice with MRI-detectable advanced PDAC were treated daily with either erlotinib (50 mg/kg bodyweight) by oral gavage or with erlotinib plus i.p. injections of 100 mg/kg gemcitabine (four doses every third day; see dosing scheme Figure 3.4A). Mice tolerated the monotherapy and the combined treatment well with no overt signs of toxicity including no induced change in body mass (Figure 3.4C). Combination-treated animals showed no significant difference in life span compared to mice with erlotinib treatment alone (median survival 63 d versus 68 d, respectively; Figure 3.4B) and showed no reduction in tumor burden by MRI (Figure 3.4D).

A

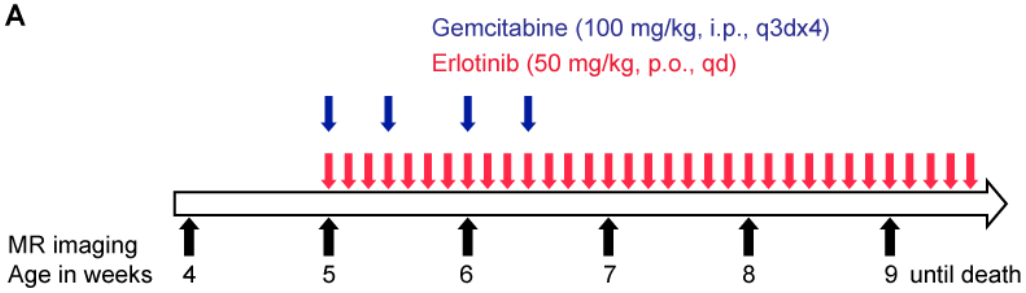

B

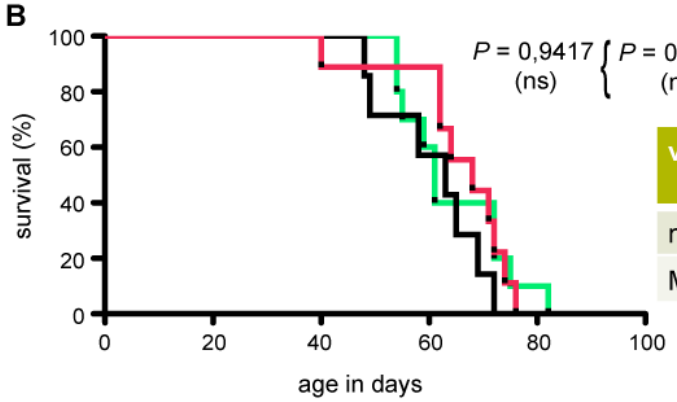

vehicle	Erlotinib	Erlotinib + Gemcitabine
n = 10	n = 7	n = 9
MS = 61 d	MS = 63 d	MS = 68 d

C

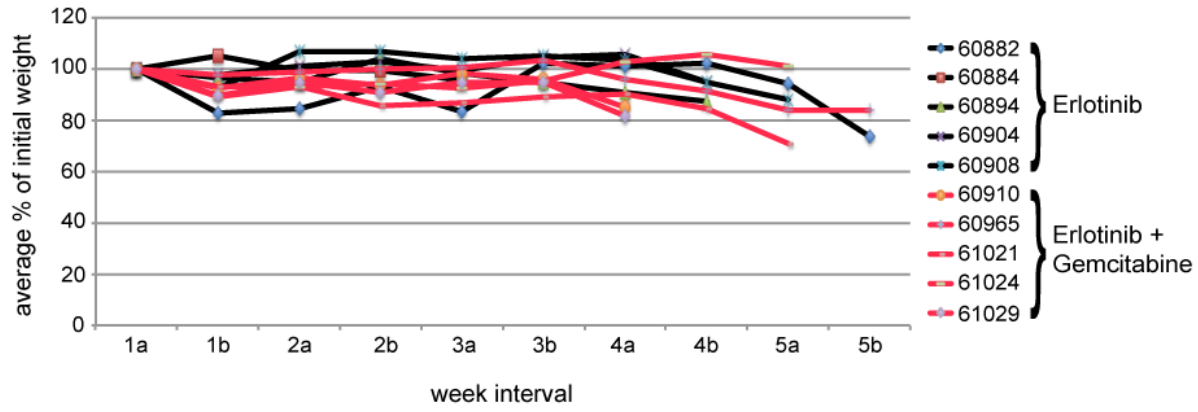

D

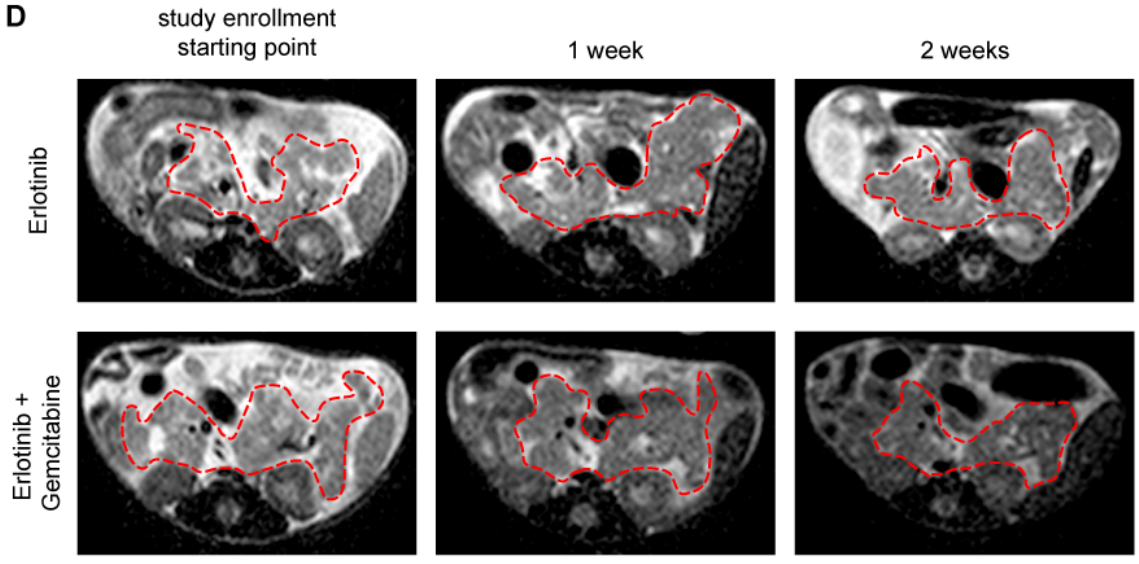

Figure 3.4 Erlotinib monotherapy* or erlotinib in combination with gemcitabine*/ are only minimally effective in *Kras*^{G12D};*p53*$^{\Delta/\Delta}$ mice.** (A) Dosing scheme for erlotinib and erlotinib plus gemcitabine *in vivo* treatment. Mice were treated either with erlotinib (50 mg/kg bodyweight; daily dosing, qd; peroral, p.o.) alone or in combination with gemcitabine (100 mg/kg bodyweight; four doses every third day, q3dx4; intraperitoneal, i.p.) or a vehicle solution. Weekly MR imaging on a clinical 1.5 T device was performed to track tumor progression during the therapy. (B) Kaplan-Meier curves depicting survival (in %) of *Kras*^{G12D};*p53*$^{\Delta/\Delta}$ mice treated with erlotinib, erlotinib plus gemcitabine or drug vehicle as indicated in the dosing scheme and refametinib for comparison (black-dotted line). *P* values (statistically not significant, ns) were determined using the log-rank test. The number (n) of mice for each group and the median survival (MS; in days, d) are denoted in the legend. (C) Body weights of erlotinib and erlotinib plus gemcitabine treated *Kras*^{G12D};*p53*$^{\Delta/\Delta}$ study mice demonstrating drug tolerance. Mice were weighed daily throughout the course of study and the weight at the beginning and the end of each week (a and b on the x-axis, respectively) are plotted. Weights are represented as the percentage of weight from the study enrollment starting point for each mouse. Five representative mice of each treatment group are shown. (D) Representative MR images of a erlotinib and an erlotinib plus gemcitabine treated *Kras*^{G12D};*p53*$^{\Delta/\Delta}$ mouse at therapy starting point as well as after one and two weeks of study enrollment. Red-doted lines illustrate the tumor location and size.

* These data are published in 'Modeling Therapy Response and Spatial Tissue Distribution of Erlotinib in Pancreatic Cancer', Molecular Cancer Therapeutics (Grüner *et al.*, 2016).

** These data are published in 'EGF Receptor is required for KRAS-induced pancreatic tumorigenesis', Cancer Cell (Ardito *et al.*, 2012).

3.1.5 Refametinib *in vivo* treatment induces a striking tumor regression leading to an overall survival benefit for *Kras*^{G12D};*p53*$^{\Delta/\Delta}$ mice

To evaluate refametinib efficacy against PDAC *in vivo*, a treatment protocol for *Kras*^{G12D};*p53*$^{\Delta/\Delta}$ animals with a detectable tumor burden, determined by a clinical MRI device, was established. Treatment was started after a visible tumor burden (around 200 mm^3) was detected in animals by weekly T2w MRI. Daily treatment for five consecutive days per week with refametinib (see dosing scheme Figure 3.5A) prolonged the survival of *Kras*^{G12D};*p53*$^{\Delta/\Delta}$ mice significantly with a median survival advantage post therapy onset of 26 days compared to their vehicle-treated counterparts - an increase in 149 % (***P* = 0.001; Figure 3.5B). To exclude drug intolerance, the body weight of enrolled *Kras*^{G12D};*p53*$^{\Delta/\Delta}$ mice was monitored throughout the course of study. All vehicle- and refametinib-dosed mice showed constant gain in weight during therapy, indicating that the dosing regimen was indeed well tolerated. Mice were euthanized, when showing signs of advanced disease (e.g. pain, non-social behavior, loss of weight) (Figure 3.5C).

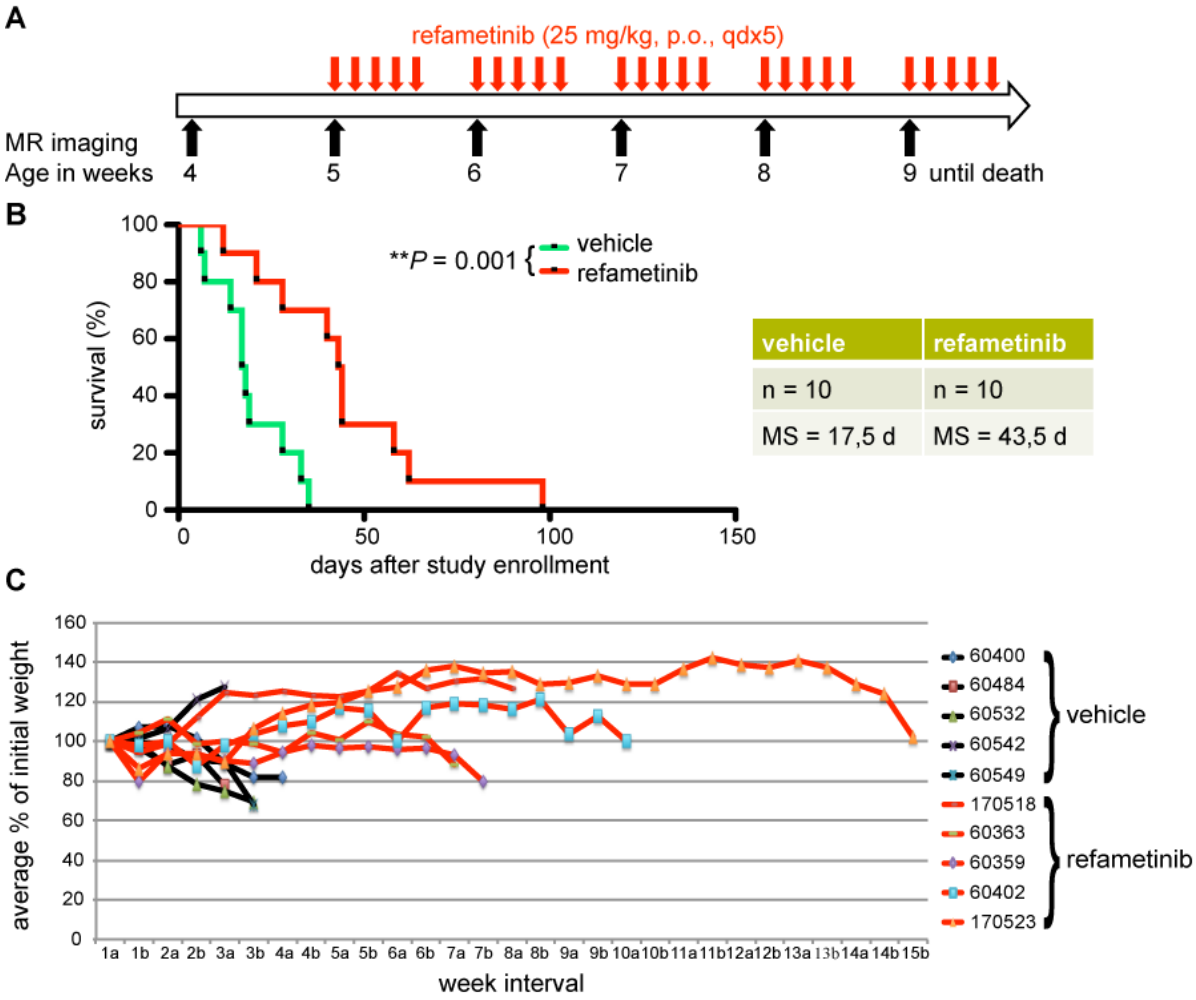

Figure 3.5 Refametinib treatment significantly prolongs the survival of *Kras*^{G12D};*p53*$^{\Delta/\Delta}$ mice. (A) Dosing scheme for refametinib *in vivo* treatment. Mice were dosed daily five consecutive days per week (qdx5) with 25 mg/kg bodyweight of refametinib or the vehicle solution consisting of 30 % HP-ß-CD-Form1 by oral gavage (peroral, p.o.). Weekly magnetic resonance imaging (MRI) on a clinical 1.5 T device was performed to track tumor progression during the therapy. (B) Kaplan-Meier curves depicting survival (in %) of *Kras*^{G12D};*p53*$^{\Delta/\Delta}$ mice treated with refametinib or drug vehicle as indicated in the dosing scheme. The significant ***P* value was determined using the log-rank test. The number (n) of mice for each group and the median survival (MS; in days, d) are denoted in the legend. (C) Body weights of vehicle- and refametinib-treated *Kras*^{G12D};*p53*$^{\Delta/\Delta}$ study mice demonstrating tolerability of drug administration. Mice were weighed five days weekly throughout the course of study and the weight at the beginning and the end of each week (a and b on the x-axis, respectively) are plotted. Weights are represented as the percentage of weight from the study enrollment starting point for each mouse. Five representative mice of each treatment group are shown.

In addition to the prolongation of survival, the most pronounced observation was an effective tumor regression in refametinib-dosed *Kras*^{G12D};*p53*$^{\Delta/\Delta}$ mice noticed already after one to two weeks of treatment by MRI (Figures 3.6A and 3.6B). In contrast, vehicle-treated animals showed a weekly tumor progression and usually died within two to four weeks of therapy due to their massive tumor burden (Figure 3.6B). Moreover, two weeks refametinib-treated pancreata showed not only ADMs and mPanINs, but also large parts of

phenotypically normal acinar tissue, whereas two weeks vehicle-treated mice developed big ductal carcinomas with rare mPanIN or ADM leftovers (Figure 3.6A).

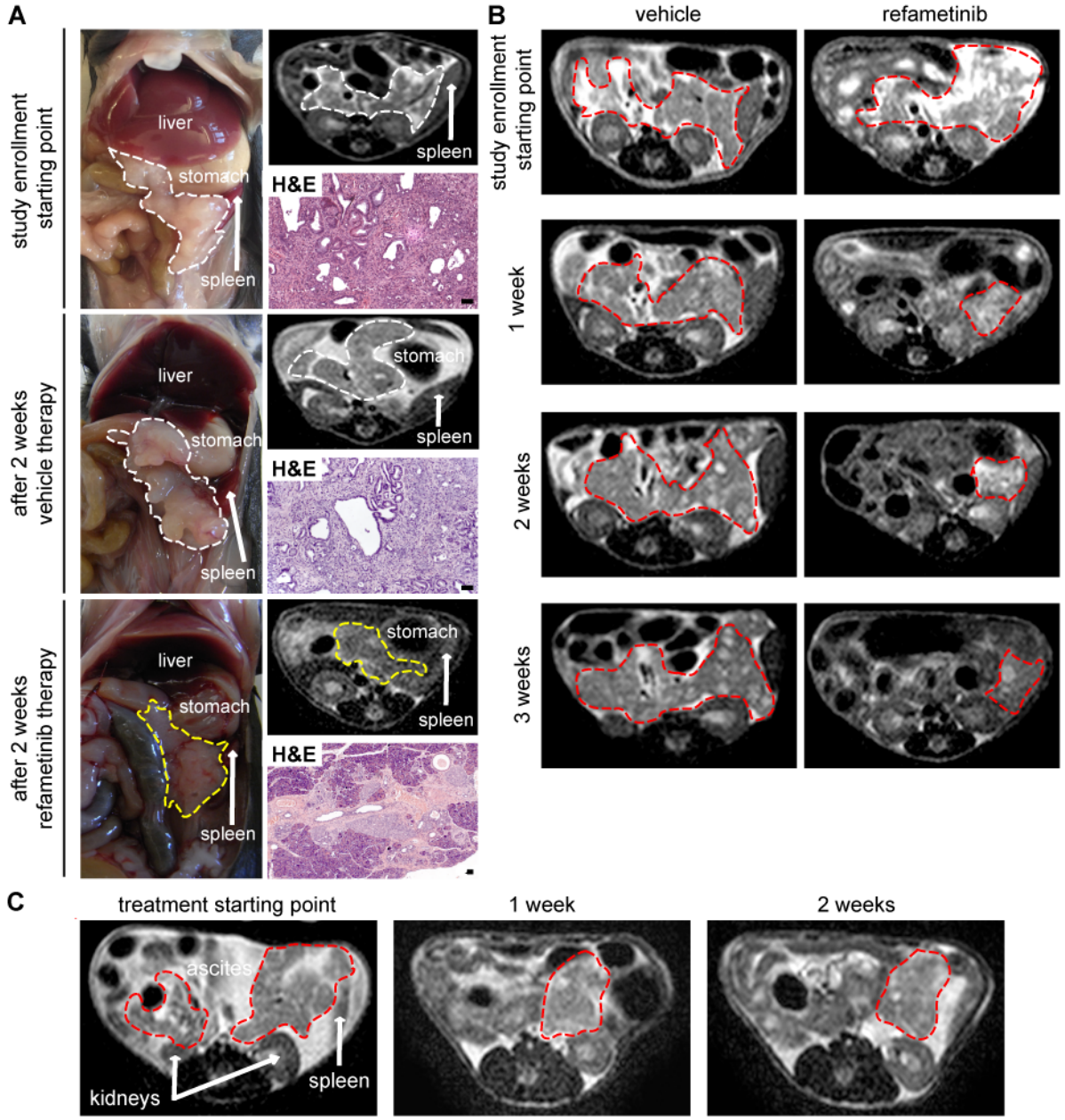

Figure 3.6 Refametinib treatment induces a massive shrinkage of tumors in *Kras^{G12D};p53$^{\Delta/\Delta}$* mice. (A) Macroscopic images of primary pancreatic *Kras^{G12D};p53$^{\Delta/\Delta}$* tumors as well as corresponding MR images and H&E staining at study enrollment starting point and after two weeks of vehicle or refametinib treatment (daily 25 mg/kg bodyweight for five consecutive days per week). White-doted lines illustrate the tumor location and size. Yellow-doted lines denote normal pancreatic tissue. (B) Representative MR images of a vehicle- and a refametinib-treated *Kras^{G12D};p53$^{\Delta/\Delta}$* mouse at therapy starting point as well as after one, two and three weeks of study enrollment. Red-doted lines illustrate the tumor location and size. (C) Refametinib treatment in mice with very advanced PDACs: Representative MR images of a refametinib-dosed *Kras^{G12D};p53$^{\Delta/\Delta}$* mouse at treatment starting point as well as after one and two weeks of therapy. Ascites (white fluid surrounding the tumor), kidneys and the spleen are denoted on the images at the treatment starting point. Red-doted lines delineate the tumor.

To evaluate whether the observed effect on tumor burden is due to treatment start in early tumor phase when the PDACs are still smaller, a group of *Kras*^{G12D};*p53*$^{\Delta/\Delta}$ mice with very advanced tumors was included in the study. The same dramatic decrease of the tumor load was observed in these animals (Figure 3.6C).

3.1.6 Refametinib *in vitro* treatment results in a remarkable cell viability reduction

The surprisingly potent antitumor activity of refametinib in *Kras*^{G12D};*p53*$^{\Delta/\Delta}$ mice prompted further analysis of the mechanism underlying the dramatic tumor mass decrease. As measured by cytotoxicity assays and colony forming assays, respectively, a number of human and primary mouse pancreatic tumor cell lines with a different genetic background displayed a remarkably reduced cell viability with very different half-maximal inhibitory concentration (IC_{50}) values when exposed to escalating concentrations of refametinib both short-term after 72 hours and long-term after 10 days (Figures 3.7A, 3.7C and 3.7D). This potent inhibitory effect on cell viability is dose-dependent and for human pancreatic tumor cell lines also dependent on their active pERK1/2 protein levels. Generally, the variability between human, murine *Kras*^{G12D} and murine *Kras*^{G12D};*p53*$^{\Delta/\Delta}$ cell lines was small with IC_{50} values ranging from 4 nM to 188 nM (Figure 3.7B). Thus, all tested cell lines independent of their genetic background were responsive to refametinib.

A

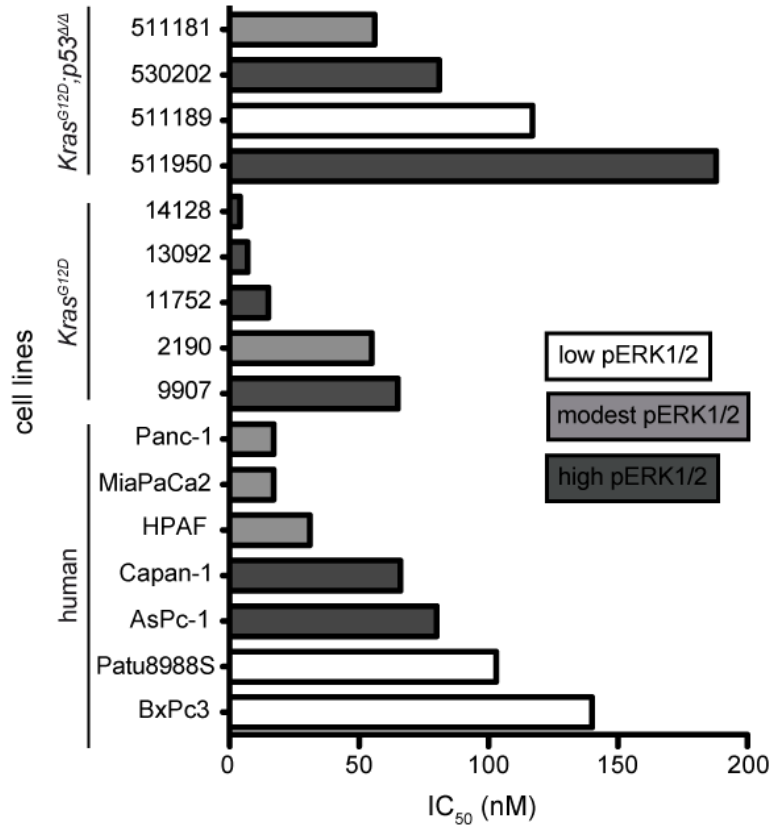

B

cell line	IC_{50} (nM)	pERK1/2 expression
511181	56	modest
530202	81	high
511189	117	low
511950	188	high
14128	4	high
13092	7	high
11752	15	high
2190	55	modest
9907	65	high
Panc-1	17	modest
MiaPaCa2	17	modest
HPAF	31	modest
Capan-1	66	high
AsPc-1	80	high
Patu8988S	103	low
BxPc3	140	low

C

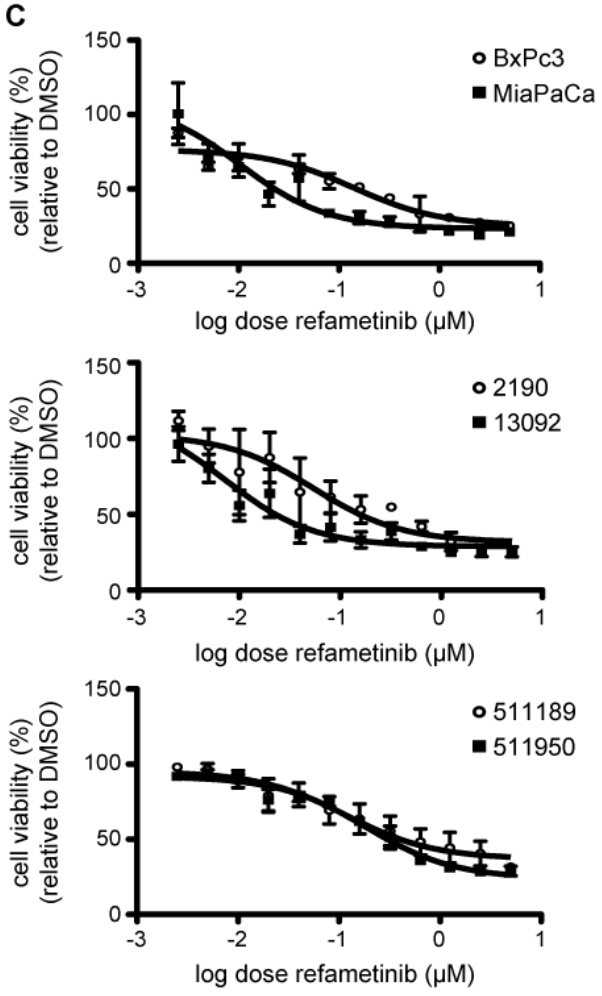

D

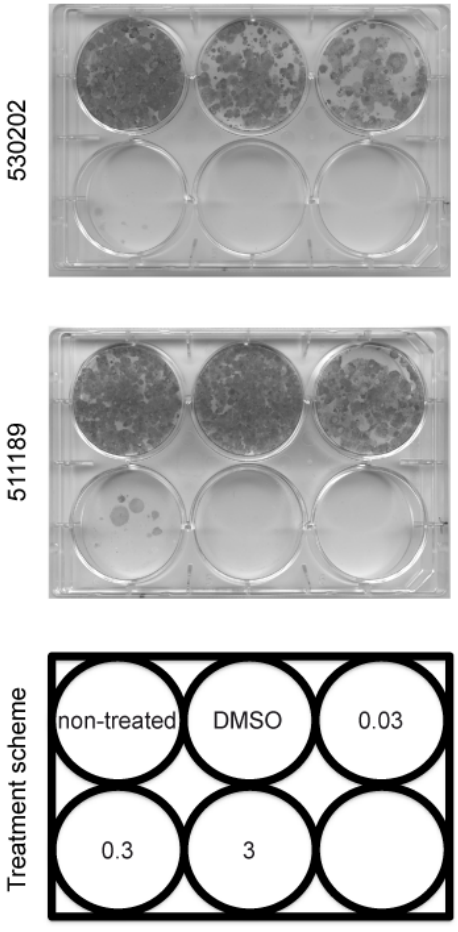

Figure 3.7 Refametinib treatment reduces the cell viability of human and murine PDAC cell lines. (A, B, C) IC_{50} measurements of several human and murine *Kras*^{G12D} and *Kras*^{G12D};*p53*$^{\Delta/\Delta}$ cell lines after 72-hour treatment with escalating concentrations of refametinib. IC_{50} (nM) values are plotted on the x-axis and corresponding cell lines on the y-axis (A). The IC_{50}, calculated from three independent performed experiments with the GraphPadPrism5 software, and the pERK1/2 expression, validated with Western blot analysis, of each cell line are shown in tabular form (B). Representative dose-response curves for a low (white circle) and high (black square) pERK1/2 expressing cell lines of each group. Cell viability (%) was calculated relative to DMSO control treatment. Values are mean ± standard deviation of triplicate wells and three independent performed experiments (C). (D) Photographic images of refametinib colony forming assays for murine *Kras*^{G12D};*p53*$^{\Delta/\Delta}$ cell lines. Colony forming assays were performed in the presence of increasing concentrations of refametinib (0.03, 0.3 and 3 µM final concentration). Plates were re-drugged every third day and fixed and stained after 10 days following plating. Images from a representative experiment of three giving similar results are shown. The name of each *Kras*^{G12D};*p53*$^{\Delta/\Delta}$ cell line is given and a schematic shows the concentration (in µM) used for each well.

To test if the combination of refametinib with the standard-of-care-agent gemcitabine induces a synergistic effect on cell viability reduction, cytotoxicity assays using the MTT reagent were conducted. Surprisingly, the combination of the allosteric MEK1/2 inhibitor plus gemcitabine did not lead to a significant synergy (Figures 3.8A and 3.8B).

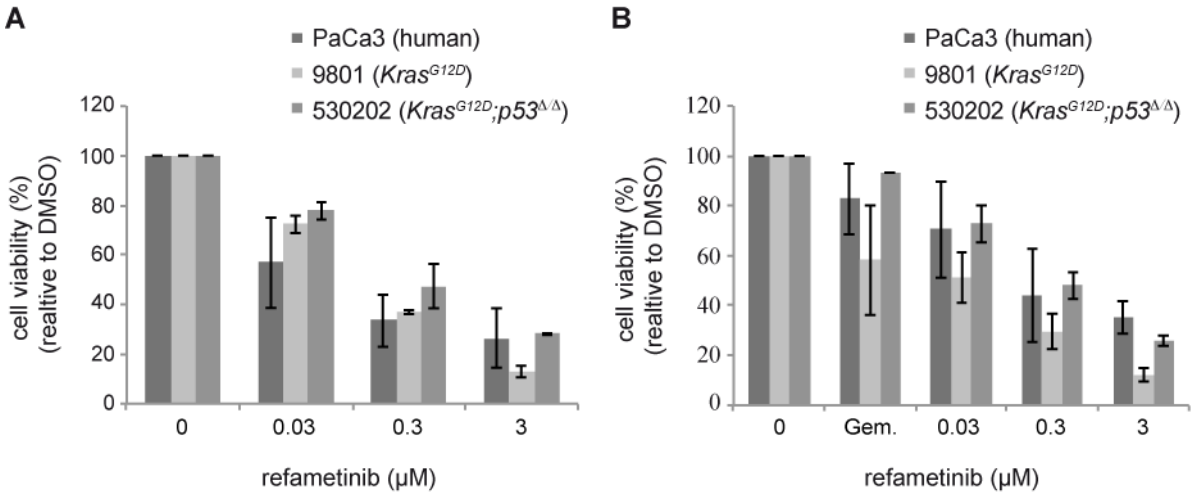

Figure 3.8 Combination of refametinib with gemcitabine leads not to a synergistic effect on cell viability reduction in human and murine PDAC cell lines. (A, B) Effect on the cell viability of indicated human and murine *Kras*^{G12D} and *Kras*^{G12D};*p53*$^{\Delta/\Delta}$ cell lines after 72-hour treatment with increasing concentrations of refametinib (0.03, 0.3 and 3 µM final concentration) alone (A) or in combination with a fixed dose of gemcitabine (Gem.; PaCa3 5 nM, 9801 and 530202 10 nM) (B) as measured with cytotoxicity assays using the MTT reagent. Cell viability (%) was calculated relative to DMSO control treatment. Values are mean ± standard deviation of triplicate wells and three independent performed experiments.

3.1.7 Refametinib *in vivo* treatment results in a potent apoptosis induction responsible for the striking tumor regression

To investigate whether the impaired cell viability after exposure to refametinib is attributable to a proliferation arrest or apoptosis induction, several cell-based *in vitro* assays were performed. Apoptosis assay of *Kras*^{G12D};*p53*$^{\Delta/\Delta}$ cells showed that ERK1/2 inhibition triggers

apoptosis via induction of CASPASE 3/7 activity (Figure 3.9A) accompanied with an increase of PARP cleavage, a CASPASE 3/7 target, as well as an upregulation of the pro-apoptotic protein BIM starting 12 hours post treatment as confirmed via Western blot analysis (Figure 3.9B). Proliferation, as measured with BrdU incorporation and with Western blot analysis of the proliferation marker PCNA, is only compromised at high concentrations (minimum dose of 3 µM; Figure 3.10), suggesting that apoptosis is mainly responsible for the observed reduction in cell viability.

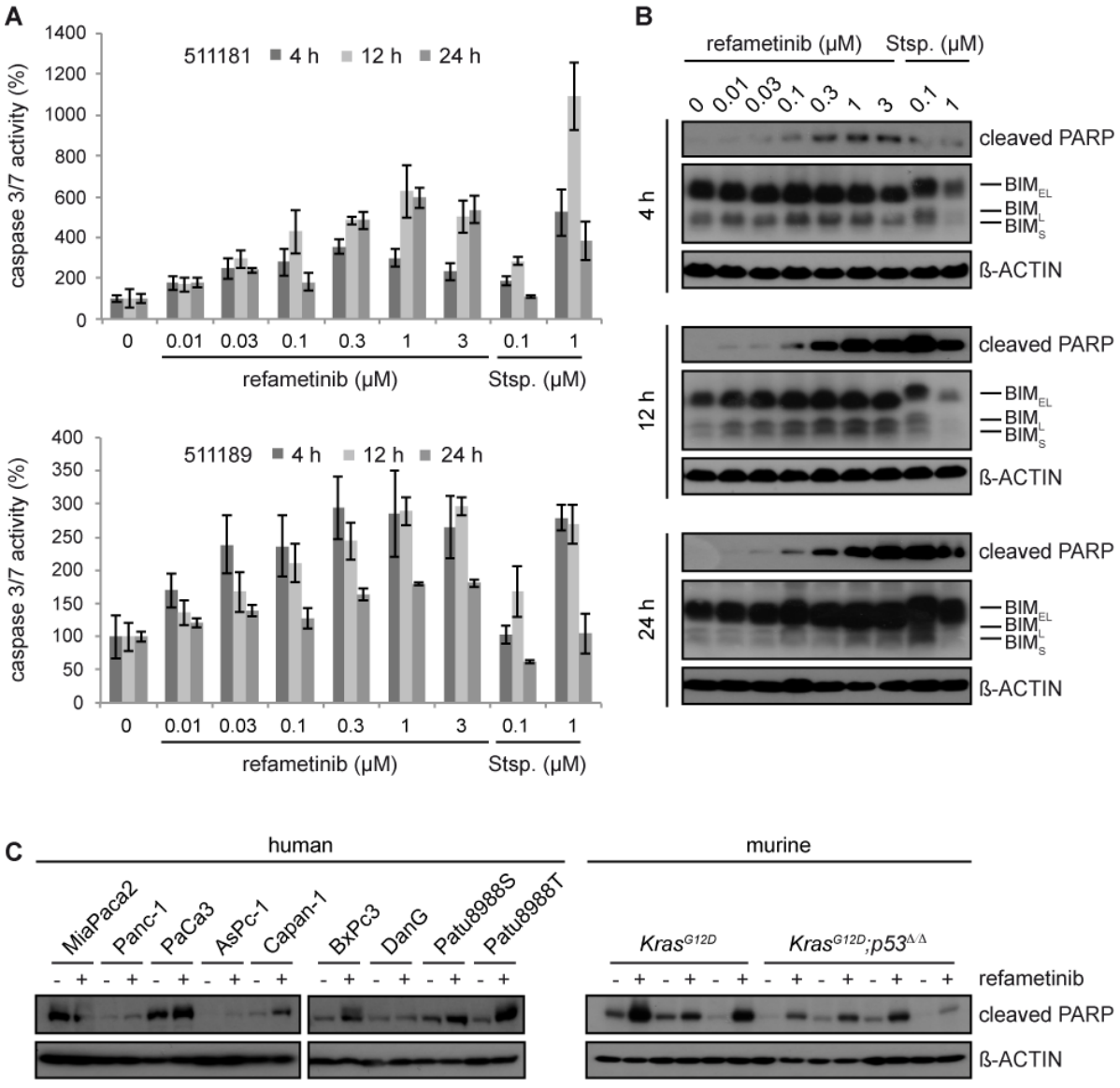

Figure 3.9 Refametinib induces apoptosis *in vitro*. (A) Induction of caspase 3/7 activity in two different murine *Kras*^{G12D};*p53*$^{\Delta/\Delta}$ cell lines (511181 and 511189) as measured by an apoptosis assay at indicated time points post refametinib treatment. Exposure to staurosporine (Stsp.), an inducer of apoptosis, served as positive control. (B) Western blot analysis for cleaved PARP and the pro-apoptotic protein BIM from lysates of a murine *Kras*^{G12D};*p53*$^{\Delta/\Delta}$ cell line (511181) after treatment with escalating concentrations of refametinib or staurosporine for the indicated time points. ß-ACTIN served as loading control. (C) Western blot analysis for cleaved PARP from lysates of several human and murine *Kras*^{G12D} and *Kras*^{G12D};*p53*$^{\Delta/\Delta}$ cell lines after treatment with 300 nM refametinib for 72 hours. ß-ACTIN served as loading control.

ERK1/2 dependent survival is also demonstrable in several human PDAC cell lines as well as murine *Kras*^{G12D} cells, which exhibit higher cleaved PARP levels after treatment with 300 nM refametinib (Figure 3.9C).

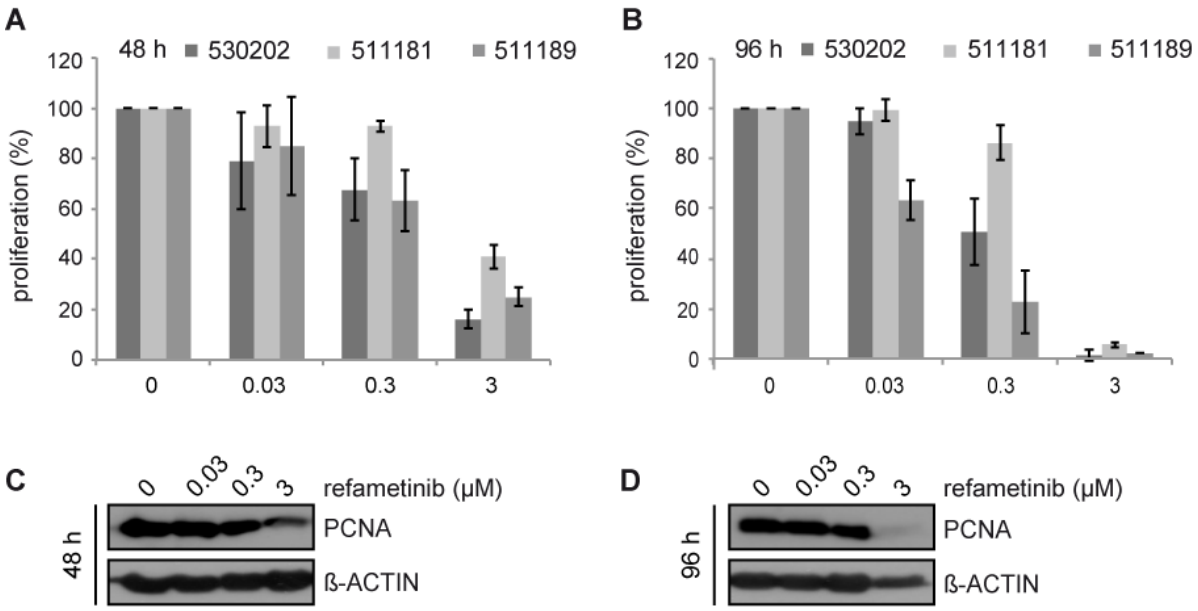

Figure 3.10 Refametinib causes only sparse cytostatic effects *in vitro*. (A, B) Proliferation of three different murine *Kras*^{G12D};*p53*$^{\Delta/\Delta}$ cell lines (530202, 511181 and 511189) was determined using a BrdU assay after exposure to increasing concentrations of refametinib for 48 hours (A) and 96 hours (B). Proliferation (%) was calculated relative to DMSO control treatment. Values are mean ± standard deviation of triplicate wells and three independent performed experiments. (C, D) Western blot analysis for the proliferation marker PCNA from lysates of a murine *Kras*^{G12D};*p53*$^{\Delta/\Delta}$ cell line (511181) after treatment with increasing concentrations of refametinib for 48 hours (C) and 96 hours (D). ß-ACTIN served as loading control.

Though a proliferation arrest might contribute to a stagnation of tumor growth, it could not explain the massive tumor shrinkage seen in refametinib treated *Kras*^{G12D};*p53*$^{\Delta/\Delta}$ mice. To test the hypothesis whether the induced cell death seen *in vitro* is also responsible for the pronounced *in vivo* effect, TUNEL staining of representative tumor sections from *Kras*^{G12D};*p53*$^{\Delta/\Delta}$ mice treated with one single dose of refametinib was performed. Already after four hours and seven hours post treatment the presence of double stranded DNA breaks as markers of apoptosis specifically in tumor cells was clearly noticed (Figure 3.11A). This prompt apoptosis induction was accompanied by CASPASE 3 activation and PARP cleavage as well as by BIM upregulation starting 12 hours post dose from *ex vivo* samples (Figure 3.11B).

Taken together, these data suggest that MEK1/2 inhibition with refametinib has potent antitumor activity both in cell lines and mouse models.

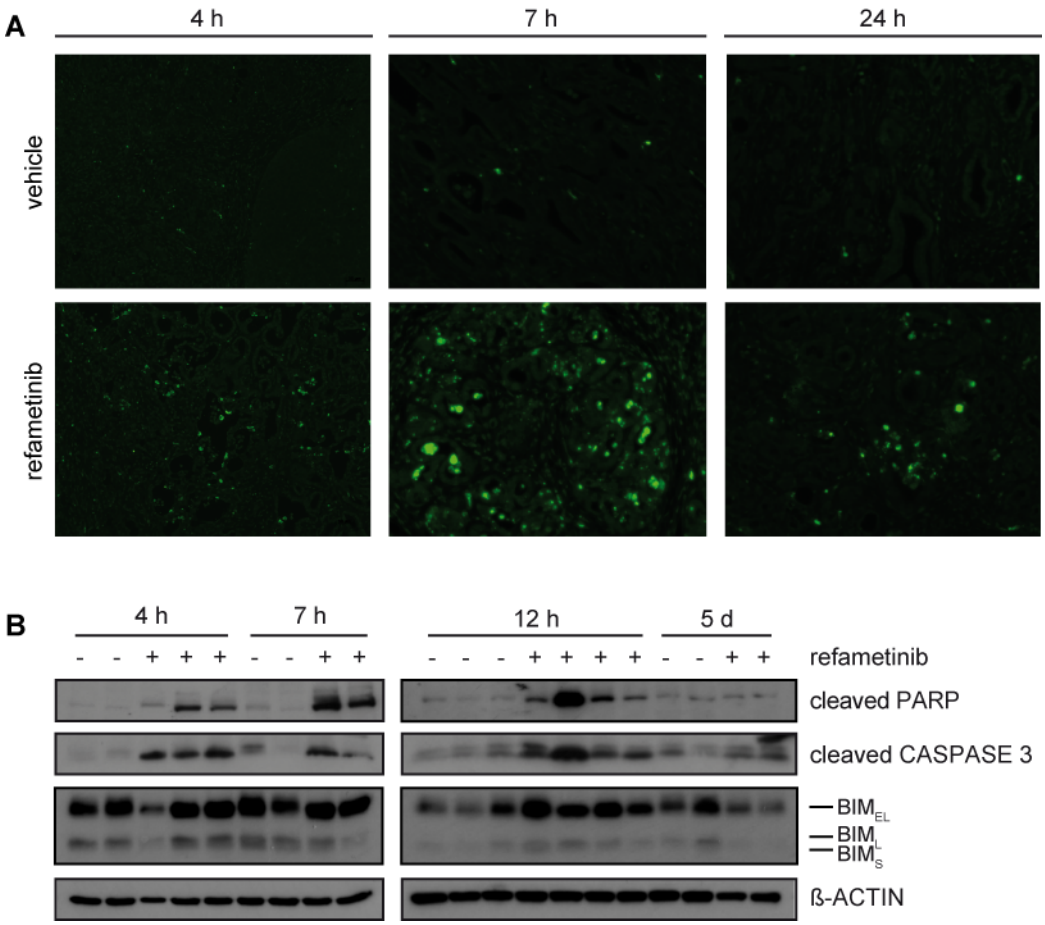

Figure 3.11 Refametinib induces apoptosis *in vivo.** (A) TUNEL stained, representative sections of *Kras*^{G12D};*p53*$^{\Delta/\Delta}$ mice treated with one single dose of refametinib (25 mg/kg bodyweight) or the vehicle solution consisting of 30 % HP-ß-CD-Form1 by oral gavage for the indicated time points. (B) Western blot analysis of whole pancreatic lysates for cleaved PARP, cleaved CASPASE 3 and BIM in *Kras*^{G12D};*p53*$^{\Delta/\Delta}$ mice after treatment with one single dose of refametinib (25 mg/kg bodyweight) or the vehicle solution consisting of 30 % HP-ß-CD-Form1 by oral gavage for the indicated time points (2-4 animals per group). ß-ACTIN served as loading control.

* These data are published in 'Apparent Diffusion Coefficient (ADC) predicts therapy response in pancreatic ductal adenocarcinoma', Scientific Reports (Trajkovic-Arsic *et al.*, 2017).

3.2 Continuous refametinib treatment led to recurrent resistant tumors

3.2.1 Relapsed refametinib resistant tumors with an EMT phenotype appear in *Kras^{G12D};p53$^{\Delta/\Delta}$* mice continuously treated with refametinib

The significant tumor shrinkage observed in refametinib treated animals was however not durable. Approximately 2-3 weeks upon therapy onset and around one week upon full tumor regression, the tumor mass re-appeared and was continuously growing till animal death (Figure 3.12).

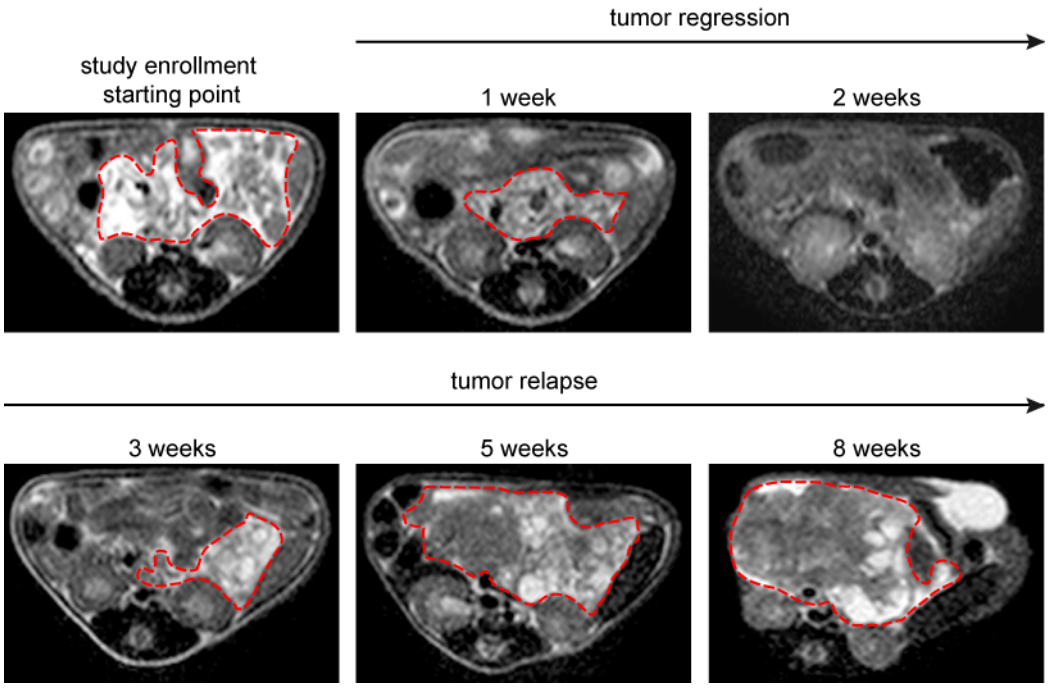

Figure 3.12 Continuous administration of refametinib led to the development of recurrent, resistant tumors in *Kras^{G12D};p53$^{\Delta/\Delta}$* mice. Representative MR images of a refametinib treated *Kras^{G12D};p53$^{\Delta/\Delta}$* mouse at therapy starting point as well as after one, two, three, five and eight weeks of study enrollment. Red-doted lines illustrate the tumor location and size.

Histopathological examination of H&E stained tumor sections from vehicle and refametinib treated *Kras^{G12D};p53$^{\Delta/\Delta}$* mice revealed that some relapsed tumors presented altered morphological features compared to the vehicle treated (Table 3.1; Figure 3.13A). Vehicle treated animals developed ductal-epithelial tumors as typically seen in *Kras^{G12D};p53$^{\Delta/\Delta}$* mice (Bardeesy *et al.*, 2006). Around 20 % of recurrent, refametinib resistant PDACs represent sarcomatoid tumor histology consisting of spindle-shaped, E-CADHERIN negative cells

(Figure 3.13A and 3.13B). Relapsed tumors with an overall ductal morphology also presented often parts (tumor lobuli) with pronounced sarcomatoid morphology. Primary tumor cell lines were isolated from relapsed ductal (animal number 60406 and 170518) and sarcomatoid (animal numbers 60409 and 70202) tumors (called *Kras^{G12D};p53$^{\Delta/\Delta}$* parental cell lines hereafter). Western blot analysis revealed that those cells not only exhibit loss of the epithelial protein E-CADHERIN, but also upregulation of mesenchymal markers including N-CADHERIN, VIMENTIN, TWIST and SNAIL (Figure 3.13C), suggesting they have undergone an epithelial-to-mesenchymal transition (EMT). Upregulation of the mesenchymal markers N-CADHERIN, VIMENTIN and SNAIL as well as the downregulation of E-CADHERIN was also noticed on mRNA level (Figures 3.13D and 3.13E). Thus, the observed EMT phenotype was apparent in relapsed, refametinib resistant carcinomas and their corresponding isolated tumor cells (Figures 3.13A-3.13E; animal numbers 60409 and 70202).

Table 3.1 Histopathological examination* of H&E stained tumor sections from vehicle and refametinib treated *Kras^{G12D};p53$^{\Delta/\Delta}$* mice.

Animal	Age at death (days)	Treatment	Carcinoma	Size (mm)	Notice
60359	79	refametinib	G2	6	infiltration in bowel wall
60389	72	vehicle	G3/4; ductal, necrosis	3	marked fibrosis
60392	72	refametinib	G4; sarcomatoid	8	infiltration in bowel wall
60396	70	refametinib	G3/4; ductal, necrosis	11	
60397	56	vehicle	G2-G4; ductal, partly sarcomatoid	7	marked fibrosis
60400	55	vehicle	G2/3; ductal	6	marked fibrosis, few PanIN1
60402	100	refametinib	G2/3; ductal	2	PanIN 1, moderate fibrosis
60406	81	refametinib	G2/3; ductal, 25 % necrosis	9	moderate fibrosis
60409	81	refametinib	G4; sarcomatoid	5	
60484	61	vehicle	G3/4; ductal	9	marked fibrosis, few PanIN1
60511	73	refametinib	G2/3; ductal	4	slight fibrosis
60531	75	vehicle	G2/3; ductal	14	
60542	61	vehicle	G2/3; ductal	14	infiltration in bowel wall
60554	54	vehicle	G2/3; ductal	9	
60590	72	vehicle	G3/4; ductal	6+2, bifocal	marked fibrosis
70202	69	refametinib	G4; sarcomatoid	8-9	moderate fibrosis
170518	89	refametinib	G2; ductal, necrosis	5	moderate fibrosis, PanIN1
170523	126	refametinib	G2/3; ductal, large necrosis	8	marked fibrosis

* The histopathological examination was kindly performed by Prof. Bence Sipos M.D., a pathologist at University Hospital Tübingen with expertise in human and mouse PDAC pathology.

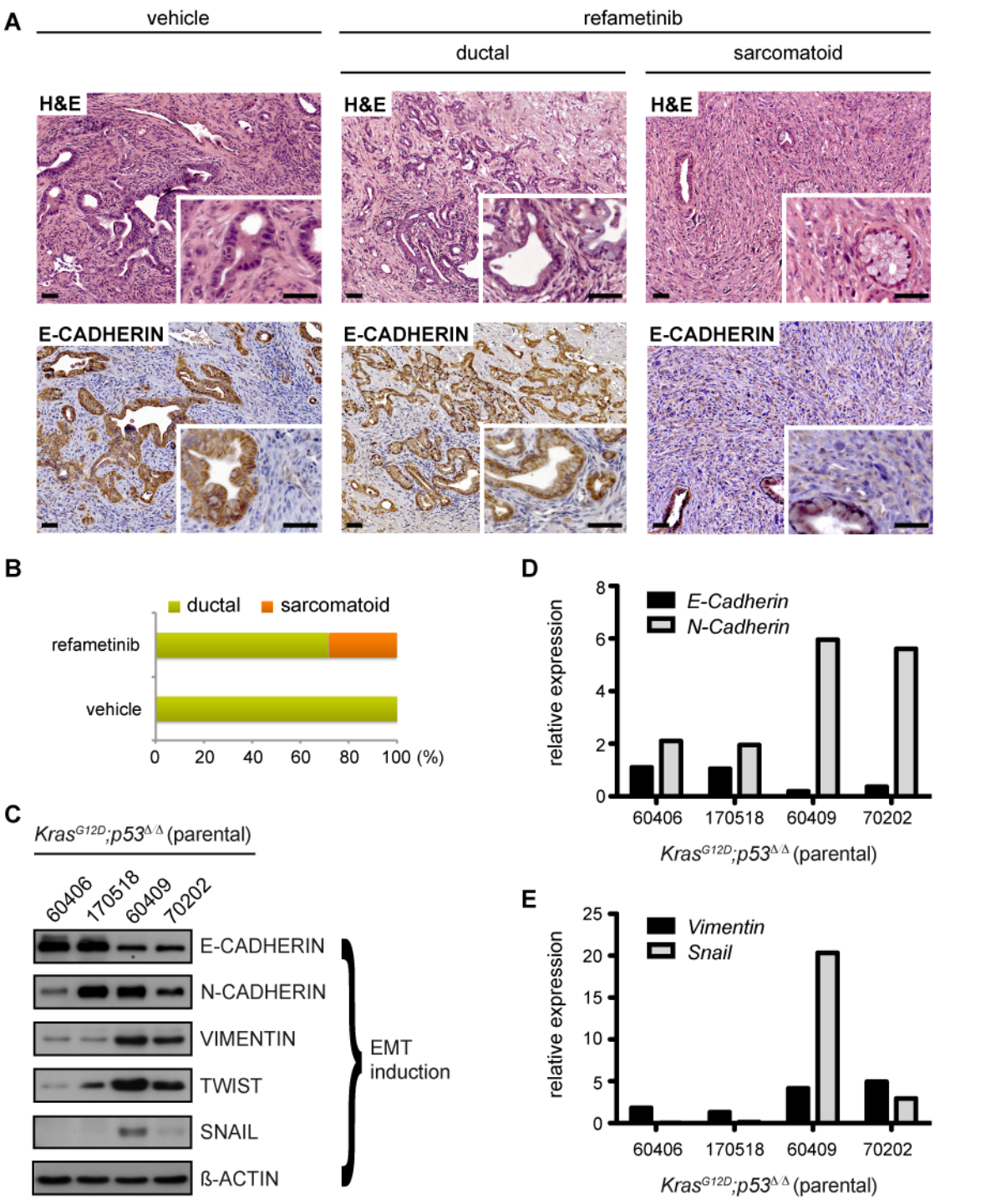

Figure 3.13 Continuous refametinib treatment leads to relapse and appearance of resistant tumors with an EMT phenotype. (A) H&E staining and IHC for E-CADHERIN in *Kras*^{G12D};*p53*$^{\Delta/\Delta}$ pancreata after continuous treatment with refametinib (25 mg/kg bodyweight) or vehicle solution consisting by oral gavage. Scale bars represent 50 µm. (B) Horizontal bar graph showing the percentage of relapsed tumors with a ductal or sarcomatoid appearance in continuously refametinib and vehicle treated *Kras*^{G12D};*p53*$^{\Delta/\Delta}$ mice. (C) Western blot analysis for the epithelial protein E-CADHERIN and the mesenchymal markers N-CADHERIN, VIMENTIN, TWIST and SNAIL from lysates of isolated *Kras*^{G12D};*p53*$^{\Delta/\Delta}$ parental cell lines. ß-ACTIN served as loading control. (D, E) Quantitative real-time-PCR (qRT-PCR) analysis for *E-Cadherin* and *N-Cadherin* (D) as well as *Vimentin* and *Snail* (E) expression levels in *Kras*^{G12D};*p53*$^{\Delta/\Delta}$ parental cell lines. Relative gene expression levels were calculated on the basis of the standard curve method. *Cyclophilin* gene expression was used for normalization. One representative analysis out of three independent performed experiments giving similar results is shown.

Additionally, expression of EMT marker was investigated in several naïve *Kras*^{G12D};*p53*$^{\Delta/\Delta}$ cell lines isolated from animals never treated with refametinib. High and uniform E-CADHERIN protein levels were observed in all of the tested cell lines with varying levels of N-CADHERIN, VIMENTIN and TWIST, suggesting a rather epithelial phenotype of naïve *Kras*^{G12D};*p53*$^{\Delta/\Delta}$ cells (Figure 3.14).

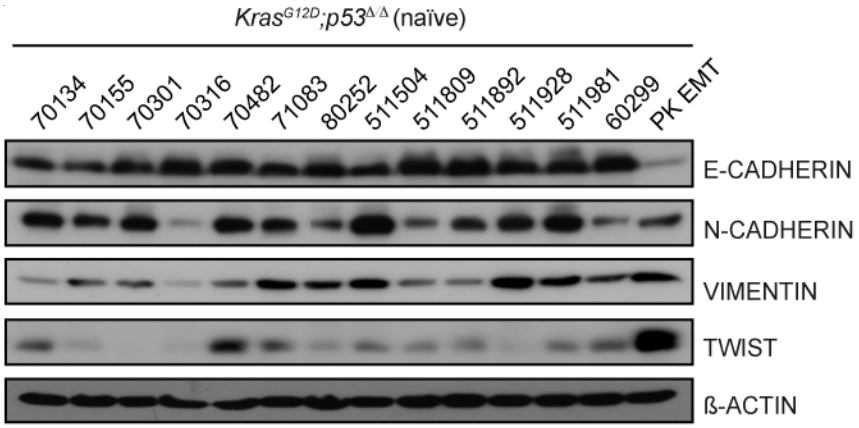

Figure 3.14 Naïve *Kras*^{G12D};*p53*$^{\Delta/\Delta}$ cell lines manifest an epithelial phenotype. Western blot analysis for the epithelial protein E-CADHERIN and the mesenchymal markers N-CADHERIN, VIMENTIN and TWIST from lysates of *Kras*^{G12D};*p53*$^{\Delta/\Delta}$ naïve cell lines isolated from non-treated mice. ß-ACTIN served as loading control.

3.2.2 Relapsed refametinib resistant tumors with persistently active Kras signaling appear in *Kras*^{G12D};*p53*$^{\Delta/\Delta}$ mice continuously treated with refametinib

Naïve *Kras*^{G12D};*p53*$^{\Delta/\Delta}$ cells were also treated for short periods of time with refametinib. Interestingly, an increase in AKT phosphorylation at Serin473 and Threonin308 as well as a KRAS upregulation was detected both on protein and mRNA level (Figure 3.15A and 3.15B).

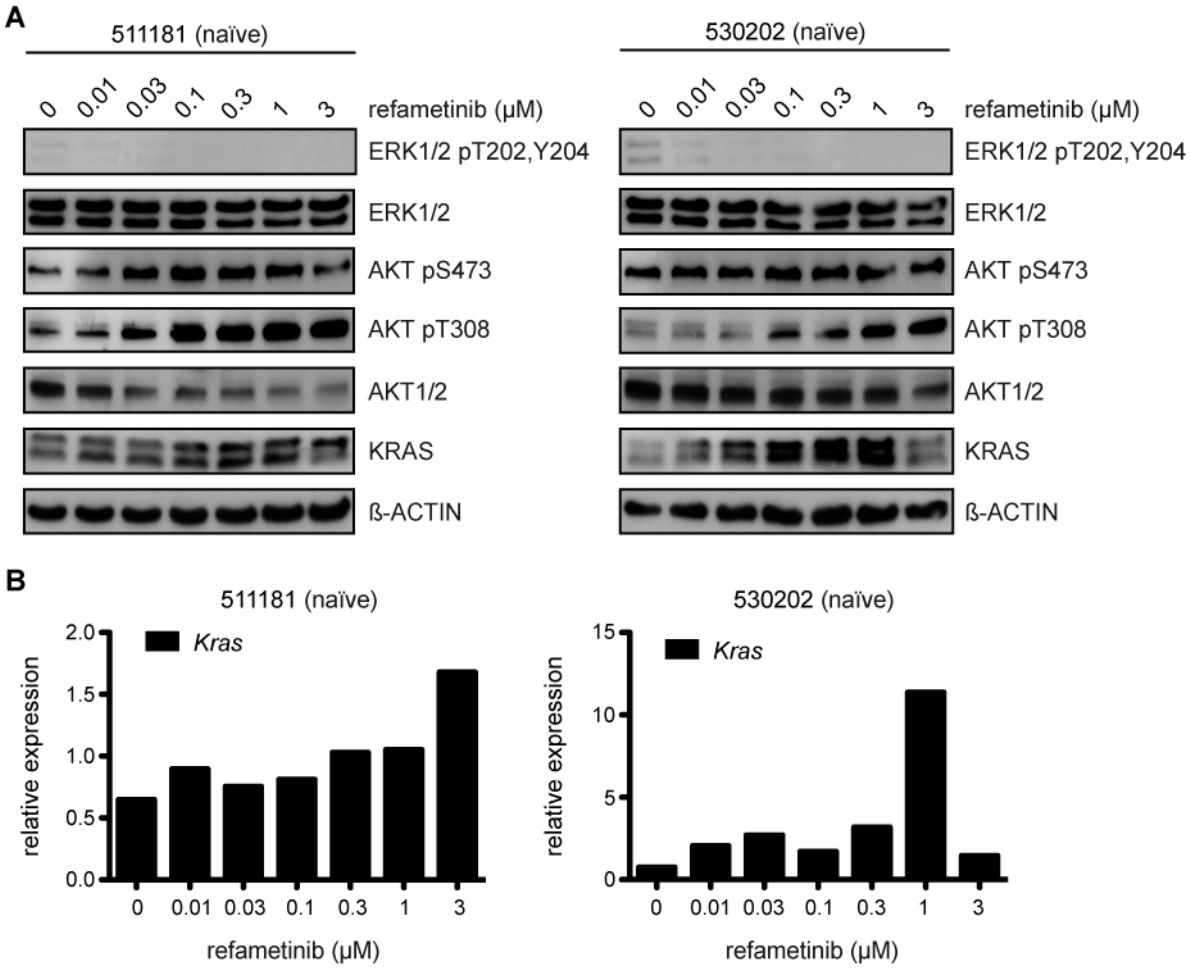

Figure 3.15 Naïve *Kras^{G12D};p53$^{Δ/Δ}$* cell lines exhibit upregulated KRAS and AKT signaling after refametinib treatment. (A) Western blot analysis for ERK1/2 pT202,pT204, AKT pS473, AKT pT308 and KRAS from lysates of *Kras^{G12D};p53$^{Δ/Δ}$* naïve cell lines after treatment with increasing concentrations of refametinib for 72 hours. ß-ACTIN served as loading control. (B) qRT-PCR analysis for *Kras* expression levels in *Kras^{G12D};p53$^{Δ/Δ}$* naïve cell lines after treatment with increasing concentrations of refametinib for 72 hours. Relative gene expression levels were calculated on the basis of the standard curve method. *Cyclophilin* gene expression was used for normalization. One representative analysis out of three independent performed experiments giving similar results is shown.

It was furthermore noted that in comparison to *Kras^{G12D};p53$^{Δ/Δ}$* parental cell lines with ductal-epithelial characteristics (60406 and 170518), also cells with a mesenchymal-like morphology (60409 and 70202) exhibit higher KRAS expression (Figure 3.16B) and active GTP-bound KRAS protein levels (Figure 3.16A) subsequently resulting in activation of RAS effector pathways seen as elevated protein levels of pERK, pAKT, pS6, and p4E-BP1 (Figure 3.16C), indicating a potential role of KRAS signaling in overriding MEK inhibition and in triggering EMT. In line with these results, IHC of relapsed tumors for active pERK1/2 revealed that all tumors independent of ductal or sarcomatoid appearance still exhibit phosphorylated ERK1/2 levels (Figure 3.16D). However, pERK1/2 staining was more

pronounced in sarcomatoid tumors and here mostly detected in the stroma of spindle-shaped mesenchymal cells (Figure 3.16D).

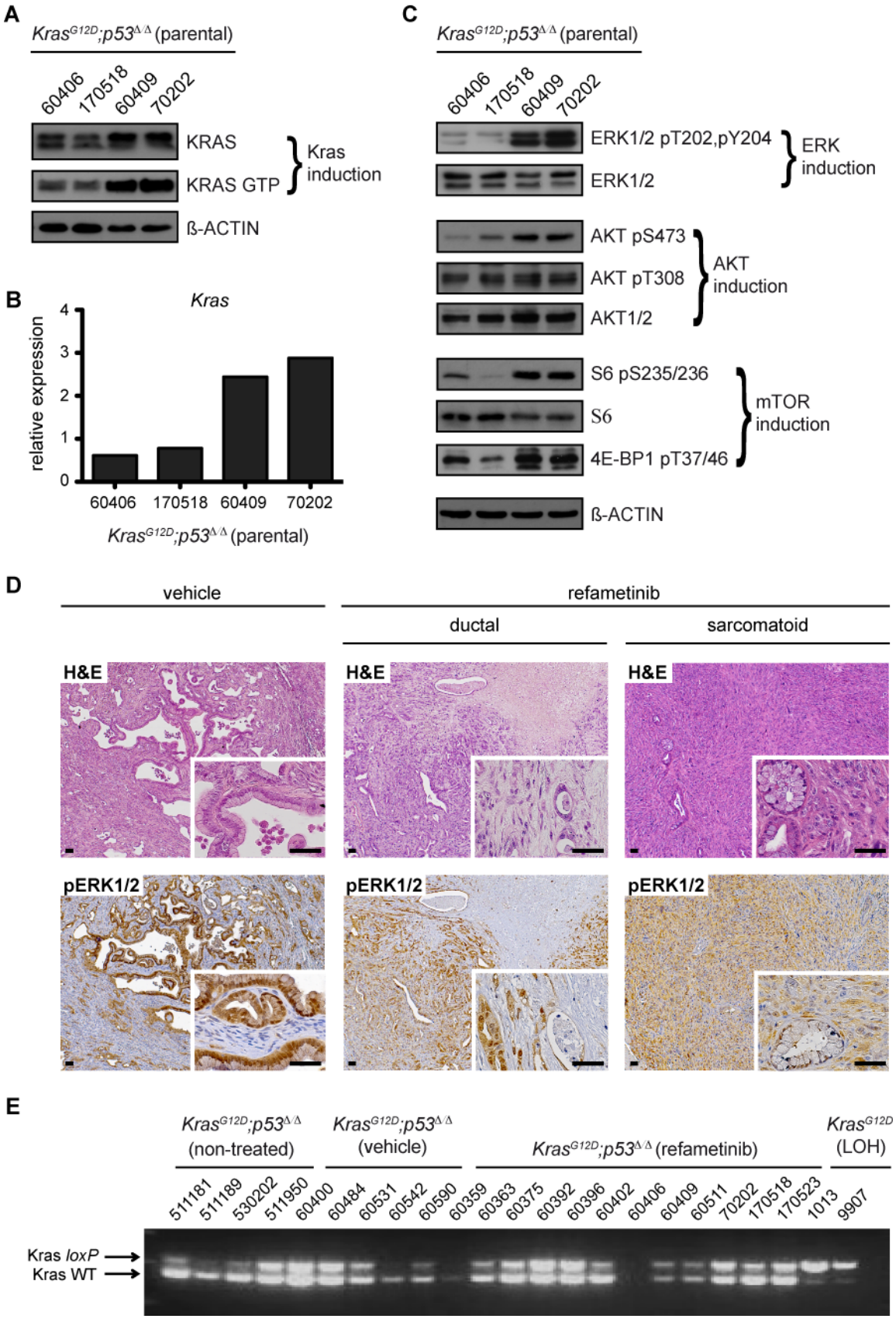

Figure 3.16 Recurrent, refametinib resistant, sarcomatoid tumors exhibit persistently active Kras signaling. (A) Western blot analysis for KRAS and active GTP-bound KRAS from lysates of isolated *Kras^{G12D};p53$^{\Delta/\Delta}$* parental cell lines. ß-ACTIN served as loading control. (B) qRT-PCR analysis for *Kras* expression levels in *Kras^{G12D};p53$^{\Delta/\Delta}$* parental cell lines. Relative gene expression levels were calculated on the basis of the standard curve method. *Cyclophilin* gene expression was used for normalization. One representative analysis out of three independent performed experiments with similar results is shown. (C) Western blot analysis for ERK1/2 pT202,pY204, AKT pS473, AKT pT308, S6 pS235/236 and 4E-BP1 pT37/46 from lysates of isolated *Kras^{G12D};p53$^{\Delta/\Delta}$* parental cell lines. ß-ACTIN served as loading control. (D) H&E staining and IHC for ERK1/2 pT202,pY204 in *Kras^{G12D};p53$^{\Delta/\Delta}$* pancreata after continuous treatment with refametinib (25 mg/kg bodyweight) or vehicle solution by oral gavage. Scale bars represent 50 µm. (E) Specific PCR analysis of genomic DNA from isolated primary murine *Kras^{G12D};p53$^{\Delta/\Delta}$* cell lines either non-, vehicle- or refametinib- treated revealed the expected stop cassette removal and *Kras^{G12D}* activation. *Kras^{G12D}* cell lines (1013 and 9907) showing loss of heterozygosity (LOH) of the remaining WT Kras allele served as positive control.

It is well known that wild-type (WT) KRAS can suppress tumor growth in the presence or absence of the oncogenic counterpart, indicating that WT RAS may have oncosuppressive properties and that loss of this remaining allele promotes tumor progression (James *et al*., 2003; Zhang *et al*., 2001). To determine whether loss of heterozygosity (LOH) is responsible for the observed KRAS induction and thus is involved in the development of resistance to refametinib, a specific PCR analysis of genomic DNA from murine *Kras^{G12D};p53$^{\Delta/\Delta}$* cell lines isolated from either non-, vehicle- or refametinib-treated pancreatic ductal adenocarcinomas was performed. However, none of these cell lines showed LOH of the WT Kras (Figure 3.16E). Consequently, oncogenic activation of mutant KRAS is not associated with a loss of the WT allele in acquiring resistance to refametinib.

3.2.3 EMT and KRAS upregulation are acquired resistance mechanisms to refametinib

Kras amplification and activation of alternative signaling cascades has been previously described as acquired resistance mechanism against MEK1/2 inhibitors (Corcoran *et al*., 2010; Little *et al*., 2011; Singh *et al*., 2009). Furthermore, pancreatic cancer cells of epithelial and mesenchymal characteristics present a different gene expression signature and different degrees of KRAS addiction (Singh *et al*., 2009).

To model MEK1/2 targeted induced resistance *in vitro* and to further investigate whether KRAS and EMT induction are parts of the underlying acquired resistance mechanisms against refametinib, refametinib resistant cell were established. Isolated *Kras^{G12D};p53$^{\Delta/\Delta}$* parental tumor cell lines were continuously treated with increasing concentrations of refametinib until a pool of drug-resistant clones capable of proliferating in a stable dose of refametinib was obtained for each cell line (hereafter referred to as *Kras^{G12D};p53$^{\Delta/\Delta}$* resistant cell lines). *Kras^{G12D};p53$^{\Delta/\Delta}$* resistant cell lines indeed acquired resistance against refametinib

as demonstrated by the dramatic increase in IC_{50} and the attenuated sensitivity (up to more than 100 times) to refametinib (Figure 3.17). Thus, *Kras*^{G12D};*p53*$^{\Delta/\Delta}$ resistant cell lines are resistant to MEK1/2 inhibition with refametinib.

A

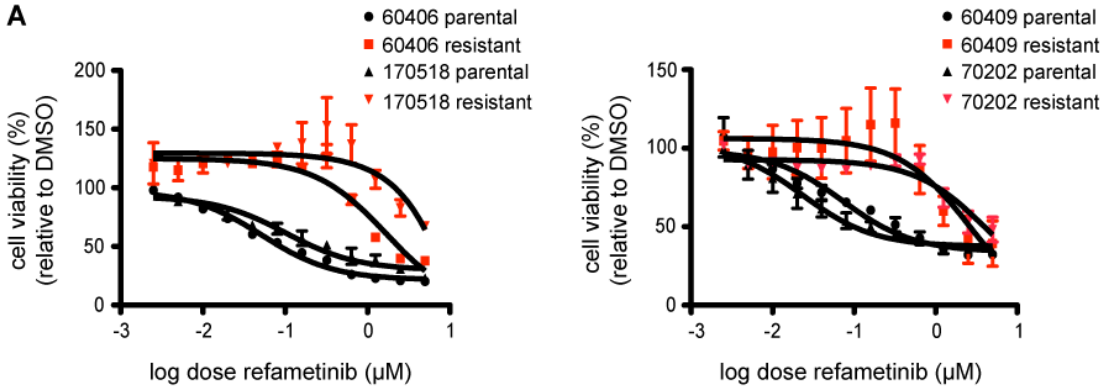

B

cell line	parental	resistant	increase IC_{50}
60406	52 nM	2,28 µM	44x
170518	103 nM	56 µM	543x
60409	73 nM	4,6 µM	63x
70202	24 nM	4,17 µM	174x

Figure 3.17 Long-term refametinib treated *Kras*^{G12D};*p53*$^{\Delta/\Delta}$ cell lines are resistant to MEK1/2 inhibition. (A, B) Dose-response curves of *Kras*^{G12D};*p53*$^{\Delta/\Delta}$ parental and their corresponding resistant cell lines after 72-hour treatment with increasing concentrations of refametinib. Cell viability (%) was calculated relative to DMSO control treatment. Values are mean ± standard deviation of triplicate wells and two independent performed experiments (A). The IC_{50} values for each *Kras*^{G12D};*p53*$^{\Delta/\Delta}$ parental and resistant cell line, as calculated from two independent performed experiments with the GraphPadPrism5 software, and the increase in IC_{50} in *Kras*^{G12D};*p53*$^{\Delta/\Delta}$ resistant cells relative to parental cells are shown in tabular form (B).

Interestingly, as it was already observed in the *Kras*^{G12D};*p53*$^{\Delta/\Delta}$ parental cell lines, all four *Kras*^{G12D};*p53*$^{\Delta/\Delta}$ resistant cells also display the cadherin switch (decrease in *E-cadherin* expression and increase in *N-cadherin* expression) both on mRNA and protein level, which is necessary for EMT induction, as well as a slight upregulation of TWIST und VIMENTIN, thus driving the cells to a mesenchymal phenotype (Figure 3.18A and 3.18B). Surprisingly, changes were most pronounced in cell lines that already demonstrated higher levels of N-CADHERIN, TWIST and VIMENTIN and lower expression of E-CADHERIN, thus suggestive of an intrinsic mesenchymal-like phenotype (60409, 70202).

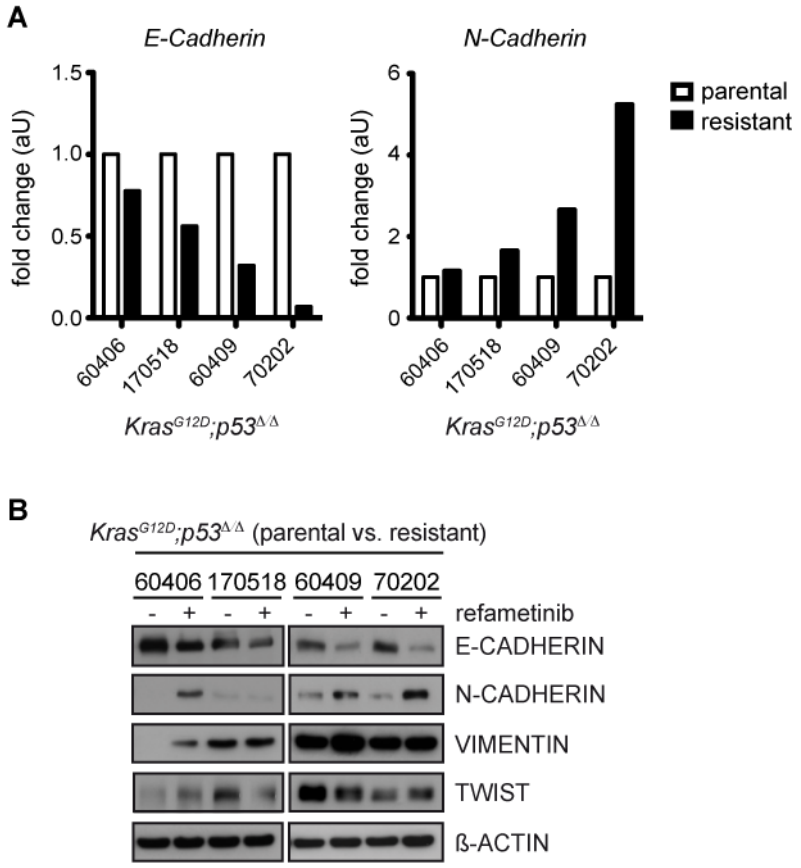

Figure 3.18 *Kras^{G12D};p53$^{Δ/Δ}$* resistant cell lines display the cadherin switch necessary for EMT induction. (A) qRT-PCR analysis for *E-Cadherin* and *N-Cadherin* expression levels in *Kras^{G12D};p53$^{Δ/Δ}$* parental and resistant cell lines. Relative gene expression levels were calculated on the basis of the standard curve method. *Gapdh* gene expression was used for normalization. Values are shown as fold change (arbitrary units, aU) of *Kras^{G12D};p53$^{Δ/Δ}$* resistant cells relative to parental cells. One representative analysis out of three independent performed experiments with similar results is presented. (B) Western blot analysis for the epithelial protein E-CADHERIN and the mesenchymal markers N-CADHERIN, VIMENTIN and TWIST from lysates of *Kras^{G12D};p53$^{Δ/Δ}$* parental and resistant cell lines. ß-ACTIN served as loading control.

Moreover, in comparison to parental cells *Kras^{G12D};p53$^{Δ/Δ}$* resistant cell lines show a markedly increase in *Kras* expression, but not *Hras* or *Nras* expression, as well as elevated KRAS protein levels (Figure 3.19A and 3.19B). Corcoran and colleagues as well as Little *et al*. have previously demonstrated, that an underlying amplification of the driving oncogene promotes the acquired resistance to MEK inhibitors in colorectal cancer and melanoma (Corcoran *et al*., 2010; Little *et al*., 2011). To test if this holds true for PDAC, qRT-PCR was performed using genomic DNA isolated from *Kras^{G12D};p53$^{Δ/Δ}$* parental and resistant cells as a template. However, there is no evidence for an amplification of the *Kras* oncogene (Figure 3.19D), rather suggesting a transcriptional regulation leading to the higher *Kras* mRNA and protein levels seen in refametinib treated resistant cells.

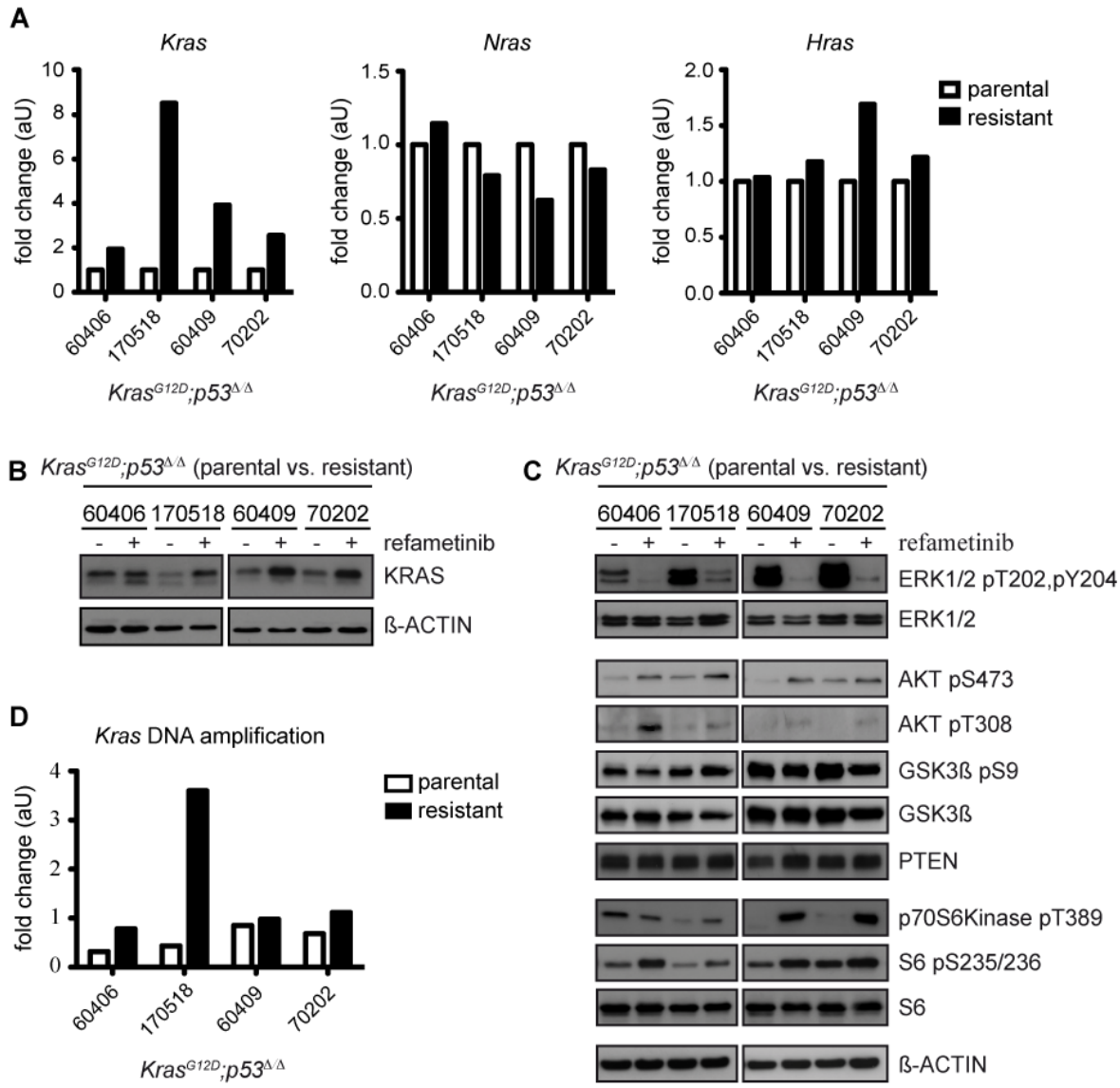

Figure 3.19 *Kras^{G12D};p53$^{Δ/Δ}$* resistant cell lines display persistently active KRAS signaling. (A) qRT-PCR analysis for *Kras*, *Nras* and *Hras* expression levels in *Kras^{G12D};p53$^{Δ/Δ}$* parental and resistant cell lines. Relative gene expression levels were calculated on the basis of the standard curve method. *Cyclophilin* gene expression was used for normalization. Values are shown as fold change (arbitrary units, aU) of *Kras^{G12D};p53$^{Δ/Δ}$* resistant cells relative to parental cells. One representative analysis out of three independent performed experiments giving similar results is presented. (B, C) Western blot analysis for KRAS (B) and other indicated proteins of RAS effector pathways including the PI3K/AKT and mTOR signaling cascade (C) from lysates of *Kras^{G12D};p53$^{Δ/Δ}$* parental and resistant cell lines. ß-ACTIN served as loading control. (D) qRT-PCR analysis of genomic DNA isolated from *Kras^{G12D};p53$^{Δ/Δ}$* parental and resistant cell lines for *Kras* amplification. Relative gene expression levels were calculated on the basis of the delta-delta-CT method. *Rplp0* gene expression was used for normalization. One representative analysis is shown.

Besides the observed KRAS activation, upregulation of phosphorylated AKT kinase (Thr308 and Ser473 residues) as well as of p70S6Kinase and S6, both direct mTOR targets, was also observed demonstrating full activation of the PI3K-AKT-mTOR signaling cascade (Figure 3.19C). Interestingly, all *Kras^{G12D};p53$^{Δ/Δ}$* parental and resistant cell lines exhibit stable protein levels of tumor suppressor phosphatase and tensin homolog deleted

on chromosome 10 (PTEN), a negative regulator of AKT activity (Figure 3.18C). In contrast to *Kras*^{G12D};*p53*$^{\Delta/\Delta}$ parental cells, ERK1/2 activation is still abrogated in *Kras*^{G12D};*p53*$^{\Delta/\Delta}$ resistant cell lines (Figure 3.19C). A compensatory increase in phosphorylation of EGF family as well as IGF1 and Insulin receptor tyrosine kinases that could also account for activation of PI3K-AKT-mTOR cascade was not observed (Figure 3.20).

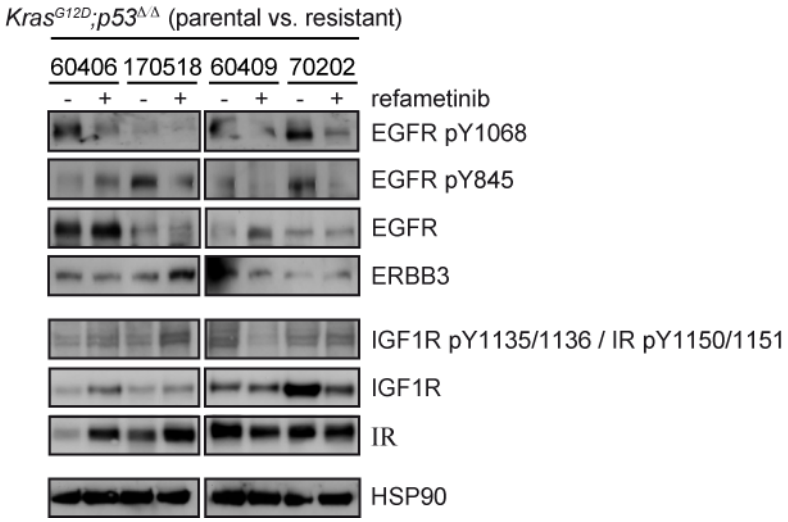

Figure 3.20 EGF receptor and IGF1/Insulin receptor signaling is not compensatory activated in *Kras*^{G12D};*p53*$^{\Delta/\Delta}$ resistant cell lines. Western blot analysis for EGFR pY1068 and pY845, EGFR, ERBB3, IGF1Rß pY1135/1136 / IRß pY1150/1151, IGF1Rß and IRß from lysates of *Kras*^{G12D};*p53*$^{\Delta/\Delta}$ parental and resistant cell lines. HSP90 served as loading control.

3.2.4 Salinomycin and gemcitabine do not selectively kill refametinib resistant cells

It was recently published that salinomycin, a polyether potassium ionophore antibiotic, shows selective toxicity for mesenchymally transdifferentiated breast epithelial cells and breast cancer stem cells as well as therapy-resistant cancer cells (Gupta *et al*., 2009; Naujokat and Steinhart, 2012). To elucidate whether salinomycin selectively kills refametinib long-term treated, resistant *Kras*^{G12D};*p53*$^{\Delta/\Delta}$ cells, cytotoxicity assays were performed to measure cell viability of resistant and parental cells after a 72-hour exposure with increasing concentrations of salinomycin. As shown in Figure 3.21, refametinib resistant *Kras*^{G12D};*p53*$^{\Delta/\Delta}$ cells are less sensitive to salinomycin treatment than their parental counterparts (Figure 3.21).

A

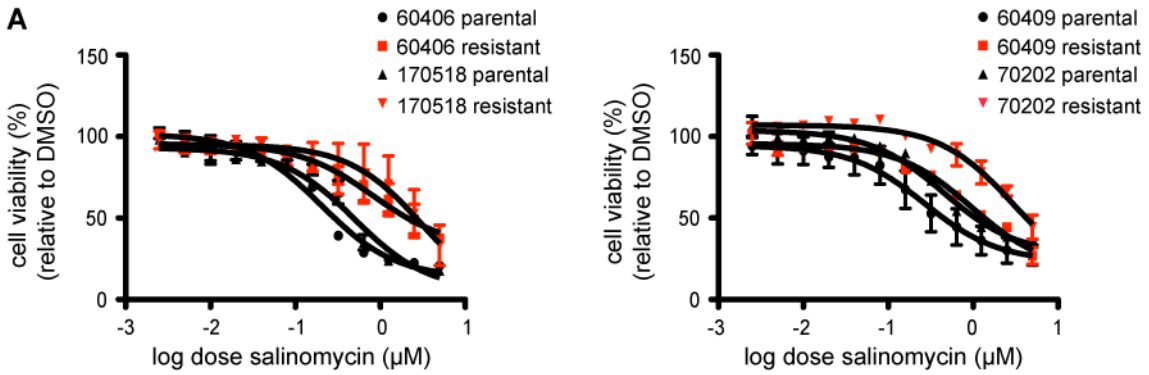

B

cell line	parental	resistant	increase IC_{50}
60406	206 nM	816 nM	4x
170518	500 nM	3,185 µM	6,4x
60409	270 nM	956 nM	3,5x
70202	451 nM	2,987 µM	6,6x

Figure 3.21 *Kras^{G12D};p53$^{\Delta/\Delta}$* resistant cell lines are less sensitive to salinomycin treatment. (A, B) Dose-response curves of *Kras^{G12D};p53$^{\Delta/\Delta}$* parental and their corresponding resistant cell lines after 72-hour treatment with increasing concentrations of salinomycin. Cell viability (%) was calculated relative to DMSO control treatment. Values are mean ± standard deviation of triplicate wells and two independent performed experiments (A). The IC_{50} values for each *Kras^{G12D};p53$^{\Delta/\Delta}$* parental and resistant cell line, as calculated from two independent performed experiments with the GraphPadPrism5 software, and the increase in IC_{50} in *Kras^{G12D};p53$^{\Delta/\Delta}$* resistant cells relative to parental cells are shown in tabular form (B).

Interestingly, similar results were obtained when *Kras^{G12D};p53$^{\Delta/\Delta}$* resistant cell lines were treated with the current standard chemotherapeutic agent for PDAC, gemcitabine. Again, all resistant cells presented lower sensitivity in comparison to their parental counterparts (Figure 3.22).

A

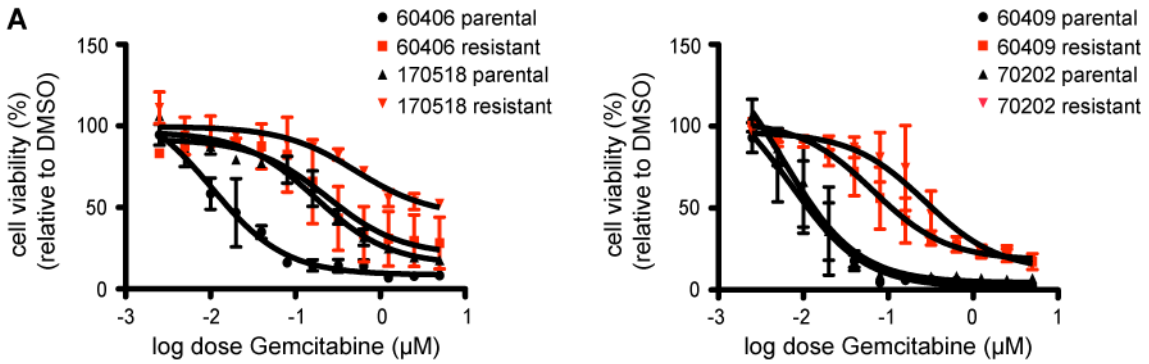

B

cell line	parental	resistant	increase IC_{50}
60406	10 nM	236 nM	24x
170518	175 nM	522 nM	3x
60409	7 nM	66 nM	9x
70202	6 nM	272 nM	45x

Figure 3.22 *Kras^{G12D};p53$^{\Delta/\Delta}$* resistant cell lines are less sensitive to gemcitabine treatment. (A, B) Dose-response curves of *Kras^{G12D};p53$^{\Delta/\Delta}$* parental and their corresponding resistant cell lines after 72-hour treatment with increasing concentrations of gemcitabine. Cell viability (%) was calculated relative to DMSO control treatment. Values are mean ± standard deviation of triplicate wells and three independent performed experiments (A). The IC_{50} values for each *Kras^{G12D};p53$^{\Delta/\Delta}$* parental and resistant cell line, as calculated from three independent performed experiments with the GraphPadPrism5 software, and the increase in IC_{50} in *Kras^{G12D};p53$^{\Delta/\Delta}$* resistant cells relative to parental cells are shown in tabular form (B).

3.2.5 mTOR inhibition with rapamycin efficiently blocks the initial compensatory upregulation of mTOR/pS6 *in vitro*

To overcome the resistance and compensatory induction of AKT induced by constant refametinib treatment, the following PI3K/AKT inhibitors were used: (1) BKM12, a PI3K/AKT inhibitor and (2) BX912, an inhibitor of 3-phosphoinositide-dependent protein kinase 1 (PDK1) - the kinase necessary for partial activation of AKT through phosphorylation at Thr308. However, *Kras^{G12D};p53$^{\Delta/\Delta}$* resistant cell lines displayed only a slightly lower sensitivity to BKM120 treatment than their parental counterparts as demonstrated by the higher BKM120 IC_{50} values measured with cytotoxicity assays (Figure 3.23B). It was also noted that even 5 µM of BKM120 failed to reduce *Kras^{G12D};p53$^{\Delta/\Delta}$* resistant cells' viability by 50 % (Figure 3.23A).

A

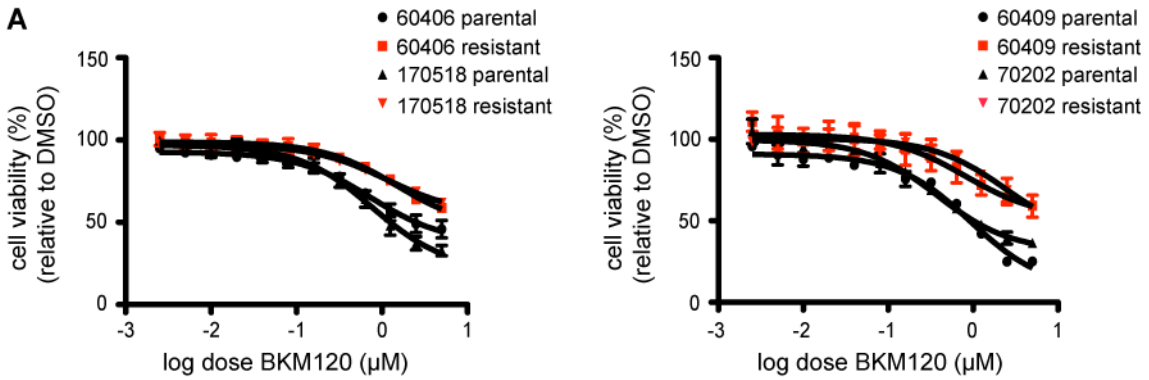

B

cell line	parental	resistant	increase IC_{50}
60406	74 nM	1,495 µM	20x
170518	779 nM	1,15 µM	1,5x
60409	940 nM	815 nM	0,9x
70202	380 nM	2,49 µM	6,6x

Figure 3.23 *Kras^{G12D};p53$^{\Delta/\Delta}$* resistant cell lines are less sensitive to PI3K inhibition with BKM120. (A, B) Dose-response curves of *Kras^{G12D};p53$^{\Delta/\Delta}$* parental and their corresponding resistant cell lines after 72-hour treatment with increasing concentrations of BKM120. Cell viability (%) was calculated relative to DMSO control treatment. Values are mean ± standard deviation of triplicate wells and three independent performed experiments (A). The IC_{50} values for each *Kras^{G12D};p53$^{\Delta/\Delta}$* parental and resistant cell line, as calculated from three independent performed experiments with the GraphPadPrism5 software, and the increase in IC_{50} in *Kras^{G12D};p53$^{\Delta/\Delta}$* resistant cells relative to parental cells are shown in tabular form (B).

Consistent with recent findings, showing that failure to suppress mTORC1 signaling indicates a common resistance mechanism for PI3K inhibitors (Corcoran *et al.*, 2013b; Elkabets *et al.*, 2013), Western blot analysis confirmed that neither the PI3K inhibitor BKM120 nor the PDK1 inhibitor BX912 alone or in combination with refametinib prevented p70S6Kinase and S6 phosphorylation in *Kras^{G12D};p53$^{\Delta/\Delta}$* resistant cells (Figure 3.24). Furthermore, either no or only slight reduction in AKT phosphorylation could be observed by BX912 and BKM120 alone or in combination with refametinib, respectively. These data also indicate that mTOR activity downstream of AKT seems to be critical in conferring resistance to refametinib for MEK1/2 targeted induced resistance and upstream AKT inhibition does not lead to inhibition of mTOR. Consequently, rapamycin (also known as sirolimus), a selective inhibitor of the mTORC1 complex (containing mTOR, RAPTOR, DEPTOR, mLST8 and PRAS40) necessary for phosphorylation of the ribosomal protein S6 kinase (p70S6Kinase) at Thr389 (reviewed in Zoncu *et al.*, 2011), was applied on *Kras^{G12D};p53$^{\Delta/\Delta}$* resistant cells. Rapamycin treatment effectively blocked mTORC1 as evidenced by a loss of p70S6Kinase and S6 phosphorylation in all *Kras^{G12D};p53$^{\Delta/\Delta}$* resistant cell lines. This observed effect was even more pronounced when rapamycin was combined with refametinib (Figure 3.24). Thus, treatment with rapamycin efficiently suppressed the

initial compensatory upregulation of mTOR/pS6 in the resistant lines. Consistent with these data, cytotoxicity assays revealed that already low doses of rapamycin (in the range of nM) decreased the cell viability of *Kras*^{G12D};*p53*$^{\Delta/\Delta}$ resistant cells by already 50 %, whereas even 5 mM of rapamycin failed to diminish parental cells' viability by 50 % (Figure 3.25). However, increasing rapamycin concentrations initiated a plateau phase without further reduction of the viability of both refametinib resistant and parental cells.

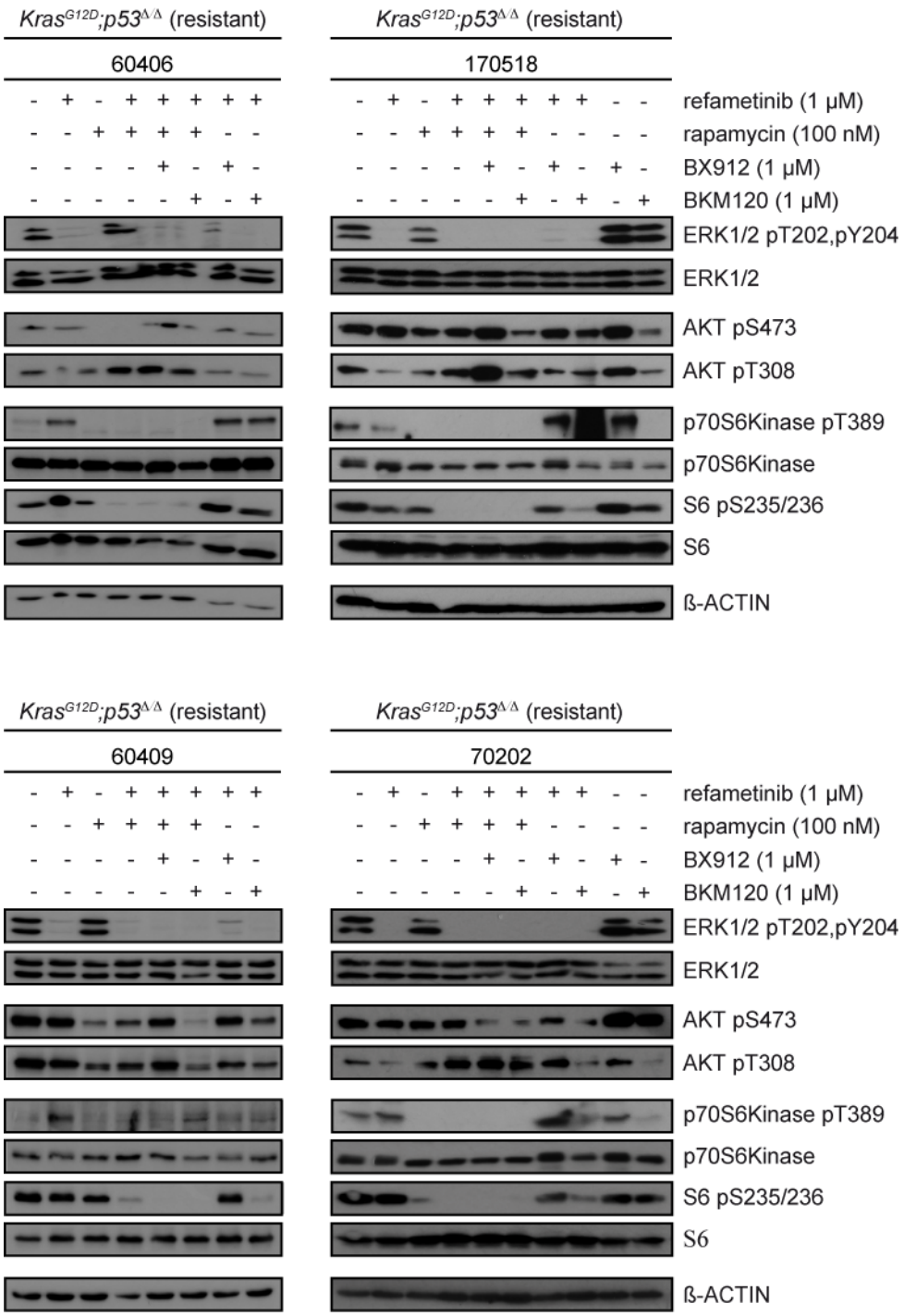

Figure 3.24 Resistance to MEK1/2 inhibition in *Kras^{G12D};p53$^{\Delta/\Delta}$* resistant cells can be partly overcome by the combination treatment with refametinib and rapamycin, but not with refametinib and BX912 or BKM120. Western blot analysis for ERK1/2 pT202,pY204, AKT1/2 pS473 and pT308, p70S6Kinase pT389 and S6 pS235/236 from lysates of *Kras^{G12D};p53$^{\Delta/\Delta}$* resistant cell lines after treatment with either refametinib (1 µM), rapamycin (100 nM), BX912 (1 µM), or BKM120 (1 µM) alone or in indicated combinations for 72 hours. ß-ACTIN served as loading control.

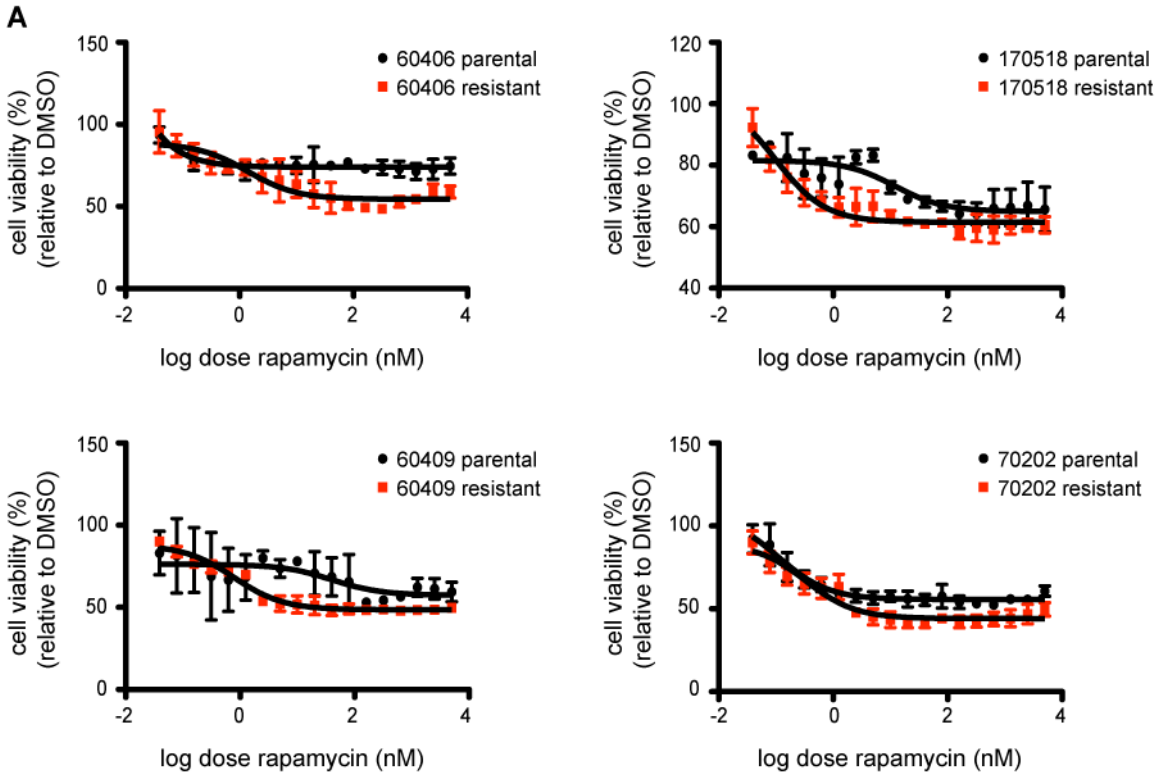

B

cell line	parental	resistant	increase IC_{50}
60406	0,01 nM	1,38 nM	138x
70202	0,11 nM	0,33 nM	3x

cell line	parental	resistant	decrease IC_{50}
170518	11,88 nM	0,1 nM	118x
60409	40,34 nM	0,78 nM	52x

Figure 3.25 Rapamycin decreases the cell viability of *Kras^{G12D};p53$^{\Delta/\Delta}$* resistant cell lines more efficiently. Dose-response curves of *Kras^{G12D};p53$^{\Delta/\Delta}$* parental and their corresponding resistant cell lines after 72-hour treatment with increasing concentrations of rapamycin. Cell viability (%) was calculated relative to DMSO control treatment. Values are mean ± standard deviation of triplicate wells and two independent performed experiments (A). The IC_{50} values for each *Kras^{G12D};p53$^{\Delta/\Delta}$* parental and resistant cell line, as calculated from two independent performed experiments with the GraphPadPrism5 software, and the increase or decrease in IC_{50} in *Kras^{G12D};p53$^{\Delta/\Delta}$* resistant cells relative to parental cells are shown in tabular form (B).

3.2.6 mTOR inhibition with rapamycin decelerates tumor relapses, but cannot overcome resistance to refametinib

The obtained *in vitro* results prompted further analysis of the efficacy of an *in vivo* therapeutic strategy combining refametinib with rapamycin. Rapamycin treatment was started upon tumor withdrawal with refametinib (see dosing scheme Figure 3.26A). If refametinib was given constantly through out the study (see dosing scheme Figure 3.26A), no overall survival benefit was observed (median survival 32 d vs. 34 d, P = 0.6335; Figure 3.26B). In contrast, mice treated with a sequential therapy approach of first 1-2 weeks refametinib and then rapamycin until death (see dosing scheme Figure 3.26A), showed a significant overall survival advantage of eight days compared to their refametinib and vehicle treated counterparts (median survival 32 d vs. 40 d, $^{*}P$ = 0.0293; Figure 3.26B). Noteworthy, a decelerated growth of tumor relapses is visible in responder mice treated with the sequential strategy by MRI (Figure 3.27). However, both treatment regimens did not produce durable responses that would have resulted in a significant survival benefit compared to the refametinib monotherapy. When refametinib was administered alone (please see chapter 3.1.3 for more details), median survival was extended to 43.5 days that could not be further prolonged by the application of rapamycin. Of note, the effects of all drug treatments did not notably affect the body weight of the mice during the treatment course. All treatment regimens were well tolerated with minimal weight losses (less than 10%) that are similar to that of vehicle control (Figure 3.26C and 3.26D).

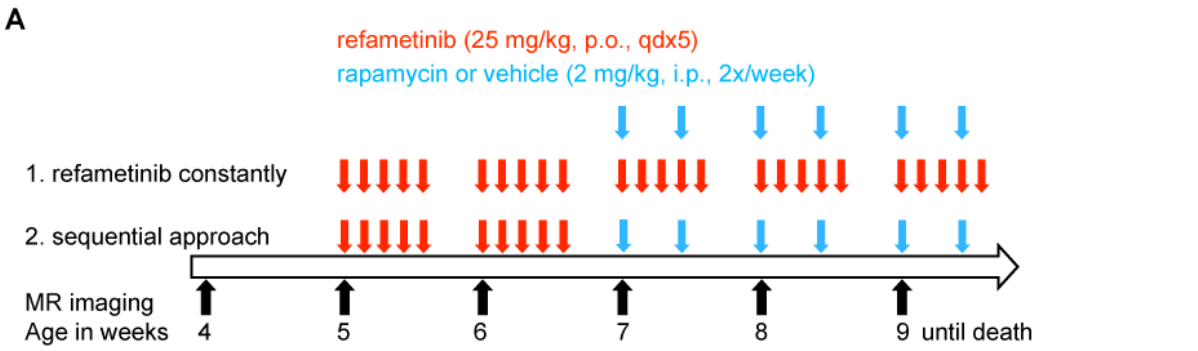

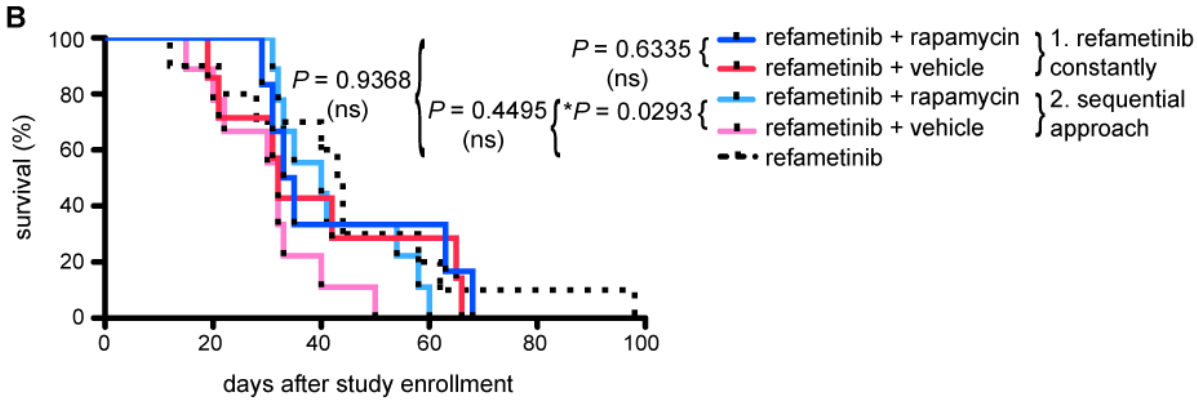

refametinib + rapamycin (constantly)	refametinib + vehicle (constantly)	refametinib + rapamycin (sequential)	refametinib + vehicle (sequential)
n = 6	n = 7	n = 9	n = 9
MS = 32 d	MS = 34 d	MS = 32 d	MS = 40 d

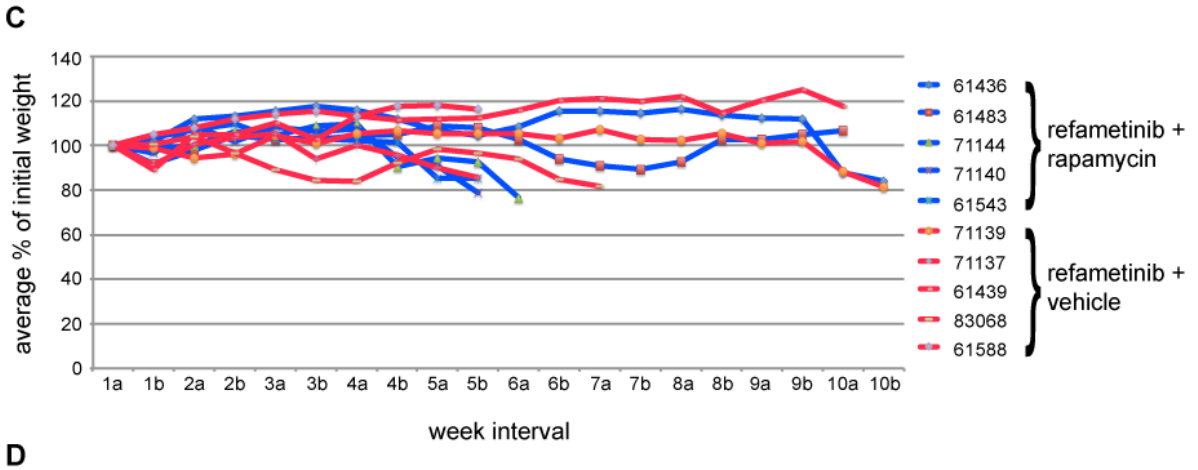

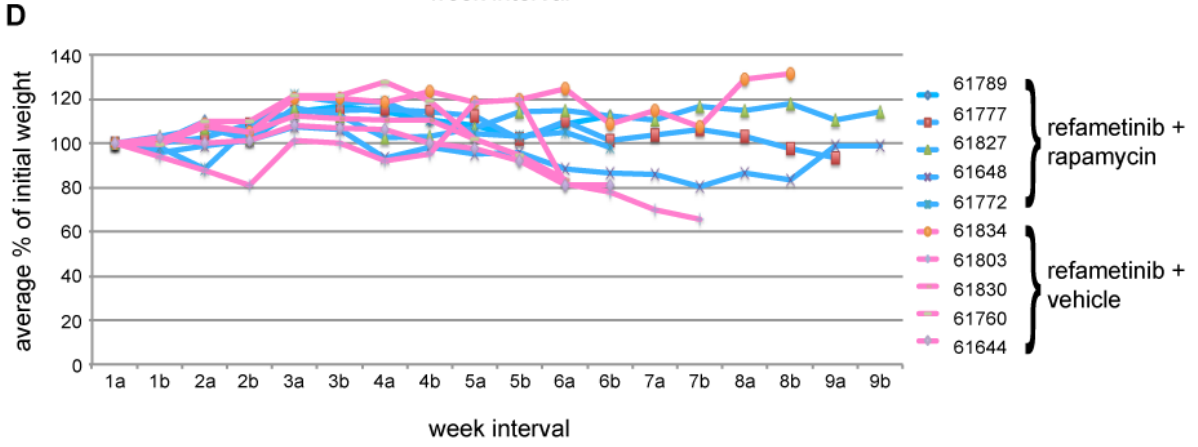

Figure 3.26 Combination of refametinib with rapamycin is not more effective than refametinib monotherapy in *Kras*^{G12D};*p53*$^{\Delta/\Delta}$ mice. (A) Dosing scheme for refametinib plus rapamycin *in vivo* therapeutic strategies. 1. Refametinib constantly: mice were either dosed with refametinib (25 mg/kg bodyweight; five consecutive days a week, qdx5; peroral, p.o.) plus rapamycin (2 mg/kg bodyweight; two doses a week, 2x/week; intraperitoneal, i.p.) or vehicle. 2. Sequential approach: mice were first treated with refametinib (25 mg/kg bodyweight; five consecutive days a week, qdx5; peroral, p.o.) until tumor regression (1-2 weeks) followed by either rapamycin (2 mg/kg bodyweight; two doses a week, 2x/week; intraperitoneal, i.p.) or vehicle injections until death. Weekly MR imaging on a clinical 1.5 T MRI scanner was performed to track tumor progression during the therapy. (B) Kaplan-Meier curves depicting survival (in %) of *Kras*^{G12D};*p53*$^{\Delta/\Delta}$ mice treated with one of the therapeutic strategies (1. refametinib constantly or 2. sequential approach) as indicated in the dosing scheme and refametinib for comparison (black-dotted line). *P* values (either significant, **P*, or statistically not significant, ns) were determined using the log-rank test. The number (n) of mice for each group and the median survival (MS; in days, d) are denoted in the legend. (C) Body weights of *Kras*^{G12D};*p53*$^{\Delta/\Delta}$ study mice treated constantly with refametinib plus either rapamycin or vehicle indicating tolerability of the drug. Mice were weighed daily throughout the course of study and the weight at the beginning and the end of each week (a and b on the x-axis, respectively) are plotted. Weights are represented as the percentage of weight from the study enrollment starting point for each mouse. Five representative mice of each treatment group are shown. (D) Body weights of *Kras*^{G12D};*p53*$^{\Delta/\Delta}$ study mice treated with the sequential approach (first refametinib and after tumor regression rapamycin or vehicle injections) indicating tolerability of drug administration. Mice were weighed daily throughout the course of study and the weight at the beginning and the end of each week (a and b on the x-axis, respectively) are plotted. Weights are represented as the percentage of weight from the study enrollment starting point for each mouse. Five representative mice of each treatment group are shown.

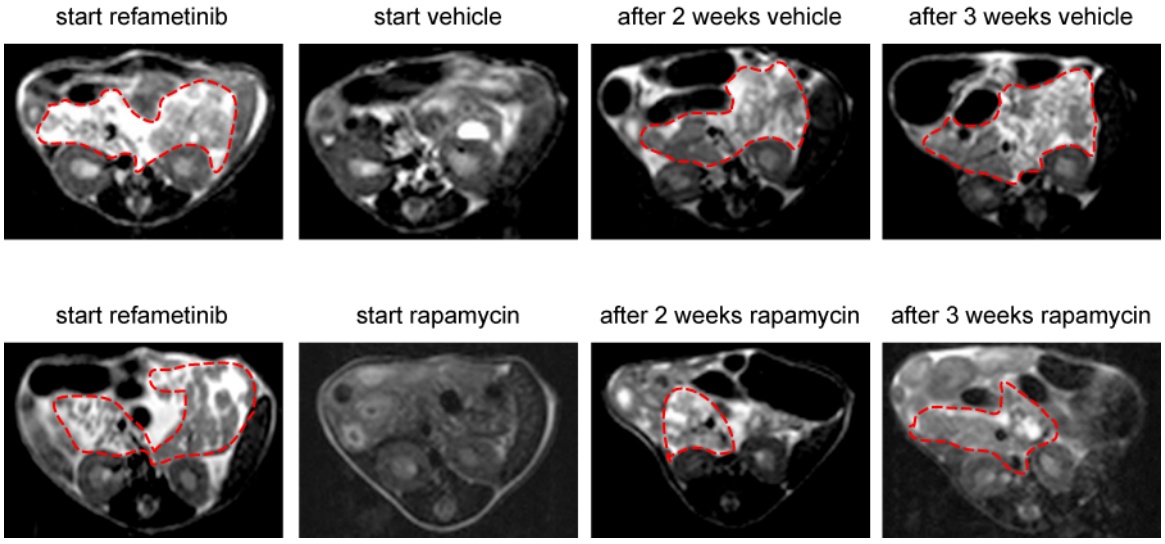

Figure 3.27 Rapamycin decelerates growth of tumor relapses. *Kras*^{G12D};*p53*$^{\Delta/\Delta}$ mice were treated with the sequential approach: first with refametinib (25 mg/kg bodyweight; five consecutive days a week, qdx5; peroral, p.o.) until tumor regression (1-2 weeks) followed by either rapamycin (2 mg/kg bodyweight; two doses a week, 2x/week; intraperitoneal, i.p.) or vehicle (absolute ethanol plus Ringer's saline solution) injections until death. Representative MR images at the therapy starting point with refametinib and either rapamycin or vehicle as well as after two and three weeks of rapamycin or vehicle treatment are shown. Red-doted lines delineate the tumor.

4. Discussion

4.1 Refametinib has potent antitumor activity against PDAC both *in vitro* and *in vivo*

Significant progress in understanding the biology of pancreatic ductal adenocarcinoma (PDAC) has been made in the last few years. Technical advancements and introduction of sophisticated methods, such as next generation DNA sequencing, have allowed whole genome sequencing analysis and identification of common and rare genetic events in PDAC samples with direct clinical implications (Bailey *et al.*, 2016). Genome and transcriptome analyses performed by different groups suggested that PDACs can be classified in genetic and molecular subtypes, which rely on different gene networks, present different histopathological appearance, and are potentially sensitive to different therapeutic approaches (Bailey *et al*., 2016; Collisson *et al*., 2011; Moffitt *et al*., 2015; Noll *et al*., 2016). Bailey and colleagues defined the following four subtypes of them three are directly overlapping with Collisson's nomenclature: (1) squamous (= Collisson's quasimesenchymal subtype); (2) pancreatic progenitor (= Collisson's classical subtype); (3) aberrantly differentiated endocrine exocrine (ADEX) (= Collisson's exocrine-like subtype); and (4) immunogenic (Bailey *et al*., 2016; Collisson *et al*., 2011). However, the Cancer Genome Atlas Network recently only confirmed the existence of two PDAC subtypes, namely the squamous/quasimesenchymal and pancreatic progenitor/classical subtype (Cancer Genome Atlas Research Network, 2017). Collisson and colleagues further showed that gemcitabine and erlotinib (one of the backbones of current treatment regimens (Moore *et al*., 2007), see also chapter 1.3) are preferentially active in these two different PDAC subtypes: the classical subtype is more sensitive to erlotinib and conversely, gemcitabine treatment is more effective in quasimesenchymal tumors (Collisson *et al*., 2011). Additionally, Noll *et al*. determined the drug sensitivity of the exocrine-like subtype showing resistance towards dasatinib, erlotinib, and paclitaxel mediated by a cell autonomous CYP3A5-dependent drug detoxification mechanism (Noll *et al*., 2016). These findings highlight the importance for an improved patient selection process based on tumor subtyping for current available treatment options and for the development of novel therapeutic strategies.

Attempts to modulate different signaling pathways using specific targeted agents has dramatically increased over the last years, but ultimately most of them have so far also failed to improve patients' survival significantly leaving the unchanged picture of PDAC as still being a major clinical challenge in oncology. PDAC belongs to the malignancies with aberrant activation of the mitogen activated protein kinase (MAPK) pathway mainly due to gain-of-function mutations in its driving oncogene KRAS that subsequently leads to constitutively active MEK/ERK signaling and high phosphorylation levels of ERK1/2 (Biankin *et al.*, 2012; Jones *et al.*, 2008). ERK1 and ERK2 are intimately involved in transducing signals from cell surface growth-factor receptors after ligand binding thereby regulating and promoting cell growth, proliferation, and survival (Chang *et al.*, 2003). The present study (Figure 3.1 and Figure 3.2) as well as others have demonstrated that phosphorylated ERK1/2 is upregulated not only in pancreatic premalignant precursor lesions (PanINs) and PDAC cell lines, but also in the vast majority of murine and human PDAC specimens including metastasis to the liver and lungs (Figure 3.1A and Figure 3.2A) (Ardito *et al*., 2012; Chadha *et al*., 2006; Collins *et al*., 2012; Ji *et al*., 2009). As murine WT pancreatic tissue shows only very low ERK1/2 phosphorylation, an upregulation of pERK1/2 during the progression of premalignant mPanIN lesions to invasive PDAC nominates ERK to be a potentially good therapeutic target (Figure 3.2A and Figure 3.2B). In humans, the upregulation of phosphorylated ERK1/2 found in surgically resected pancreatic cancer specimens is associated with a significant shorter median survival of PDAC patients (Chadha *et al*., 2006). Surprisingly, this was not observed in our patient cohort (Figure 3.1D). Patients with low pERK1/2 expression in the PDAC did not survive significantly longer than patients with high pERK1/2 levels (Figure 3.1D).

There are currently no small molecule inhibitors available that can directly modulate ERK1/2 function. Also oncogenic KRAS has been proven to be refractory to direct pharmacological targeting and an effective anti-RAS drug has yet to reach the clinic (Berndt *et al*., 2011; Zeitouni *et al*., 2016). As a consequence, therapeutic approaches for PDAC focus on RAS effector molecules (Cox *et al*., 2014). MEK/ERK signaling is susceptible to pharmacologic intervention (Caunt *et al*., 2015; Samatar and Poulikakos, 2014) and thus dual-specificity protein kinases MEK1 and MEK2 have emerged as an attractive therapeutic target not only due to the fact that they appear to have only one main catalytic substrate ERK1/2, but also due to their unique hydrophobic pocket that allows binding of highly selective allosteric inhibitors that do not compete with ATP binding (non-ATP competitive). To date, small molecule MEK1/2 inhibitors represent the most specific and effective strategy tested to suppress MAPK activity in KRAS mutant cancers (Garnett *et al*., 2012). Furthermore, the use of compounds targeting components of the MAPK

pathway, such as BRAF and MEK1/2 inhibitors, has led to substantial improvement in clinical outcome in metastatic melanoma and has shown promising clinical activity in additional tumor types (reviewed in Samatar and Poulikakos, 2014; Sullivan and Flaherty, 2013). Thus, targeting pERK1/2 seems to be a potential treatment strategy for PDAC.

The selective allosteric MEK1/2 inhibitor CI-1040 first reached phase II clinical evaluation, but its development was then stopped due to insufficient efficacy (Rinehart *et al*., 2004). Two 2nd generation MEK1/2 inhibitors, AZD6244 and PD0325901, which have shown better efficacy than CI-1040 in preclinical models, have then been brought to early clinical development (Adjei *et al*., 2008; Leijen *et al*., 2011; LoRusso *et al*., 2010). Both showed clinical activity, however their effectiveness was mostly limited by their toxicities including skin rash, blurred vision and acute neurotoxicity (Adjei *et al*., 2008; LoRusso *et al*., 2010). As a result of these studies, development of PD0325901 was halted and there has not been an advocacy for AZD6244 as a monotherapy. Refametinib is another highly selective oral allosteric MEK1/2 inhibitor and the only cyclopropane-1-sulfonamide derivative with single-agent activity in preclinical models of melanoma, colon, epidermal, and hepotacellular carcinoma xenografts (Iverson *et al*., 2009; Schmieder *et al*., 2013). Additionally, refametinib has shown potent antitumor activity in human orthotopic primary pancreatic cancer xenografts and a synergistic effect between refametinib and erlotinib was reported in a subset of pancreatic cancer cells and xenografts harboring wild-type KRAS (Chang *et al*., 2010; Diep *et al*., 2011). The aim of this work was to investigate the efficacy and mechanisms of action of refametinib in a GEMM of pancreatic cancer. The current study revealed that refametinib treatment resulted in a marked down-regulation of active pERK1/2 not only at nanomolar concentrations in a broad range of human and murine $Kras^{G12D};p53^{\Delta/\Delta}$ pancreatic tumor cell lines (Figure 3.3A and Figure 3.3.B), but also at clinically achievable concentrations in a GEMM of PDAC driven by the activation of KRAS and the inactivation of p53 ($Ptf1a^{+/Cre};Kras^{+/LSL\text{-}G12D};Trp53^{fl/fl}$; designated $Kras^{G12D};p53^{\Delta/\Delta}$ mice) (Figure 3.3C and Figure 3.3.D). In nearly all animals an unanimous response to refametinib and significant decrease in tumor mass in shortest time was observed. First signs of tumor volume decrease were visible already few days after the onset of therapy (Figure 3.5). Though limited drug delivery to poorly perfused and poorly vascularized PDAC tissue of $Kras^{G12D/+};Trp53^{R172H/+};Pdx\text{-}1\text{-}Cre$ mice as a consequence of strongly developed stroma is often mentioned in PDAC field (Hingorani *et al*., 2005; Jacobetz *et al*., 2013; Olive *et al*., 2009; Provenzano *et al*., 2012), it seems that this was here not the case. *In vivo* experiments presented in this study indicated that the target MEK/ERK pathway was effectively suppressed already after four hours of refametinib administration (Figure 3.3C and Figure 3.3D), suggesting no limitation to drug delivery in this case.

GEMMs have been used as tools to address many different important issues in PDAC, such as tumor development, progression, and resistance as well as characterization and validation of diagnostic strategies (Mazur *et al*., 2015b). Furthermore, their role in preclinical trials as therapy models is still indispensable (Cook *et al*., 2012; Mazur *et al*., 2015b; Mazur and Siveke, 2012). These preclinical models not only take into account the inflammatory response at the tumor side and the vascular network, but also reflect the intratumoral genetic heterogeneity, the strong desmoplastic reaction, and the development of spontaneous metastases. A plethora of mouse models of pancreatic cancer have been developed (reviewed by Mazur and Siveke, 2012) approaching different questions and have dramatically helped our understanding of PDAC. Of them $Kras^{G12D};p53^{\Delta/\Delta}$ mice have been described before (Bardeesy *et al*., 2006). These animals develop highly aggressive PDAC with 100% penetration already in the 5th week of life. Thus, their short life span of 6-8 weeks makes them compelling for preclinical trials needed to be performed in reasonable time periods. Furthermore, these animals develop PDACs histologically resembling the human-like morphology with moderate to poor epithelial differentiation and with an abundant desmoplasia. The predictive value of these mice has been shown in preclinical trials with gemcitabine, where response similar to human was observed (Ardito *et al*., 2012; Olive *et al*., 2009). In this work, a survival study was conducted evaluating the approved first-line combination therapy of gemcitabine plus erlotinib (Moore *et al*., 2007) in $Kras^{G12D};p53^{\Delta/\Delta}$ mice. In comparison to only erlotinib-dosed animals, combination-treated mice showed neither a significant survival benefit nor a reduction in tumor burden (Figure 3.4). Thus, erlotinib does not limit PDAC progression in $Kras^{G12D};p53^{\Delta/\Delta}$ mice. These results reflect the rather limited efficacy of erlotinib plus gemcitabine observed in patients. Therefore, *in vivo* efficacy of refametinib as a single agent was also tested using this mouse model. A dramatic tumor regression seen in all $Kras^{G12D};p53^{\Delta/\Delta}$ animals as early as 1-2 weeks post therapy start subsequently resulting in a pronounced prolongation of survival was not documented for PDAC in any single-agent therapeutic trial so far (Mazur *et al*., 2015a; Morton *et al*., 2010; Olive *et al*., 2009; Singh *et al*., 2010) and hence, these data strongly support potentials of MEK targeting in PDAC. Diep *et al*. showed refametinib being much more effective when combined with erlotinib only in a subset of pancreatic cancer cells and xenografts harboring wild-type KRAS (Diep *et al*., 2011). Other studies also favor MEK1/2 inhibitors as a backbone for combination therapies instead of single agent treatment in PDAC and other KRAS mutant cancers. Alagesan et al. described the MEK1/2 inhibitor AZD6244 as best efficient in a screen on 500 human cancer cell lines and in combination with PI3K inhibitors (Alagesan *et al*., 2015). Corcoran and colleagues reported combined MEK/BCL-XL inhibition as successful in KRAS-driven lung cancer

(Corcoran *et al*., 2013a), Ying *et al*. observed major metabolic reprogramming in a PDAC cancer cell upon MAPK inhibition (Ying *et al*., 2012), and Appleman *et al*. suggest that MEK1/2 inhibitors are successful only in combination with IGF1R inhibitors in pancreatic ductal epithelial cell lines (Appleman *et al*., 2012). Lamba *et al*. have recently reported an excellent synergism of MEK1/2 and RAF inhibitors in KRAS mutant colon and lung cancer cells (Lamba *et al*., 2014), and Roberts *et al*. successfully applied the combination of AZD6244 with the PI3K inhibitor BEZ235 in a melanoma mouse model and two breast cancer GEMMs (Roberts *et al*., 2012). The preclinical study presented here further supports the potential of MEK inhibition as treatment in PDAC.

4.2 Inhibition of MEK1/2 signaling with refametinib induces tumor cell apoptosis

To further address the underlying molecular mechanisms upon MEK1/2 inhibition with refametinib, several *in vitro* assays with a number of human and primary mouse pancreatic tumor cell lines harboring different genetic backgrounds were performed. Cytotoxicity assays and colony forming assays (Figure 3.7) revealed a remarkably reduced cell viability of all tested cell lines irrelevant of their *Kras* mutational status after refametinib exposure with half-maximal inhibitory concentration (IC_{50}) values ranging from 4 nM to 188 nM as similarly observed by Schmieder *et al*. in hepatocellular carcinoma cell lines (Schmieder *et al*., 2013) and similar sensitivity profiles in pancreatic cancer cell lines as reported by Diep *et al*. and Iverson and colleagues (Diep *et al*., 2011; Iverson *et al*., 2009). Also KRAS wild-type BxPc3 cells were sensitive to refametinib single-agent therapy with an IC_{50} of 140 nM. In contrast, the MEK1/2 inhibitor AZD6244 and PD0325901 were described to have only minimal effects on cell viability of BxPc3 cells (Wee *et al*., 2009; Yeh *et al*., 2007). Additionally, *Kras* mutated cell lines were less responsive upon AZD6244 treatment (Yeh *et al*., 2007), whereas refametinib shows a pronounced efficacy especially in cells harboring *Kras* mutations.

The massive tumor regression in $Kras^{G12D};p53^{\Delta/\Delta}$ animals observed even after short exposal to refametinib can potentially be explained by dramatic induction of apoptosis observed both in cell lines and in tumor tissue upon exposure to refametinib (Figure 3.11). In good relation with recent publications (Gillings *et al*., 2009; Ley *et al*., 2003; Wickenden *et al*., 2008), the decrease in cell viability in the present study was a consequence of CASPASE 3/7 dependent apoptosis induction associated with cleaved PARP (Figure 3.9). The Bcl-2 family represents a critical checkpoint for the hierarchical regulation of intrinsic (mitochondrial) apoptosis at a cellular and molecular level (Certo *et al*., 2006; Kim *et al*.,

2006; Willis *et al*., 2003). Others have shown that cell death of human monocytic leukemia cells with the first generation MEK1/2 inhibitor CI-1040 in combination with other agents (e.g. paclitaxel) was dependent in part on the Bcl-2 family (Yu *et al*., 2001). Meng *et al*. found that BIM in particular was key to AZD6244-induced apoptosis in a lung cancer model and Bhalla and colleagues demonstrated that AZD6244 resulted in upregulation of several pro-apoptotic mediators (e.g. p53-up-regulated modulator of apoptosis (PUMA) and BIM) and down-regulation of anti-apoptotic proteins (e.g. Mcl-1 and Bcl-2) (Bhalla *et al*., 2011; Meng *et al*., 2010b). Furthermore, it is known that ERK1/2 can inhibit the activity of several pro-apoptotic proteins, especially of BIM, by promoting its ubiquitination for proteasome-dependent degradation (Ewings *et al*., 2007; Hubner *et al*., 2008; Ley *et al*., 2003). Consistent with these reported findings, an upregulation of all three BIM isoforms in murine $Kras^{G12D};p53^{\Delta/\Delta}$ pancreatic tumor cell lines was observed as early as only 12 hours post treatment (Figure 3.9B). *In vivo*, BIM upregulation was also noticed 12-hour post-dose refametinib administration as seen in Western blot analysis of the tissues (Figure 3.11B). These data suggest that refametinib is possibly responsible for a massive induction of apoptosis in pancreatic cancer tissue that is probably the cause of the striking cancer regression. This strong apoptotic effect of refametinib as monotherapy in murine PDAC has not been observed with other MEK inhibitors so far. Abrogation of MEK-ERK signaling with either AZD6244 or PD0325901 alone appears to stop tumor cell proliferation, but fails to induce apoptosis in KRAS-mutant cell lines of pancreatic, lung, and colorectal tissue (Alagesan *et al*., 2015; Collisson *et al*., 2012; Corcoran *et al*., 2013a; Lamba *et al*., 2014; Wee *et al*., 2009). Only the combination of AZD6244 with additional therapeutic modalities, such as the chemical BCL-XL inhibitor ABT-263 or the PI3K inhibitor BEZ235 or BKM-120, exclusively leads to augmented levels of apoptosis and marked synergistic tumor regressions in KRAS-driven lung and pancreatic cancer mouse models, HRAS-driven melanoma as well as breast cancer GEMMs (Alagesan *et al*., 2015; Corcoran *et al*., 2013a; Engelman *et al*., 2008; Roberts *et al*., 2012).

4.3 Continuous refametinib treatment led to recurrent resistant tumors

Despite the initial enthusiasm and only 2-3 weeks after full regression of the tumor, PDACs did relapse with a penetration rate of 100% (Figure 3.12) that was associated with retained sufficient active pERK1/2 levels in the presence of refametinib (Figure 3.16C and Figure 3.16D). These results reflect the current clinical situation with temporary responses to ERK signaling inhibitors (RAF inhibitors (vemurafenib, dabrafenib) or combinations of

RAF and MEK inhibitors (dabrafenib and trametinib)) in melanoma patients with most relapsing in less than a year (Sullivan and Flaherty, 2013). Several reasons may account for this observation.

Activating mutations within the RAS-RAF-MEK-ERK pathway could contribute to the mechanism of resistance to MEK1/2 inhibitors leading to persistently active ERK1/2 signaling even in the presence of the drug. Even though not evaluated in the present study, acquired mutations of MEK1/2 are very unlikely and are so far only found in very low prevalence of human lung and colon tumors as well as in melanoma, but not in PDAC (Emery *et al*., 2009; Marks *et al*., 2008; Murugan *et al*., 2009; Wang *et al*., 2011). Furthermore, it is a rare exception that a tumor possesses both KRAS and BRAF mutations (Rajagopalan *et al*., 2002). Hence, it is unlikely that BRAF mutations have occurred in the used models to significantly attenuate the ability of refametinib to block ERK1/2 signaling. This needs to be addressed in further analyses.

A number of studies have demonstrated that oncogenic amplification of driving KRAS or BRAF confers decreased susceptibility to AZD6244 (Corcoran *et al*., 2010; Little *et al*., 2011). In this study, no evidence for an underlying amplification of the driving oncogene *Kras* in refametinib resistant PDAC cell lines was observed (Figure 3.19D). However, refametinib treated relapsing tumors did present higher mRNA and protein levels of KRAS (Figure 3.16A and Figure 3.16B) as well as activation of the Kras activity (Figure 3.16A) what has been also observed in mice and humans (Aguirre *et al*., 2003; Heidenblad *et al*., 2002).

Another possibility is that the resistant tumor evolves decreased dependency on ERK1/2 signaling for its growth and survival and activates compensatory signaling cascades of its colossal signaling network. The typical compensatory mechanism involves activation of phosphoinositide-3-kinase (PI3K) signaling. The PI3K-AKT-mTOR and MAPK pathways share RAS as a common upstream activator (Steelman *et al*., 2011). Consequently, activation of KRAS, despite the down-regulation of ERK activity by refametinib, could lead to compensatory signaling through this parallel pathway. Evidence also suggest that MEK and PI3K cascade regulate each other and determine sensitivity of PDAC cells to inhibitors via different mechanisms (Soares *et al*., 2015; Toulany *et al*., 2014; Wee *et al*., 2009). Soares *et al*. proposed that inhibition of the PI3K-AKT-mTOR pathway suppress a novel negative feedback loop mediated by mTORC2, which phosphorylates AKT at Ser473, thereby leading to enhanced MEK/ERK signaling in pancreatic cancer cells (Soares *et al*., 2015). Wee and colleagues have also shown the reverse effect in *KRAS* mutant cells: MEK1/2 inhibition leads to PI3K pathway activation (Wee *et al*., 2009). Additionally, Zmajkovicova *et al.* have shed some light on the mechanism how the MEK/ERK and

PI3K/AKT pathway negatively regulate each other: phosphorylation of MEK1 kinase at Thr292 by activated ERK1/2 is necessary for PTEN membrane recruitment leading in turn to a dephosphorylation of PIP_3 and thus a decreasing PI3K and AKT activity (Zmajkovicova *et al.*, 2013). In the present study, treatment with refametinib indeed resulted in a compensatory activation of AKT/mTOR as observed in *Kras*^{G12D};*p53*$^{\Delta/\Delta}$ parental tumor cell lines isolated from refametinib relapsed tumors (Figure 3.16C). Furthermore, an increase in Kras mRNA and protein levels was also observed in these cells (Figure 3.16A and Figure 3.16B). Both mechanisms have been previously described as response to MEK inhibitors (Corcoran *et al*., 2010; Emery *et al*., 2009; Little *et al*., 2011; Marks *et al*., 2008; Turke *et al*., 2012; Zmajkovicova *et al*., 2013), and are thus likely to be happening in this system, too. It is however worth noting that these two events might not be independent here. Namely, higher KRAS expression levels are very well followed by a higher pAKT/pS6 signaling in cell lines isolated from resistant tumors. Additionally, all of the isolated cell lines responded to further refametinib administration with an increase of KRAS and even further activation of pAKT/pS6 signaling (Figure 3.18). Moreover, the same pattern is observed once naïve *Kras*^{G12D};*p53*$^{\Delta/\Delta}$ cells are short-term dosed with refametinib (Figure 3.15) suggesting that the selective pressure of refametinib treatment is potentially responsible for these changes. This observation imposes the question whether an increase in KRAS levels simultaneously means development of a more prominent RAS dependency and whether this has any effect on therapy outcome? Singh and colleagues recently published that RAS dependency in PDAC implies higher KRAS protein levels connected with expression of markers of a well-differentiated epithelial cancer cell type and general better sensitivity to EGFR and MEK inhibitors. Moreover, KRAS protein levels in KRAS-dependent cells were well correlated with *Kras* gene amplification (Singh *et al*., 2009). Even in primary lung tumors of squamous carcinoma and adenocarcinoma subtypes, well-to-moderately differentiated tumors present a gene expression signature associated with higher KRAS levels (high Ras dependency) while poorly differentiated cancers are associated with a low RAS dependency score. This relationship of a RAS dependency gene signature linked with an epithelial differentiation state was further validated in a *Kras*-driven mouse pancreatic cancer model that develops tumors with varying degrees of differentiated ductal morphology (Singh *et al*., 2009). The increase in KRAS protein levels observed in the current work is in therapy-induced context and cohabitates with a mesenchymal phenotype suggesting a potential role of KRAS in overriding MEK1/2 inhibition by triggering an epithelial-to-mesenchymal transition (EMT) through cadherin switching (Figure 3.18). This phenomenon was also described in primary pancreatic duct epithelial cells (PDECs), where oncogenic KRAS^{V12} promotes the loss of epithelial E-CADHERIN and the gain of

mesenchymal N-CADHERIN (Agbunag and Bar-Sagi, 2004). Induction of EMT is a resistance mechanism observed under treatment with the MEK1/2 inhibitor GSK1120212, too (Jing *et al*., 2012). Indeed, phenotypic status, mesenchymal or epithelial, can determine the sensitivity of pancreatic cancer cells to MEK and EGFR inhibitors and their combination (Mirzoeva *et al*., 2013). Those of mesenchymal phenotype are described as less sensitive to either single inhibitor or the MEK/EGFR combination and once their phenotype is reversed to epithelial, their sensitivity is re-established (Mirzoeva *et al*., 2013). It is thus possible that selective pressure of refametinib on the MEK1 and MEK2 kinases has enforced an EMT switch and appearance of a resistant cancer cell that is not anymore affected by refametinib and that became less dependent on the MAPK pathway. The current results suggest that indeed refametinib is an inducer of EMT. While all PDACs of vehicle-dosed animals are classified as epithelial-ductal, around 20 % of recurrent, refametinib resistant PDACs are found to be sarcomatoid histopathology (Figure 3.13B). Furthermore, areas undifferentiated histopathologies are often seen in relapsing tumors of ductal phenotype. Cancer cell lines that were isolated from relapsed tumors showed also different degrees of epithelial/mesenchymal phenotypes, with 60409 and 70202 being more mesenchymal and 60406 and 170518 being more epithelial (Figure 3.13). However, when isolated and kept in culture under constant selective pressure of refametinib (so established $Kras^{G12D};p53^{\Delta/\Delta}$ resistant cells), they all respond with a decrease in E-CADHERIN, a marker for differentiated epithelia, as well as an increase in different mesenchymal markers already on mRNA level, suggesting even the transcriptional regulation of EMT. This result speaks in favor of an EMT mechanism as part of an acquired resistance mechanism against refametinib. Interestingly, EMT induction was happening in parallel with KRAS induction with being most pronounced in mesenchymal cells (60409 and 70202) (Figure 3.13, Figure 3.16, Figure 3.18 and Figure 3.19). Furthermore, mesenchymal PDACs have also been described as resistant to the combinatorial regimen of MEK and EGFR inhibitors (Mirzoeva *et al*., 2013) going well in line with the quasi-mesenchymal subtype or the squamous subtype when considering the new nomenclature from Bailey and colleagues (Bailey *et al*., 2016) being more sensitive to gemcitabine (Collisson *et al*., 2011). Conversely, erlotinib was found to be more effective in classical or pancreatic progenitor (Bailey *et al*., 2016) PDAC cell lines that not only harbor elevated *Kras* mRNA levels and high expression of adhesion-associated and epithelial genes, but also are relatively more dependent on KRAS itself (Collisson *et al*., 2011). In the present study, treatment with a MEK1/2 inhibitor potentially induced resistance in the originally ductal, epithelial tumor initially sensitive to inhibition of the MEK cascade, as witnessed by initial reduction in tumor volume. Upon longer treatment, the remaining cancer cell changes

its phenotype from ductal and MEK1/2 inhibition sensitive to mesenchymal and MEK1/2 resistant. However, salinomycin failed to selectively kill the refametinib long-term treated, resistant *Kras*^{G12D};*p53*$^{\Delta/\Delta}$ cells (Figure 3.21) and any subtype-specific response to gemcitabine (Figure 3.22), as previously reported for mesenchymal cells by Collisson and colleagues, could not be detected (Collisson *et al*., 2011). Indeed these results are in line with the observations currently reported by Zheng *et al*., who demonstrated an increased sensitivity to gemcitabine only for EMT-negative pancreatic cancer cells isolated from respective pancreatic GEMMs (Zheng *et al*., 2015). Previous studies have confirmed the concept of the cancer cell EMT program being associated with gemcitabine drug resistance in PDAC cell lines, too (Arumugam *et al*., 2009; Shah *et al*., 2007; Wang *et al*., 2009; Yin *et al*., 2007). Such gemcitabine-resistant pancreatic cancer cells were more invasive and migratory and have acquired a spindle-shaped, mesenchymal morphology (Shah *et al*., 2007) through EMT, the most prominent example of cellular plasticity (Smigiel *et al*., 2018). Seminal work by Mani *et al*. and Morel *et al*. now link EMT with the acquisition of cancer stem cell (CSC) properties (Mani *et al*., 2008; Morel *et al*., 2008), and cells harboring CSC properties are afforded an enhanced ability to survive therapy (Smigiel *et al*., 2018). Consistently, an enhanced frequency of EMT-positive cancer cells in pancreatic tumors is associated with poor survival (Javle *et al*., 2007; Masugi *et al*., 2010). Additionally, it was shown by Collisson *et al.* that individuals with classical subtype tumors fared better than individuals with quasimesenchymal-PDAC subtype tumors after resection (Collisson *et al*., 2011). Bailey and colleagues further identified the squamous PDAC subtype as an independent poor prognostic factor (Bailey *et al*., 2016). More recent studies have shown that not only cell-intrinsic, but more importantly also external stimuli, such as oncogenes (e.g. *Kras*) and cytotoxic therapies (e.g. gemcitabine), induce cellular plasticity within epithelial/non-CSC cells, thus driving their transitioning through intermediary stages until reaching a mesenchymal/CSC state (Baer *et al*., 2014; Krebs *et al*., 2017; Smigiel *et al*., 2017). Mueller and colleagues further associated the mesenchymal phenotype with *Kras*^{G12D} expression above a certain threshold supporting a role of *Kras*^{G12D} dosage variation in shaping cellular phenotypes (Mueller *et al*., 2018). The results of this work underpin these current hypotheses of cells undergoing cellular plasticity suggesting a role of oncogenic *Kras* in rendering cells from their original, epithelial, drug-tolerant state to a cell state escaping the targeted therapy with refametinib followed by a repopulation of the original tumor at the primary site.

4.4 Rapamycin cannot overcome refametinib acquired resistance

It has been noted in the literature that disruption of the EGFR-MAPK signaling pathway can shift signaling to PI3K-AKT as a mode to maintain cell survival (Buck *et al*., 2008; Normanno *et al*., 2006; Sergina *et al*., 2007). Hence, a novel, EGFR-dependent functional feedback loop was discovered in breast and colorectal cancer cell lines harboring RAS mutations that resulted in PI3K activation upon MEK inhibition (Ebi *et al*., 2011; Mirzoeva *et al*., 2009). A similar feedback mechanism was then described by Diep and colleagues for KRAS wild-type PDAC cells (Diep *et al*., 2011) that was further confirmed by Collisson *et al.* in both KRAS wild-type and mutated human PDAC cell lines (Collisson *et al*., 2012). In line with these results, compensatory PI3K-AKT-mTOR pathway activation, as determined by markedly enhanced protein levels of AKT pSer473 and pThr308 as well as p70S6Kinase pT389 and S6 pSer235/236, was observed in response to MEK1/2 inhibition with refametinib in this study (Figure 3.16). However, an enhanced phosphorylation of EGFR in the $Kras^{G12D};p53^{\Delta/\Delta}$ refametinib resistant cell lines could not be detected (Figure 3.20) and thus, a EGFR dependency of PI3K activation, as recently described also for a panel of human PDAC cell lines by Mirzoeva *et al.* under different experimental conditions (Mirzoeva *et al*., 2013), could be ruled out in my system. Furthermore, the previously published autocrine activation of IGF1R downstream of MEK1/2 in PDECs (Appleman *et al*., 2012) could also not account for the subsequent compensatory stimulation of PI3K/AKT signaling in my system as an increased phosphorylation of IGF1R was not observed (Figure 3.20). Thus, these results speak in favor for oncogenic KRAS itself being predominantly responsible for the direct activation of the PI3K-AKT-mTOR cascade underlining the hypothesis that refametinib resistant cells are still dependent on KRAS function despite their reduced MAPK pathway dependency.

One approach to overcome the extensive crosstalk between MEK and PI3K pathways in KRAS mutant cancer types is the combinatorial targeting of both MEK1/2 and PI3K/AKT. This therapeutic strategy has led to synergistic effects in PDAC and lung cancer cell lines (Collisson *et al*., 2012; Meng *et al*., 2010a) and synergistically enhanced tumor apoptosis *in vivo* (Engelman *et al*., 2008; Wee *et al*., 2009). However, downstream of PI3K/AKT functions mTOR, a catalytic subunit of two distinct multiprotein complexes: mTORC1 and mTORC2 (Zoncu *et al*., 2011). Activation of mTORC1, a key regulator of cellular growth and protein synthesis containing mTOR, RAPTOR, DEPTOR, mLST8, and proline-rich Akt substrate of 40 kDa (PRAS40), is at least mediated by phosphorylated AKT (at Thr308) that negatively regulates tuberous sclerosis protein complex 1 (TSC1) and TSC2. Activated

mTORC1 in turn phosphorylates and controls the 40S ribosomal protein subunit S6 kinase (p70S6Kinase) and the translational repressor 4E-binding protein 1, referred to as 4E-BP1. mTORC2, a complex including mTOR, rapamycin-insensitive companion of mTOR (RICTOR), protein observed with RICTOR-2 (PROTOR2), DEPTOR, mLST8, and mammalian stress-activated map kinase-interacting protein 1 (mSIN1), is responsible for the phosphorylation of several protein kinases, such as AKT at Ser473 leading to its full activation (Zoncu *et al*., 2011). Recent findings demonstrated that failure to suppress mTORC1 signaling represents a common resistance mechanism for PI3K inhibitors (Corcoran *et al*., 2013b; Elkabets *et al*., 2013). Moreover, there is equilibrium between the mTORC1 and mTORC2 complexes in cells, meaning that the assembly of the mTORC1 complex in cancer cells with elevated levels of AKT is higher than in those cells that do not exhibit markedly AKT overexpression and are thus characterized by a higher assembly rate of mTORC2 (Chappell *et al*., 2011). Subsequently, cancer cells with high levels of activated AKT should be more sensitive to mTORC1-inhibiting agents, such as rapamycin. As a consequence, mTORC1 has emerged as an attractive therapeutic target in PDAC and other common malignancies. The relevance of mTOR-mediated signals to PDAC is further supported by reports demonstrating that mTOR and its downstream components are constitutively active in pancreatic cancer cell lines and tissues and that rapamycin inhibits the proliferation of pancreatic cancer cells (Grewe *et al*., 1999; Shah *et al*., 2001). Additionally, mTOR functions to maintain the stem cell-like properties of pancreatic CSCs (Matsubara *et al*., 2013). In line with this recently identified critical role, targeting mTOR alone (Matsubara *et al*., 2013) or in combination with c-MET signaling (Zeng *et al*., 2014) showed a striking reduction in the viability of a $CD133^+$ CSC population. Thus, it was reasonable to rely on mTOR inhibition by the macrolide rapamycin in a tryout to overcome MEK1/2 inhibitor treatment induced resistance, as was also previously published for PDAC xenografts (Chang *et al*., 2010). Indeed, rapamycin decreased p70S6Kinase and S6 phosphorylation in all $Kras^{G12D};p53^{\Delta/\Delta}$ refametinib resistant cells and this observed effect was even more pronounced upon combined rapamycin and refametinib administration (Figure 3.24). Additionally, a potent growth-inhibitory effect of all refametinib resistant cells was detected in response to rapamycin (Figure 3.25). However *in vivo*, neither the combination of refametinib and rapamycin, nor a sequential therapy of refametinib first and rapamycin once the PDACs regressed provided a survival benefit for $Kras^{G12D};p53^{\Delta/\Delta}$ animals compared to the refametinib monotherapy (Figure 3.26). Thus, these findings suggest that the combination therapy may not offer marked improvement although signaling studies indicate that target pathways are effectively suppressed.

4.5 Conclusion

Limited progress has been made in treating PDAC over the recent years, and it is often challenging to evaluate new agents in patients due to the rapid progression of disease and the difficulty in monitoring the response to therapies. Overall, the results of the present study intriguingly demonstrate that uncoupling the hyperactivated RAS-RAF-MEK-ERK cascade in pancreatic cancer is possible with refametinib and provides clinically significant responses in a genetically and histologically faithful GEMM of PDAC never seen before with any MEK1/2 inhibitor single-agent therapy in any tumor entity. My results also emphasize the fact that monotherapeutic approaches, though initially successful, are still not curative and provide only a short-term benefit as resistance emerges rapidly. Hence, detailed characterization and overcoming this resistance are major hurdles in PDAC clinical management. The in this study identified acquired resistance mechanism to refametinib involving KRAS upregulation, AKT/mTOR activation and EMT ultimately needs to be validated through the analysis of pancreatic cancer specimens from PDAC patients, who have received refametinib. Nevertheless, determining the correct combination necessary to completely suppress RAS-MEK-ERK signaling without causing unacceptable toxicities is also desperately needed to improve the clinical success rate of targeted therapies especially for KRAS mutant tumors, such as PDAC, and the benefit to patients. Based on my findings, ongoing clinical development of refametinib as well as the exploration of novel combinatorial strategies involving MEK inhibitors and agents capable of reversing EMT is warranted.

5. Summary

Pancreatic ductal adenocarcinoma (PDAC) is still lacking curative approaches despite intensive academic research and tremendous industrial efforts within the past decades and thus remains one of the deadliest malignancies in western countries with a dismal average life expectancy of less than six month after diagnosis. Driven by its fundamental hallmark, the widely considered undruggable *KRAS* oncogene, PDAC harbors a significant proportion of constitutively activated signaling cascades, such as the RAS-RAF-MEK-ERK or MAPK pathway, that not only regulate proliferation and survival, but are also important players in pancreatic tumor development and maintenance. Given the pivotal position that MEK1/2 occupies within the MAPK signal transduction cascade, its narrow substrate specificity to only native ERK1/2 proteins and its unique hydrophobic pocket that allows for the interaction of selective “allosteric” inhibitors, targeting the MEK molecule has become an attractive approach of blocking the hyperactivated RAS-RAF-MEK-ERK pathway in different tumor entities. In particular, the present study aims to evaluate the novel, allosteric MEK1/2 inhibitor refametinib as a potential therapeutic strategy for PDAC using a GEMM-based preclinical research platform.

First of all, ERK1 and ERK2 were validated as therapeutic targets for pancreatic cancer. Using $Kras^{G12D}$-driven genetically engineered mouse models (GEMMs) and murine PDAC cells it was demonstrated that both kinases are upregulated during the progression of premalignant mPanIN lesions to invasive PDAC. In addition, elevated levels of phosphorylated ERK1/2 were noted in human PDAC specimens and human PDAC cell lines with only a few samples being completely pERK1/2-negative implying also an important role of active pERK1/2 during human pancreatic tumorigenesis. Consequently, pERK1/2 seems to be an ideal candidate for a targeted therapy of PDAC.

Secondly, *in vitro* and *in vivo* responses to the highly selective MEK1/2 inhibitor refametinib as well as the underlying molecular mechanisms upon MEK1/2 inhibition were closely elucidated. Refametinib treatment efficiently blocked phosphorylation of ERK1/2 *in vitro* in human and murine primary pancreatic cancer cell lines as well as *in vivo* in $Kras^{G12D};p53^{\Delta/\Delta}$ mice. Hence, ERK1/2 substrates were down-regulated by refametinib including the pro-apoptotic protein BIM leading to a time- and dose-dependent cell viability reduction mainly attributable to an apoptosis induction in all tested human and murine pancreatic cancer cells. This pronounced cytotoxic effect was also responsible for the massive tumor shrinkage seen in all refametinib-dosed $Kras^{G12D};p53^{\Delta/\Delta}$ mice with nearly no cancer tissue

remainings observable by MRI one to two weeks after treatment start. Cell death was both caspase 3/7 dependent and associated with cleaved PARP. Additionally, the profound and durable ERK1/2 inhibition combined with the striking tumor regression prolonged the overall survival of *Kras*^{G12D};*p53*$^{\Delta/\Delta}$ mice significantly with a median survival advantage of 26 days compared to their vehicle-treated counterparts. In contrast, the standard-of-care combination therapy gemcitabine plus erlotinib failed to limit PDAC progression in *Kras*^{G12D};*p53*$^{\Delta/\Delta}$ mice with no reduction in tumor burden and no increase in life expectancy. Thus, these preclinical data strongly support the notion that refametinib is a novel promising chemotherapeutic agent for the treatment of pancreatic cancer.

Despite continuous treatment with refametinib, pancreatic cancers reappeared in all animals approximately three weeks post-therapy onset and were successively growing till death. This relapse was partly followed by a change in PDAC subtype. Tumors in around 20 % of refametinib-treated animals showed mesenchymal characteristics including the typical cadherin switch (N-cadherin upregulation and E-cadherin down-regulation) and were histologically characterized as sarcomatoid. Furthermore, recurrent, refametinib resistant tumors with an EMT phenotype exhibited persistently active KRAS signaling subsequently resulting in compensatory activation of the downstream PI3K-AKT-mTOR cascade. Finally, it was shown that the induction of a mesenchymal phenotype as well as the amplification of KRAS signaling, but without an underlying amplification of the *Kras* oncogene itself, and RAS effector pathways are indeed acquired resistance mechanisms to refametinib and that refametinib resistance can partly be overcome by rapamycin treatment *in vitro*. Rapamycin, an inhibitor of the mTOR kinase, also decelerates tumor relapses *in vivo* when applied in a sequential approach to refametinib, but could not further prolong the overall survival of *Kras*^{G12D};*p53*$^{\Delta/\Delta}$ mice compared to the refametinib monotherapy.

Taken together, the provoking results of the current work not only give an insight how pharmacological intervention of the MAPK pathway limits PDAC progression, but also are of great benefit for further enhancing existing treatment strategies targeting this colossal signaling network to improve pancreatic cancer patient’s quality of life.

6. References

Adachi, M., Fukuda, M., and Nishida, E. (2000). Nuclear export of MAP kinase (ERK) involves a MAP kinase kinase (MEK)-dependent active transport mechanism. J Cell Biol *148*, 849-856.

Adamska, A., Domenichini, A., and Falasca, M. (2017). Pancreatic Ductal Adenocarcinoma: Current and Evolving Therapies. Int J Mol Sci *18*.

Adell, T., Gomez-Cuadrado, A., Skoudy, A., Pettengill, O. S., Longnecker, D. S., and Real, F. X. (2000). Role of the basic helix-loop-helix transcription factor p48 in the differentiation phenotype of exocrine pancreas cancer cells. Cell Growth Differ *11*, 137-147.

Adjei, A. A., Cohen, R. B., Franklin, W., Morris, C., Wilson, D., Molina, J. R., Hanson, L. J., Gore, L., Chow, L., Leong, S.*, et al.* (2008). Phase I pharmacokinetic and pharmacodynamic study of the oral, small-molecule mitogen-activated protein kinase kinase 1/2 inhibitor AZD6244 (ARRY-142886) in patients with advanced cancers. J Clin Oncol *26*, 2139-2146.

Agbunag, C., and Bar-Sagi, D. (2004). Oncogenic K-ras drives cell cycle progression and phenotypic conversion of primary pancreatic duct epithelial cells. Cancer Res *64*, 5659-5663.

Aguirre, A. J., Bardeesy, N., Sinha, M., Lopez, L., Tuveson, D. A., Horner, J., Redston, M. S., and DePinho, R. A. (2003). Activated Kras and Ink4a/Arf deficiency cooperate to produce metastatic pancreatic ductal adenocarcinoma. Genes Dev *17*, 3112-3126.

Aichler, M., Seiler, C., Tost, M., Siveke, J., Mazur, P. K., Da Silva-Buttkus, P., Bartsch, D. K., Langer, P., Chiblak, S., Durr, A.*, et al.* (2012). Origin of pancreatic ductal adenocarcinoma from atypical flat lesions: a comparative study in transgenic mice and human tissues. J Pathol *226*, 723-734.

Alagesan, B., Contino, G., Guimaraes, A. R., Corcoran, R. B., Deshpande, V., Wojtkiewicz, G. R., Hezel, A. F., Wong, K. K., Loda, M., Weissleder, R.*, et al.* (2015). Combined MEK and PI3K inhibition in a mouse model of pancreatic cancer. Clin Cancer Res *21*, 396-404.

Anderson, N. G., Maller, J. L., Tonks, N. K., and Sturgill, T. W. (1990). Requirement for integration of signals from two distinct phosphorylation pathways for activation of MAP kinase. Nature *343*, 651-653.

Apelqvist, A., Li, H., Sommer, L., Beatus, P., Anderson, D. J., Honjo, T., Hrabe de Angelis, M., Lendahl, U., and Edlund, H. (1999). Notch signalling controls pancreatic cell differentiation. Nature *400*, 877-881.

Appleman, V. A., Ahronian, L. G., Cai, J., Klimstra, D. S., and Lewis, B. C. (2012). KRAS(G12D)- and BRAF(V600E)-induced transformation of murine pancreatic epithelial cells requires MEK/ERK-stimulated IGF1R signaling. Mol Cancer Res *10*, 1228-1239.

Ardito, C. M., Grüner, B. M., Takeuchi, K. K., Lubeseder-Martellato, C., Teichmann, N., Mazur, P. K., Delgiorno, K. E., Carpenter, E. S., Halbrook, C. J., Hall, J. C.*, et al.* (2012). EGF receptor is required for KRAS-induced pancreatic tumorigenesis. Cancer Cell *22*, 304-317.

Arumugam, T., Ramachandran, V., Fournier, K. F., Wang, H., Marquis, L., Abbruzzese, J. L., Gallick, G. E., Logsdon, C. D., McConkey, D. J., and Choi, W. (2009). Epithelial to mesenchymal transition contributes to drug resistance in pancreatic cancer. Cancer Res *69*, 5820-5828.

Baer, R., Cintas, C., Dufresne, M., Cassant-Sourdy, S., Schonhuber, N., Planque, L., Lulka, H., Couderc, B., Bousquet, C., Garmy-Susini, B.*, et al.* (2014). Pancreatic cell plasticity and cancer initiation induced by oncogenic Kras is completely dependent on wild-type PI 3-kinase p110alpha. Genes Dev *28*, 2621-2635.

Bailey, P., Chang, D. K., Nones, K., Johns, A. L., Patch, A. M., Gingras, M. C., Miller, D. K., Christ, A. N., Bruxner, T. J., Quinn, M. C.*, et al.* (2016). Genomic analyses identify molecular subtypes of pancreatic cancer. Nature *531*, 47-52.

Bardeesy, N., Aguirre, A. J., Chu, G. C., Cheng, K. H., Lopez, L. V., Hezel, A. F., Feng, B., Brennan, C., Weissleder, R., Mahmood, U.*, et al.* (2006). Both p16(Ink4a) and the p19(Arf)-p53 pathway constrain progression of pancreatic adenocarcinoma in the mouse. Proc Natl Acad Sci U S A *103*, 5947-5952.

Bardeesy, N., and DePinho, R. A. (2002). Pancreatic cancer biology and genetics. Nat Rev Cancer *2*, 897-909.

Bay, N. S., and Bay, B. H. (2010). Greek anatomist herophilus: the father of anatomy. Anat Cell Biol *43*, 280-283.

Beer, R. L., Parsons, M. J., and Rovira, M. (2016). Centroacinar cells: At the center of pancreas regeneration. Dev Biol *413*, 8-15.

Belanger, L. F., Roy, S., Tremblay, M., Brott, B., Steff, A. M., Mourad, W., Hugo, P., Erikson, R., and Charron, J. (2003). Mek2 is dispensable for mouse growth and development. Mol Cell Biol *23*, 4778-4787.

Bendetz-Nezer, S., and Seger, R. (2005). Full molecular page of MEK1. AfCS/Nature Signaling Gateway (doi:10.1038/mp.a001505.01).

Berndt, N., Hamilton, A. D., and Sebti, S. M. (2011). Targeting protein prenylation for cancer therapy. Nat Rev Cancer *11*, 775-791.

Bhalla, S., Evens, A. M., Dai, B., Prachand, S., Gordon, L. I., and Gartenhaus, R. B. (2011). The novel anti-MEK small molecule AZD6244 induces BIM-dependent and AKT-independent apoptosis in diffuse large B-cell lymphoma. Blood *118*, 1052-1061.

Biankin, A. V., Kench, J. G., Dijkman, F. P., Biankin, S. A., and Henshall, S. M. (2003). Molecular pathogenesis of precursor lesions of pancreatic ductal adenocarcinoma. Pathology *35*, 14-24.

Biankin, A. V., Waddell, N., Kassahn, K. S., Gingras, M. C., Muthuswamy, L. B., Johns, A. L., Miller, D. K., Wilson, P. J., Patch, A. M., Wu, J.*, et al.* (2012). Pancreatic cancer genomes reveal aberrations in axon guidance pathway genes. Nature *491*, 399-405.

Branda, C. S., and Dymecki, S. M. (2004). Talking about a revolution: The impact of site-specific recombinases on genetic analyses in mice. Dev Cell *6*, 7-28.

Brennan, D. F., Dar, A. C., Hertz, N. T., Chao, W. C., Burlingame, A. L., Shokat, K. M., and Barford, D. (2011). A Raf-induced allosteric transition of KSR stimulates phosphorylation of MEK. Nature *472*, 366-369.

Brott, B. K., Alessandrini, A., Largaespada, D. A., Copeland, N. G., Jenkins, N. A., Crews, C. M., and Erikson, R. L. (1993). MEK2 is a kinase related to MEK1 and is differentially expressed in murine tissues. Cell Growth Differ *4*, 921-929.

Brune, K. A., and Klein, A. P. (2008). Familial Pancreatic Cancer. In A. M. Lowy *et al*. (eds.), Pancreatic Cancer, 65-79. Springer (ISBN 9780387692500).

Buck, E., Eyzaguirre, A., Rosenfeld-Franklin, M., Thomson, S., Mulvihill, M., Barr, S., Brown, E., O'Connor, M., Yao, Y., Pachter, J.*, et al.* (2008). Feedback mechanisms promote cooperativity for small molecule inhibitors of epidermal and insulin-like growth factor receptors. Cancer Res *68*, 8322-8332.

Bulle, A., Dekervel, J., van der Merwe, S., Van Cutsem, E., Verslype, S., and van Pelt, J. (2017). Relevance of the stroma in pancreatic ductal adenocarcinoma and its challenges for translational research. J Cancer Treat & Diagnosis *2*,1-15.

Burris, H. A., 3rd, Moore, M. J., Andersen, J., Green, M. R., Rothenberg, M. L., Modiano, M. R., Cripps, M. C., Portenoy, R. K., Storniolo, A. M., Tarassoff, P.*, et al.* (1997). Improvements in survival and clinical benefit with gemcitabine as first-line therapy for patients with advanced pancreas cancer: a randomized trial. J Clin Oncol *15*, 2403-2413.

Caldas, C., and Kern, S. E. (1995). K-ras mutation and pancreatic adenocarcinoma. Int J Pancreatol *18*, 1-6.

Cancer Genome Atlas Research Network. Electronic address, a. a. d. h. e., and Cancer Genome Atlas Research, N. (2017). Integrated Genomic Characterization of Pancreatic Ductal Adenocarcinoma. Cancer Cell *32*, 185-203 e113.

Catalanotti, F., Reyes, G., Jesenberger, V., Galabova-Kovacs, G., de Matos Simoes, R., Carugo, O., and Baccarini, M. (2009). A Mek1-Mek2 heterodimer determines the strength and duration of the Erk signal. Nat Struct Mol Biol *16*, 294-303.

Caunt, C. J., Sale, M. J., Smith, P. D., and Cook, S. J. (2015). MEK1 and MEK2 inhibitors and cancer therapy: the long and winding road. Nat Rev Cancer *15*, 577-592.

Certo, M., Del Gaizo Moore, V., Nishino, M., Wei, G., Korsmeyer, S., Armstrong, S. A., and Letai, A. (2006). Mitochondria primed by death signals determine cellular addiction to antiapoptotic BCL-2 family members. Cancer Cell *9*, 351-365.

Chadha, K. S., Khoury, T., Yu, J., Black, J. D., Gibbs, J. F., Kuvshinoff, B. W., Tan, D., Brattain, M. G., and Javle, M. M. (2006). Activated Akt and Erk expression and survival after surgery in pancreatic carcinoma. Ann Surg Oncol *13*, 933-939.

Chang, F., Steelman, L. S., Lee, J. T., Shelton, J. G., Navolanic, P. M., Blalock, W. L., Franklin, R. A., and McCubrey, J. A. (2003). Signal transduction mediated by the Ras/Raf/MEK/ERK pathway from cytokine receptors to transcription factors: potential targeting for therapeutic intervention. Leukemia *17*, 1263-1293.

Chang, Q., Chapman, M. S., Miner, J. N., and Hedley, D. W. (2010). Antitumour activity of a potent MEK inhibitor RDEA119/BAY 869766 combined with rapamycin in human orthotopic primary pancreatic cancer xenografts. BMC Cancer *10*, 515.

Chappell, W. H., Steelman, L. S., Long, J. M., Kempf, R. C., Abrams, S. L., Franklin, R. A., Basecke, J., Stivala, F., Donia, M., Fagone, P*., et al.* (2011). Ras/Raf/MEK/ERK and PI3K/PTEN/Akt/mTOR inhibitors: rationale and importance to inhibiting these pathways in human health. Oncotarget *2*, 135-164.

Collins, M. A., Bednar, F., Zhang, Y., Brisset, J. C., Galban, S., Galban, C. J., Rakshit, S., Flannagan, K. S., Adsay, N. V., and Pasca di Magliano, M. (2012). Oncogenic Kras is required for both the initiation and maintenance of pancreatic cancer in mice. J Clin Invest *122*, 639-653.

Collisson, E. A., Sadanandam, A., Olson, P., Gibb, W. J., Truitt, M., Gu, S., Cooc, J., Weinkle, J., Kim, G. E., Jakkula, L*., et al.* (2011). Subtypes of pancreatic ductal adenocarcinoma and their differing responses to therapy. Nat Med *17*, 500-503.

Collisson, E. A., Trejo, C. L., Silva, J. M., Gu, S., Korkola, J. E., Heiser, L. M., Charles, R. P., Rabinovich, B. A., Hann, B., Dankort, D*., et al.* (2012). A central role for RAF-->MEK-->ERK signaling in the genesis of pancreatic ductal adenocarcinoma. Cancer Discov *2*, 685-693.

Conroy, T., Desseigne, F., Ychou, M., Bouche, O., Guimbaud, R., Becouarn, Y., Adenis, A., Raoul, J. L., Gourgou-Bourgade, S., de la Fouchardiere, C*., et al.* (2011). FOLFIRINOX versus gemcitabine for metastatic pancreatic cancer. N Engl J Med *364*, 1817-1825.

Cook, N., Jodrell, D. I., and Tuveson, D. A. (2012). Predictive in vivo animal models and translation to clinical trials. Drug Discov Today *17*, 253-260.

Cook, N., Olive, K. P., Frese, K., and Tuveson, D. A. (2008). K-Ras-driven pancreatic cancer mouse model for anticancer inhibitor analyses. Methods in enzymology *439*, 73-85.

Corcoran, R. B., Cheng, K. A., Hata, A. N., Faber, A. C., Ebi, H., Coffee, E. M., Greninger, P., Brown, R. D., Godfrey, J. T., Cohoon, T. J*., et al.* (2013a). Synthetic lethal interaction of combined BCL-XL and MEK inhibition promotes tumor regressions in KRAS mutant cancer models. Cancer Cell *23*, 121-128.

Corcoran, R. B., Dias-Santagata, D., Bergethon, K., Iafrate, A. J., Settleman, J., and Engelman, J. A. (2010). BRAF gene amplification can promote acquired resistance to MEK inhibitors in cancer cells harboring the BRAF V600E mutation. Science signaling *3*, ra84.

Corcoran, R. B., Rothenberg, S. M., Hata, A. N., Faber, A. C., Piris, A., Nazarian, R. M., Brown, R. D., Godfrey, J. T., Winokur, D., Walsh, J.*, et al.* (2013b). TORC1 suppression predicts responsiveness to RAF and MEK inhibition in BRAF-mutant melanoma. Science translational medicine *5*, 196ra198.

Cox, A. D., Fesik, S. W., Kimmelman, A. C., Luo, J., and Der, C. J. (2014). Drugging the undruggable RAS: Mission possible? Nat Rev Drug Discov *13*, 828-851.

Crews, C. M., Alessandrini, A., and Erikson, R. L. (1992). The primary structure of MEK, a protein kinase that phosphorylates the ERK gene product. Science *258*, 478-480.

Davies, B. R., Logie, A., McKay, J. S., Martin, P., Steele, S., Jenkins, R., Cockerill, M., Cartlidge, S., and Smith, P. D. (2007). AZD6244 (ARRY-142886), a potent inhibitor of mitogen-activated protein kinase/extracellular signal-regulated kinase kinase 1/2 kinases: mechanism of action in vivo, pharmacokinetic/pharmacodynamic relationship, and potential for combination in preclinical models. Mol Cancer Ther *6*, 2209-2219.

Diep, C. H., Munoz, R. M., Choudhary, A., Von Hoff, D. D., and Han, H. (2011). Synergistic effect between erlotinib and MEK inhibitors in KRAS wild-type human pancreatic cancer cells. Clin Cancer Res *17*, 2744-2756.

Dudley, D. T., Pang, L., Decker, S. J., Bridges, A. J., and Saltiel, A. R. (1995). A synthetic inhibitor of the mitogen-activated protein kinase cascade. Proc Natl Acad Sci U S A *92*, 7686-7689.

Ebi, H., Corcoran, R. B., Singh, A., Chen, Z., Song, Y., Lifshits, E., Ryan, D. P., Meyerhardt, J. A., Benes, C., Settleman, J.*, et al.* (2011). Receptor tyrosine kinases exert dominant control over PI3K signaling in human KRAS mutant colorectal cancers. J Clin Invest *121*, 4311-4321.

Edlund, H. (2002). Pancreatic organogenesis--developmental mechanisms and implications for therapy. Nat Rev Genet *3*, 524-532.

Elkabets, M., Vora, S., Juric, D., Morse, N., Mino-Kenudson, M., Muranen, T., Tao, J., Campos, A. B., Rodon, J., Ibrahim, Y. H.*, et al.* (2013). mTORC1 inhibition is required for sensitivity to PI3K p110alpha inhibitors in PIK3CA-mutant breast cancer. Science translational medicine *5*, 196ra199.

Emery, C. M., Vijayendran, K. G., Zipser, M. C., Sawyer, A. M., Niu, L., Kim, J. J., Hatton, C., Chopra, R., Oberholzer, P. A., Karpova, M. B.*, et al.* (2009). MEK1 mutations confer resistance to MEK and B-RAF inhibition. Proc Natl Acad Sci U S A *106*, 20411-20416.

Engelman, J. A., Chen, L., Tan, X., Crosby, K., Guimaraes, A. R., Upadhyay, R., Maira, M., McNamara, K., Perera, S. A., Song, Y.*, et al.* (2008). Effective use of PI3K and MEK inhibitors to treat mutant Kras G12D and PIK3CA H1047R murine lung cancers. Nat Med *14*, 1351-1356.

Eser, S., Schnieke, A., Schneider, G., and Saur, D. (2014). Oncogenic KRAS signalling in pancreatic cancer. Br J Cancer *111*, 817-822.

Esposito, I., Konukiewitz, B., Schlitter, A. M., and Kloppel, G. (2012). [New insights into the origin of pancreatic cancer. Role of atypical flat lesions in pancreatic carcinogenesis]. Pathologe *33 Suppl 2*, 189-193.

Esposito, I., Konukiewitz, B., Schlitter, A. M., and Kloppel, G. (2014). Pathology of pancreatic ductal adenocarcinoma: facts, challenges and future developments. World J Gastroenterol *20*, 13833-13841.

Ewings, K. E., Hadfield-Moorhouse, K., Wiggins, C. M., Wickenden, J. A., Balmanno, K., Gilley, R., Degenhardt, K., White, E., and Cook, S. J. (2007). ERK1/2-dependent phosphorylation of BimEL promotes its rapid dissociation from Mcl-1 and Bcl-xL. Embo J *26*, 2856-2867.

Falchook, G. S., Long, G. V., Kurzrock, R., Kim, K. B., Arkenau, T. H., Brown, M. P., Hamid, O., Infante, J. R., Millward, M., Pavlick, A. C.*, et al.* (2012). Dabrafenib in patients with melanoma, untreated brain metastases, and other solid tumours: a phase 1 dose-escalation trial. Lancet *379*, 1893-1901.

Ferrell, J. E., Jr., and Bhatt, R. R. (1997). Mechanistic studies of the dual phosphorylation of mitogen-activated protein kinase. J Biol Chem *272*, 19008-19016.

Flaherty, K. T., Puzanov, I., Kim, K. B., Ribas, A., McArthur, G. A., Sosman, J. A., O'Dwyer, P. J., Lee, R. J., Grippo, J. F., Nolop, K., and Chapman, P. B. (2010). Inhibition of mutated, activated BRAF in metastatic melanoma. N Engl J Med *363*, 809-819.

Frese, K. K., Neesse, A., Cook, N., Bapiro, T. E., Lolkema, M. P., Jodrell, D. I., and Tuveson, D. A. (2012). nab-Paclitaxel potentiates gemcitabine activity by reducing cytidine deaminase levels in a mouse model of pancreatic cancer. Cancer Discov *2*, 260-269.

Fukuda, M., Gotoh, I., Adachi, M., Gotoh, Y., and Nishida, E. (1997a). A novel regulatory mechanism in the mitogen-activated protein (MAP) kinase cascade. Role of nuclear export signal of MAP kinase kinase. J Biol Chem *272*, 32642-32648.

Fukuda, M., Gotoh, Y., and Nishida, E. (1997b). Interaction of MAP kinase with MAP kinase kinase: its possible role in the control of nucleocytoplasmic transport of MAP kinase. Embo J *16*, 1901-1908.

Garber, K. (2009). From human to mouse and back: 'tumorgraft' models surge in popularity. J Natl Cancer Inst *101*, 6-8.

Garnett, M. J., Edelman, E. J., Heidorn, S. J., Greenman, C. D., Dastur, A., Lau, K. W., Greninger, P., Thompson, I. R., Luo, X., Soares, J.*, et al.* (2012). Systematic identification of genomic markers of drug sensitivity in cancer cells. Nature *483*, 570-575.

Ghaneh, P., Costello, E., and Neoptolemos, J. P. (2007). Biology and management of pancreatic cancer. Gut *56*, 1134-1152.

Gillings, A. S., Balmanno, K., Wiggins, C. M., Johnson, M., and Cook, S. J. (2009). Apoptosis and autophagy: BIM as a mediator of tumour cell death in response to oncogene-targeted therapeutics. Febs J *276*, 6050-6062.

Giroux, S., Tremblay, M., Bernard, D., Cardin-Girard, J. F., Aubry, S., Larouche, L., Rousseau, S., Huot, J., Landry, J., Jeannotte, L., and Charron, J. (1999). Embryonic death of Mek1-deficient mice reveals a role for this kinase in angiogenesis in the labyrinthine region of the placenta. Curr Biol *9*, 369-372.

Grewe, M., Gansauge, F., Schmid, R. M., Adler, G., and Seufferlein, T. (1999). Regulation of cell growth and cyclin D1 expression by the constitutively active FRAP-p70s6K pathway in human pancreatic cancer cells. Cancer Res *59*, 3581-3587.

Grüner, B. M., Winkelmann, I., Feuchtinger, A., Sun, N., Balluff, B., Teichmann, N., Herner, A., Kalideris, E., Steiger, K., Braren, R.*, et al.* (2016). Modeling Therapy Response and Spatial Tissue Distribution of Erlotinib in Pancreatic Cancer. Mol Cancer Ther *15*, 1145-1152.

Gu, G., Brown, J. R., and Melton, D. A. (2003). Direct lineage tracing reveals the ontogeny of pancreatic cell fates during mouse embryogenesis. Mech Dev *120*, 35-43.

Gupta, P. B., Onder, T. T., Jiang, G., Tao, K., Kuperwasser, C., Weinberg, R. A., and Lander, E. S. (2009). Identification of selective inhibitors of cancer stem cells by high-throughput screening. Cell *138*, 645-659.

Hahn, S. A., Schutte, M., Hoque, A. T., Moskaluk, C. A., da Costa, L. T., Rozenblum, E., Weinstein, C. L., Fischer, A., Yeo, C. J., Hruban, R. H., and Kern, S. E. (1996). DPC4, a candidate tumor suppressor gene at human chromosome 18q21.1. Science *271*, 350-353.

Hansel, D. E., Kern, S. E., and Hruban, R. H. (2003). Molecular pathogenesis of pancreatic cancer. Annu Rev Genomics Hum Genet *4*, 237-256.

Harding, A., and Hancock, J. F. (2008). Ras nanoclusters: combining digital and analog signaling. Cell Cycle *7*, 127-134.

Hart, A., Papadopoulou, S., and Edlund, H. (2003). Fgf10 maintains notch activation, stimulates proliferation, and blocks differentiation of pancreatic epithelial cells. Dev Dyn *228*, 185-193.

Hatzivassiliou, G., Song, K., Yen, I., Brandhuber, B. J., Anderson, D. J., Alvarado, R., Ludlam, M. J., Stokoe, D., Gloor, S. L., Vigers, G.*, et al.* (2010). RAF inhibitors prime wild-type RAF to activate the MAPK pathway and enhance growth. Nature *464*, 431-435.

Heid, I., Steiger, K., Trajkovic-Arsic, M., Settles, M., Esswein, M. R., Erkan, M., Kleeff, J., Jager, C., Friess, H., Haller, B., *et al.* (2017). Co-clinical Assessment of Tumor Cellularity in Pancreatic Cancer. Clin Cancer Res *23*, 1461-1470.

Heidenblad, M., Jonson, T., Mahlamaki, E. H., Gorunova, L., Karhu, R., Johansson, B., and Hoglund, M. (2002). Detailed genomic mapping and expression analyses of 12p amplifications in pancreatic carcinomas reveal a 3.5-Mb target region for amplification. Genes Chromosomes Cancer *34*, 211-223.

Heidorn, S. J., Milagre, C., Whittaker, S., Nourry, A., Niculescu-Duvas, I., Dhomen, N., Hussain, J., Reis-Filho, J. S., Springer, C. J., Pritchard, C., and Marais, R. (2010). Kinase-dead BRAF and oncogenic RAS cooperate to drive tumor progression through CRAF. Cell *140*, 209-221.

Hezel, A. F., Kimmelman, A. C., Stanger, B. Z., Bardeesy, N., and Depinho, R. A. (2006). Genetics and biology of pancreatic ductal adenocarcinoma. Genes Dev *20*, 1218-1249.

Hingorani, S. R., Petricoin, E. F., Maitra, A., Rajapakse, V., King, C., Jacobetz, M. A., Ross, S., Conrads, T. P., Veenstra, T. D., Hitt, B. A.*, et al.* (2003). Preinvasive and invasive ductal pancreatic cancer and its early detection in the mouse. Cancer Cell *4*, 437-450.

Hingorani, S. R., Wang, L., Multani, A. S., Combs, C., Deramaudt, T. B., Hruban, R. H., Rustgi, A. K., Chang, S., and Tuveson, D. A. (2005). Trp53R172H and KrasG12D cooperate to promote chromosomal instability and widely metastatic pancreatic ductal adenocarcinoma in mice. Cancer Cell *7*, 469-483.

Hruban, R. H., Adsay, N. V., Albores-Saavedra, J., Compton, C., Garrett, E. S., Goodman, S. N., Kern, S. E., Klimstra, D. S., Kloppel, G., Longnecker, D. S.*, et al.* (2001). Pancreatic intraepithelial neoplasia: a new nomenclature and classification system for pancreatic duct lesions. Am J Surg Pathol *25*, 579-586.

Hruban, R. H., Maitra, A., and Goggins, M. (2008). Update on pancreatic intraepithelial neoplasia. Int J Clin Exp Pathol *1*, 306-316.

Hruban, R. H., Takaori, K., Klimstra, D. S., Adsay, N. V., Albores-Saavedra, J., Biankin, A. V., Biankin, S. A., Compton, C., Fukushima, N., Furukawa, T.*, et al.* (2004). An illustrated consensus on the classification of pancreatic intraepithelial neoplasia and intraductal papillary mucinous neoplasms. Am J Surg Pathol *28*, 977-987.

Hubner, A., Barrett, T., Flavell, R. A., and Davis, R. J. (2008). Multisite phosphorylation regulates Bim stability and apoptotic activity. Mol Cell *30*, 415-425.

Iacobuzio-Donahue, C. A., Klimstra, D. S., Adsay, N. V., Wilentz, R. E., Argani, P., Sohn, T. A., Yeo, C. J., Cameron, J. L., Kern, S. E., and Hruban, R. H. (2000). Dpc-4 protein is expressed in virtually all human intraductal papillary mucinous neoplasms of the pancreas: comparison with conventional ductal adenocarcinomas. Am J Pathol *157*, 755-761.

Ishimura, N., Yamasawa, K., Karim Rumi, M. A., Kadowaki, Y., Ishihara, S., Amano, Y., Nio, Y., Higami, T., and Kinoshita, Y. (2003). BRAF and K-ras gene mutations in human pancreatic cancers. Cancer Lett *199*, 169-173.

Iverson, C., Larson, G., Lai, C., Yeh, L. T., Dadson, C., Weingarten, P., Appleby, T., Vo, T., Maderna, A., Vernier, J. M.*, et al.* (2009). RDEA119/BAY 869766: a potent, selective, allosteric inhibitor of MEK1/2 for the treatment of cancer. Cancer Res *69*, 6839-6847.

Jackson, E. L., Willis, N., Mercer, K., Bronson, R. T., Crowley, D., Montoya, R., Jacks, T., and Tuveson, D. A. (2001). Analysis of lung tumor initiation and progression using conditional expression of oncogenic K-ras. Genes Dev *15*, 3243-3248.

Jacobetz, M. A., Chan, D. S., Neesse, A., Bapiro, T. E., Cook, N., Frese, K. K., Feig, C., Nakagawa, T., Caldwell, M. E., Zecchini, H. I.*, et al.* (2013). Hyaluronan impairs vascular function and drug delivery in a mouse model of pancreatic cancer. Gut *62*, 112-120.

James, R. M., Arends, M. J., Plowman, S. J., Brooks, D. G., Miles, C. G., West, J. D., and Patek, C. E. (2003). K-ras proto-oncogene exhibits tumor suppressor activity as its absence promotes tumorigenesis in murine teratomas. Mol Cancer Res *1*, 820-825.

Janne, P. A., Shaw, A. T., Pereira, J. R., Jeannin, G., Vansteenkiste, J., Barrios, C., Franke, F. A., Grinsted, L., Zazulina, V., Smith, P.*, et al.* (2013). Selumetinib plus docetaxel for KRAS-mutant advanced non-small-cell lung cancer: a randomised, multicentre, placebo-controlled, phase 2 study. The Lancet Oncology *14*, 38-47.

Javle, M. M., Gibbs, J. F., Iwata, K. K., Pak, Y., Rutledge, P., Yu, J., Black, J. D., Tan, D., and Khoury, T. (2007). Epithelial-mesenchymal transition (EMT) and activated extracellular signal-regulated kinase (p-Erk) in surgically resected pancreatic cancer. Ann Surg Oncol *14*, 3527-3533.

Jemal, A., Siegel, R., Xu, J., and Ward, E. (2010). Cancer statistics, 2010. CA Cancer J Clin *60*, 277-300.

Ji, B., Tsou, L., Wang, H., Gaiser, S., Chang, D. Z., Daniluk, J., Bi, Y., Grote, T., Longnecker, D. S., and Logsdon, C. D. (2009). Ras activity levels control the development of pancreatic diseases. Gastroenterology *137*, 1072-1082, 1082 e1071-1076.

Jing, J., Greshock, J., Holbrook, J. D., Gilmartin, A., Zhang, X., McNeil, E., Conway, T., Moy, C., Laquerre, S., Bachman, K.*, et al.* (2012). Comprehensive predictive biomarker analysis for MEK inhibitor GSK1120212. Mol Cancer Ther *11*, 720-729.

Jones, S., Zhang, X., Parsons, D. W., Lin, J. C., Leary, R. J., Angenendt, P., Mankoo, P., Carter, H., Kamiyama, H., Jimeno, A.*, et al.* (2008). Core signaling pathways in human pancreatic cancers revealed by global genomic analyses. Science *321*, 1801-1806.

Jonkers, J., and Berns, A. (2002). Conditional mouse models of sporadic cancer. Nat Rev Cancer *2*, 251-265.

Kawaguchi, Y., Cooper, B., Gannon, M., Ray, M., MacDonald, R. J., and Wright, C. V. (2002). The role of the transcriptional regulator Ptf1a in converting intestinal to pancreatic progenitors. Nat Genet *32*, 128-134.

Kim, S. K., and Hebrok, M. (2001). Intercellular signals regulating pancreas development and function. Genes Dev *15*, 111-127.

Kim, H., Rafiuddin-Shah, M., Tu, H. C., Jeffers, J. R., Zambetti, G. P., Hsieh, J. J., and Cheng, E. H. (2006). Hierarchical regulation of mitochondrion-dependent apoptosis by BCL-2 subfamilies. Nat Cell Biol *8*, 1348-1358.

Klimstra, D. S., and Longnecker, D. S. (1994). K-ras mutations in pancreatic ductal proliferative lesions. Am J Pathol *145*, 1547-1550.

Klimstra, D. S., Pitman, M. B., and Hruban, R. H. (2009). An algorithmic approach to the diagnosis of pancreatic neoplasms. Arch Pathol Lab Med *133*, 454-464.

Kolch, W. (2005). Coordinating ERK/MAPK signalling through scaffolds and inhibitors. Nat Rev Mol Cell Biol *6*, 827-837.

Krapp, A., Knofler, M., Frutiger, S., Hughes, G. J., Hagenbuchle, O., and Wellauer, P. K. (1996). The p48 DNA-binding subunit of transcription factor PTF1 is a new exocrine pancreas-specific basic helix-loop-helix protein. Embo J *15*, 4317-4329.

Krapp, A., Knofler, M., Ledermann, B., Burki, K., Berney, C., Zoerkler, N., Hagenbuchle, O., and Wellauer, P. K. (1998). The bHLH protein PTF1-p48 is essential for the formation of the exocrine and the correct spatial organization of the endocrine pancreas. Genes Dev *12*, 3752-3763.

Krebs, A. M., Mitschke, J., Lasierra Losada, M., Schmalhofer, O., Boerries, M., Busch, H., Boettcher, M., Mougiakakos, D., Reichardt, W., Bronsert, P.*, et al.* (2017). The EMT-activator Zeb1 is a key factor for cell plasticity and promotes metastasis in pancreatic cancer. Nat Cell Biol *19*, 518-529.

Lahat, G., Sever, R., Lubezky, N., Nachmany, I., Gerstenhaber, F., Ben-Haim, M., Nakache, R., Koriansky, J., and Klausner, J. M. (2011). Pancreatic cancer: surgery is a feasible therapeutic option for elderly patients. World J Surg Oncol *9*, 10.

Lamba, S., Russo, M., Sun, C., Lazzari, L., Cancelliere, C., Grernrum, W., Lieftink, C., Bernards, R., Di Nicolantonio, F., and Bardelli, A. (2014). RAF suppression synergizes with MEK inhibition in KRAS mutant cancer cells. Cell Rep *8*, 1475-1483.

Lee, J., Jang, K. T., Ki, C. S., Lim, T., Park, Y. S., Lim, H. Y., Choi, D. W., Kang, W. K., Park, K., and Park, J. O. (2007). Impact of epidermal growth factor receptor (EGFR) kinase mutations, EGFR gene amplifications, and KRAS mutations on survival of pancreatic adenocarcinoma. Cancer *109*, 1561-1569.

Leijen, S., Soetekouw, P. M., Jeffry Evans, T. R., Nicolson, M., Schellens, J. H., Learoyd, M., Grinsted, L., Zazulina, V., Pwint, T., and Middleton, M. (2011). A phase I, open-label, randomized crossover study to assess the effect of dosing of the MEK 1/2 inhibitor Selumetinib (AZD6244; ARRY-142866) in the presence and absence of food in patients with advanced solid tumors. Cancer Chemother Pharmacol *68*, 1619-1628.

Ley, R., Balmanno, K., Hadfield, K., Weston, C., and Cook, S. J. (2003). Activation of the ERK1/2 signaling pathway promotes phosphorylation and proteasome-dependent degradation of the BH3-only protein, Bim. J Biol Chem *278*, 18811-18816.

Little, A. S., Balmanno, K., Sale, M. J., Newman, S., Dry, J. R., Hampson, M., Edwards, P. A., Smith, P. D., and Cook, S. J. (2011). Amplification of the driving oncogene, KRAS or BRAF, underpins acquired resistance to MEK1/2 inhibitors in colorectal cancer cells. Science signaling *4*, ra17.

Lorusso, P. M., Adjei, A. A., Varterasian, M., Gadgeel, S., Reid, J., Mitchell, D. Y., Hanson, L., DeLuca, P., Bruzek, L., Piens, J.*, et al.* (2005). Phase I and pharmacodynamic study of the oral MEK inhibitor CI-1040 in patients with advanced malignancies. J Clin Oncol *23*, 5281-5293.

LoRusso, P. M., Krishnamurthi, S. S., Rinehart, J. J., Nabell, L. M., Malburg, L., Chapman, P. B., DePrimo, S. E., Bentivegna, S., Wilner, K. D., Tan, W., and Ricart, A. D. (2010). Phase I pharmacokinetic and pharmacodynamic study of the oral MAPK/ERK kinase inhibitor PD-0325901 in patients with advanced cancers. Clin Cancer Res *16*, 1924-1937.

Lowenfels, A. B., and Maisonneuve, P. (2006). Epidemiology and risk factors for pancreatic cancer. Best Pract Res Clin Gastroenterol *20*, 197-209.

Luo, G., Long, J., Qiu, L., Liu, C., Xu, J., and Yu, X. (2011). Role of epidermal growth factor receptor expression on patient survival in pancreatic cancer: a meta-analysis. Pancreatology *11*, 595-600.

Luttges, J., Galehdari, H., Brocker, V., Schwarte-Waldhoff, I., Henne-Bruns, D., Kloppel, G., Schmiegel, W., and Hahn, S. A. (2001). Allelic loss is often the first hit in the biallelic inactivation of the p53 and DPC4 genes during pancreatic carcinogenesis. Am J Pathol *158*, 1677-1683.

Maitra, A., and Hruban, R. H. (2008). Pancreatic cancer. Annu Rev Pathol *3*, 157-188.

Mani, S. A., Guo, W., Liao, M. J., Eaton, E. N., Ayyanan, A., Zhou, A. Y., Brooks, M., Reinhard, F., Zhang, C. C., Shipitsin, M.*, et al.* (2008). The epithelial-mesenchymal transition generates cells with properties of stem cells. Cell *133*, 704-715.

Marino, S., Vooijs, M., van Der Gulden, H., Jonkers, J., and Berns, A. (2000). Induction of medulloblastomas in p53-null mutant mice by somatic inactivation of Rb in the external granular layer cells of the cerebellum. Genes Dev *14*, 994-1004.

Marks, J. L., Gong, Y., Chitale, D., Golas, B., McLellan, M. D., Kasai, Y., Ding, L., Mardis, E. R., Wilson, R. K., Solit, D.*, et al.* (2008). Novel MEK1 mutation identified by mutational analysis of epidermal growth factor receptor signaling pathway genes in lung adenocarcinoma. Cancer Res *68*, 5524-5528.

Masugi, Y., Yamazaki, K., Hibi, T., Aiura, K., Kitagawa, Y., and Sakamoto, M. (2010). Solitary cell infiltration is a novel indicator of poor prognosis and epithelial-mesenchymal transition in pancreatic cancer. Hum Pathol *41*, 1061-1068.

Matsubara, S., Ding, Q., Miyazaki, Y., Kuwahata, T., Tsukasa, K., and Takao, S. (2013). mTOR plays critical roles in pancreatic cancer stem cells through specific and stemness-related functions. Sci Rep *3*, 3230.

Matthaei, H., Schulick, R. D., Hruban, R. H., and Maitra, A. (2011). Cystic precursors to invasive pancreatic cancer. Nat Rev Gastroenterol Hepatol *8*, 141-150.

Mazur, P. K., Einwachter, H., Lee, M., Sipos, B., Nakhai, H., Rad, R., Zimber-Strobl, U., Strobl, L. J., Radtke, F., Kloppel, G.*, et al.* (2010). Notch2 is required for progression of pancreatic intraepithelial neoplasia and development of pancreatic ductal adenocarcinoma. Proc Natl Acad Sci U S A *107*, 13438-13443.

Mazur, P. K., Herner, A., Mello, S. S., Wirth, M., Hausmann, S., Sanchez-Rivera, F. J., Lofgren, S. M., Kuschma, T., Hahn, S. A., Vangala, D.*, et al.* (2015a). Combined inhibition of BET family proteins and histone deacetylases as a potential epigenetics-based therapy for pancreatic ductal adenocarcinoma. Nat Med *21*, 1163-1171.

Mazur, P. K., Herner, A., Neff, F., and Siveke, J. T. (2015b). Current methods in mouse models of pancreatic cancer. Methods Mol Biol *1267*, 185-215.

Mazur, P. K., and Siveke, J. T. (2012). Genetically engineered mouse models of pancreatic cancer: unravelling tumour biology and progressing translational oncology. Gut *61*, 1488-1500.

Meng, J., Dai, B., Fang, B., Bekele, B. N., Bornmann, W. G., Sun, D., Peng, Z., Herbst, R. S., Papadimitrakopoulou, V., Minna, J. D.*, et al.* (2010a). Combination treatment with MEK and AKT inhibitors is more effective than each drug alone in human non-small cell lung cancer in vitro and in vivo. PLoS One *5*, e14124.

Meng, J., Fang, B., Liao, Y., Chresta, C. M., Smith, P. D., and Roth, J. A. (2010b). Apoptosis induction by MEK inhibition in human lung cancer cells is mediated by Bim. PLoS One *5*, e13026.

Melstrom, L. G., and Grippo, P. J. (2008). Models of Pancreatic Cancer: Understanding Disease Progression. In A. M. Lowy *et al*. (eds.), Pancreatic Cancer, 137-158. Springer (ISBN 9780387692500).

Mirzoeva, O. K., Collisson, E. A., Schaefer, P. M., Hann, B., Hom, Y. K., Ko, A. H., and Korn, W. M. (2013). Subtype-specific MEK-PI3 kinase feedback as a therapeutic target in pancreatic adenocarcinoma. Mol Cancer Ther *12*, 2213-2225.

Mirzoeva, O. K., Das, D., Heiser, L. M., Bhattacharya, S., Siwak, D., Gendelman, R., Bayani, N., Wang, N. J., Neve, R. M., Guan, Y.*, et al.* (2009). Basal subtype and MAPK/ERK kinase (MEK)-phosphoinositide 3-kinase feedback signaling determine susceptibility of breast cancer cells to MEK inhibition. Cancer Res *69*, 565-572.

Moffitt, R. A., Marayati, R., Flate, E. L., Volmar, K. E., Loeza, S. G., Hoadley, K. A., Rashid, N. U., Williams, L. A., Eaton, S. C., Chung, A. H., *et al.* (2015). Virtual microdissection identifies distinct tumor- and stroma-specific subtypes of pancreatic ductal adenocarcinoma. Nat Genet *47*, 1168-1178.

Moore, M. J., Goldstein, D., Hamm, J., Figer, A., Hecht, J. R., Gallinger, S., Au, H. J., Murawa, P., Walde, D., Wolff, R. A.*, et al.* (2007). Erlotinib plus gemcitabine compared with gemcitabine alone in patients with advanced pancreatic cancer: a phase III trial of the National Cancer Institute of Canada Clinical Trials Group. J Clin Oncol *25*, 1960-1966.

Moore, P. S., Sipos, B., Orlandini, S., Sorio, C., Real, F. X., Lemoine, N. R., Gress, T., Bassi, C., Kloppel, G., Kalthoff, H.*, et al.* (2001). Genetic profile of 22 pancreatic carcinoma cell lines. Analysis of K-ras, p53, p16 and DPC4/Smad4. Virchows Arch *439*, 798-802.

Morel, A. P., Lievre, M., Thomas, C., Hinkal, G., Ansieau, S., and Puisieux, A. (2008). Generation of breast cancer stem cells through epithelial-mesenchymal transition. PLoS One *3*, e2888.

Morton, J. P., Karim, S. A., Graham, K., Timpson, P., Jamieson, N., Athineos, D., Doyle, B., McKay, C., Heung, M. Y., Oien, K. A.*, et al.* (2010). Dasatinib inhibits the development of metastases in a mouse model of pancreatic ductal adenocarcinoma. Gastroenterology *139*, 292-303.

Mueller, S., Engleitner, T., Maresch, R., Zukowska, M., Lange, S., Kaltenbacher, T., Konukiewitz, B., Ollinger, R., Zwiebel, M., Strong, A.*, et al.* (2018). Evolutionary routes and KRAS dosage define pancreatic cancer phenotypes. Nature *554*, 62-68.

Murugan, A. K., Dong, J., Xie, J., and Xing, M. (2009). MEK1 mutations, but not ERK2 mutations, occur in melanomas and colon carcinomas, but none in thyroid carcinomas. Cell Cycle *8*, 2122-2124.

Nakhai, H., Sel, S., Favor, J., Mendoza-Torres, L., Paulsen, F., Duncker, G. I., and Schmid, R. M. (2007). Ptf1a is essential for the differentiation of GABAergic and glycinergic amacrine cells and horizontal cells in the mouse retina. Development *134*, 1151-1160.

Naujokat, C., and Steinhart, R. (2012). Salinomycin as a drug for targeting human cancer stem cells. J Biomed Biotechnol *2012*, 950658.

Neuzillet, C., Hammel, P., Tijeras-Raballand, A., Couvelard, A., and Raymond, E. (2013). Targeting the Ras-ERK pathway in pancreatic adenocarcinoma. Cancer Metastasis Rev *32*, 147-162.

Noll, E. M., Eisen, C., Stenzinger, A., Espinet, E., Muckenhuber, A., Klein, C., Vogel, V., Klaus, B., Nadler, W., Rosli, C.*, et al.* (2016). CYP3A5 mediates basal and acquired therapy resistance in different subtypes of pancreatic ductal adenocarcinoma. Nat Med *22*, 278-287.

Norgaard, G. A., Jensen, J. N., and Jensen, J. (2003). FGF10 signaling maintains the pancreatic progenitor cell state revealing a novel role of Notch in organ development. Dev Biol *264*, 323-338.

Normanno, N., De Luca, A., Maiello, M. R., Campiglio, M., Napolitano, M., Mancino, M., Carotenuto, A., Viglietto, G., and Menard, S. (2006). The MEK/MAPK pathway is involved in the resistance of breast cancer cells to the EGFR tyrosine kinase inhibitor gefitinib. J Cell Physiol *207*, 420-427.

Obata, J., Yano, M., Mimura, H., Goto, T., Nakayama, R., Mibu, Y., Oka, C., and Kawaichi, M. (2001). p48 subunit of mouse PTF1 binds to RBP-Jkappa/CBF-1, the intracellular mediator of Notch signalling, and is expressed in the neural tube of early stage embryos. Genes to cells : devoted to molecular & cellular mechanisms *6*, 345-360.

Ohren, J. F., Chen, H., Pavlovsky, A., Whitehead, C., Zhang, E., Kuffa, P., Yan, C., McConnell, P., Spessard, C., Banotai, C.*, et al.* (2004). Structures of human MAP kinase kinase 1 (MEK1) and MEK2 describe novel noncompetitive kinase inhibition. Nat Struct Mol Biol *11*, 1192-1197.

Olive, K. P., Jacobetz, M. A., Davidson, C. J., Gopinathan, A., McIntyre, D., Honess, D., Madhu, B., Goldgraben, M. A., Caldwell, M. E., Allard, D.*, et al.* (2009). Inhibition of Hedgehog signaling enhances delivery of chemotherapy in a mouse model of pancreatic cancer. Science *324*, 1457-1461.

Orton, R. J., Sturm, O. E., Vyshemirsky, V., Calder, M., Gilbert, D. R., and Kolch, W. (2005). Computational modelling of the receptor-tyrosine-kinase-activated MAPK pathway. Biochem J *392*, 249-261.

Parada, L. F., and Weinberg, R. A. (1983). Presence of a Kirsten murine sarcoma virus ras oncogene in cells transformed by 3-methylcholanthrene. Mol Cell Biol *3*, 2298-2301.

Poulikakos, P. I., Zhang, C., Bollag, G., Shokat, K. M., and Rosen, N. (2010). RAF inhibitors transactivate RAF dimers and ERK signalling in cells with wild-type BRAF. Nature *464*, 427-430.

Provenzano, P. P., Cuevas, C., Chang, A. E., Goel, V. K., Von Hoff, D. D., and Hingorani, S. R. (2012). Enzymatic targeting of the stroma ablates physical barriers to treatment of pancreatic ductal adenocarcinoma. Cancer Cell *21*, 418-429.

Pylayeva-Gupta, Y., Grabocka, E., and Bar-Sagi, D. (2011). RAS oncogenes: weaving a tumorigenic web. Nat Rev Cancer *11*, 761-774.

Rahib, L., Smith, B. D., Aizenberg, R., Rosenzweig, A. B., Fleshman, J. M., and Matrisian, L. M. (2014). Projecting cancer incidence and deaths to 2030: the unexpected burden of thyroid, liver, and pancreas cancers in the United States. Cancer Res *74*, 2913-2921.

Rajagopalan, H., Bardelli, A., Lengauer, C., Kinzler, K. W., Vogelstein, B., and Velculescu, V. E. (2002). Tumorigenesis: RAF/RAS oncogenes and mismatch-repair status. Nature *418*, 934.

Redston, M. S., Caldas, C., Seymour, A. B., Hruban, R. H., da Costa, L., Yeo, C. J., and Kern, S. E. (1994). p53 mutations in pancreatic carcinoma and evidence of common involvement of homocopolymer tracts in DNA microdeletions. Cancer Res *54*, 3025-3033.

Rinehart, J., Adjei, A. A., Lorusso, P. M., Waterhouse, D., Hecht, J. R., Natale, R. B., Hamid, O., Varterasian, M., Asbury, P., Kaldjian, E. P.*, et al.* (2004). Multicenter phase II study of the oral MEK inhibitor, CI-1040, in patients with advanced non-small-cell lung, breast, colon, and pancreatic cancer. J Clin Oncol *22*, 4456-4462.

Roberts, P. J., Usary, J. E., Darr, D. B., Dillon, P. M., Pfefferle, A. D., Whittle, M. C., Duncan, J. S., Johnson, S. M., Combest, A. J., Jin, J.*, et al.* (2012). Combined PI3K/mTOR and MEK inhibition provides broad antitumor activity in faithful murine cancer models. Clin Cancer Res *18*, 5290-5303.

Roskoski, R., Jr. (2012). MEK1/2 dual-specificity protein kinases: structure and regulation. Biochem Biophys Res Commun *417*, 5-10.

Rozenblum, E., Schutte, M., Goggins, M., Hahn, S. A., Panzer, S., Zahurak, M., Goodman, S. N., Sohn, T. A., Hruban, R. H., Yeo, C. J., and Kern, S. E. (1997). Tumor-suppressive pathways in pancreatic carcinoma. Cancer Res *57*, 1731-1734.

Rubinfeld, H., Hanoch, T., and Seger, R. (1999). Identification of a cytoplasmic-retention sequence in ERK2. J Biol Chem *274*, 30349-30352.

Salomon, D. S., Brandt, R., Ciardiello, F., and Normanno, N. (1995). Epidermal growth factor-related peptides and their receptors in human malignancies. Crit Rev Oncol Hematol *19*, 183-232.

Samatar, A. A., and Poulikakos, P. I. (2014). Targeting RAS-ERK signalling in cancer: promises and challenges. Nat Rev Drug Discov *13*, 928-942.

Sarbassov, D. D., Ali, S. M., Sengupta, S., Sheen, J. H., Hsu, P. P., Bagley, A. F., Markhard, A. L., and Sabatini, D. M. (2006). Prolonged rapamycin treatment inhibits mTORC2 assembly and Akt/PKB. Mol Cell *22*, 159-168.

Sauer, B. (1998). Inducible gene targeting in mice using the Cre/lox system. Methods *14*, 381-392.

Schmieder, R., Puehler, F., Neuhaus, R., Kissel, M., Adjei, A. A., Miner, J. N., Mumberg, D., Ziegelbauer, K., and Scholz, A. (2013). Allosteric MEK1/2 inhibitor refametinib (BAY 86-9766) in combination with sorafenib exhibits antitumor activity in preclinical murine and rat models of hepatocellular carcinoma. Neoplasia *15*, 1161-1171.

Schneider, G., and Schmid, R. M. (2003). Genetic alterations in pancreatic carcinoma. Mol Cancer *2*, 15.

Scholl, F. A., Dumesic, P. A., Barragan, D. I., Harada, K., Bissonauth, V., Charron, J., and Khavari, P. A. (2007). Mek1/2 MAPK kinases are essential for Mammalian development, homeostasis, and Raf-induced hyperplasia. Dev Cell *12*, 615-629.

Schonleben, F., Qiu, W., Ciau, N. T., Ho, D. J., Li, X., Allendorf, J. D., Remotti, H. E., and Su, G. H. (2006). PIK3CA mutations in intraductal papillary mucinous neoplasm/carcinoma of the pancreas. Clin Cancer Res *12*, 3851-3855.

Sebolt-Leopold, J. S., and Herrera, R. (2004). Targeting the mitogen-activated protein kinase cascade to treat cancer. Nat Rev Cancer *4*, 937-947.

Sergina, N. V., Rausch, M., Wang, D., Blair, J., Hann, B., Shokat, K. M., and Moasser, M. M. (2007). Escape from HER-family tyrosine kinase inhibitor therapy by the kinase-inactive HER3. Nature *445*, 437-441.

Shah, A. N., Summy, J. M., Zhang, J., Park, S. I., Parikh, N. U., and Gallick, G. E. (2007). Development and characterization of gemcitabine-resistant pancreatic tumor cells. Ann Surg Oncol *14*, 3629-3637.

Shah, S. A., Potter, M. W., Ricciardi, R., Perugini, R. A., and Callery, M. P. (2001). FRAP-p70s6K signaling is required for pancreatic cancer cell proliferation. J Surg Res *97*, 123-130.

Shih, H. P., Wang, A., and Sander, M. (2013). Pancreas organogenesis: from lineage determination to morphogenesis. Annu Rev Cell Dev Biol *29*, 81-105.

Siegel, R., Naishadham, D., and Jemal, A. (2013). Cancer statistics, 2013. CA Cancer J Clin *63*, 11-30.

Singh, A., Greninger, P., Rhodes, D., Koopman, L., Violette, S., Bardeesy, N., and Settleman, J. (2009). A gene expression signature associated with "K-Ras addiction" reveals regulators of EMT and tumor cell survival. Cancer Cell *15*, 489-500.

Singh, M., Lima, A., Molina, R., Hamilton, P., Clermont, A. C., Devasthali, V., Thompson, J. D., Cheng, J. H., Bou Reslan, H., Ho, C. C.*, et al.* (2010). Assessing therapeutic responses in Kras mutant cancers using genetically engineered mouse models. Nat Biotechnol *28*, 585-593.

Smigiel, J. M., Parameswaran, N., and Jackson, M. W. (2017). Potent EMT and CSC Phenotypes Are Induced By Oncostatin-M in Pancreatic Cancer. Mol Cancer Res *15*, 478-488.

Smigiel, J. M., Parameswaran, N., and Jackson, M. W. (2018). Targeting Pancreatic Cancer Cell Plasticity: The Latest in Therapeutics. Cancers (Basel) *10*.

Soares, H. P., Ming, M., Mellon, M., Young, S. H., Han, L., Sinnet-Smith, J., and Rozengurt, E. (2015). Dual PI3K/mTOR Inhibitors Induce Rapid Overactivation of the MEK/ERK Pathway in Human Pancreatic Cancer Cells through Suppression of mTORC2. Mol Cancer Ther *14*, 1014-1023.

Solit, D. B., Garraway, L. A., Pratilas, C. A., Sawai, A., Getz, G., Basso, A., Ye, Q., Lobo, J. M., She, Y., Osman, I.*, et al.* (2006). BRAF mutation predicts sensitivity to MEK inhibition. Nature *439*, 358-362.

Spratlin, J. L., and Mackey, J. R. (2010). Human Equilibrative Nucleoside Transporter 1 (hENT1) in Pancreatic Adenocarcinoma: Towards Individualized Treatment Decisions. Cancers (Basel) *2*, 2044-2054.

Steelman, L. S., Chappell, W. H., Abrams, S. L., Kempf, R. C., Long, J., Laidler, P., Mijatovic, S., Maksimovic-Ivanic, D., Stivala, F., Mazzarino, M. C.*, et al.* (2011). Roles of the Raf/MEK/ERK and PI3K/PTEN/Akt/mTOR pathways in controlling growth and sensitivity to therapy-implications for cancer and aging. Aging (Albany NY) *3*, 192-222.

Su, G. H., Hruban, R. H., Bansal, R. K., Bova, G. S., Tang, D. J., Shekher, M. C., Westerman, A. M., Entius, M. M., Goggins, M., Yeo, C. J., and Kern, S. E. (1999). Germline and somatic mutations of the STK11/LKB1 Peutz-Jeghers gene in pancreatic and biliary cancers. Am J Pathol *154*, 1835-1840.

Sullivan, R. J., and Flaherty, K. T. (2013). Resistance to BRAF-targeted therapy in melanoma. Eur J Cancer *49*, 1297-1304.

Tobita, K., Kijima, H., Dowaki, S., Kashiwagi, H., Ohtani, Y., Oida, Y., Yamazaki, H., Nakamura, M., Ueyama, Y., Tanaka, M.*, et al.* (2003). Epidermal growth factor receptor expression in human pancreatic cancer: Significance for liver metastasis. Int J Mol Med *11*, 305-309.

Toulany, M., Minjgee, M., Saki, M., Holler, M., Meier, F., Eicheler, W., and Rodemann, H. P. (2014). ERK2-dependent reactivation of Akt mediates the limited response of tumor cells with constitutive K-RAS activity to PI3K inhibition. Cancer Biol Ther *15*, 317-328.

Tran, K. T., Smeenk, H. G., van Eijck, C. H., Kazemier, G., Hop, W. C., Greve, J. W., Terpstra, O. T., Zijlstra, J. A., Klinkert, P., and Jeekel, H. (2004). Pylorus preserving pancreaticoduodenectomy versus standard Whipple procedure: a prospective, randomized, multicenter analysis of 170 patients with pancreatic and periampullary tumors. Ann Surg *240*, 738-745.

Trajkovic-Arsic, M., Heid, I., Steiger, K., Gupta, A., Fingerle, A., Worner, C., Teichmann, N., Sengkwawoh-Lueong, S., Wenzel, P., Beer, A. J.*, et al.* (2017). Apparent Diffusion Coefficient (ADC) predicts therapy response in pancreatic ductal adenocarcinoma. Sci Rep *7*, 17038.

Turke, A. B., Song, Y., Costa, C., Cook, R., Arteaga, C. L., Asara, J. M., and Engelman, J. A. (2012). MEK inhibition leads to PI3K/AKT activation by relieving a negative feedback on ERBB receptors. Cancer Res *72*, 3228-3237.

Ueda, S., Ogata, S., Tsuda, H., Kawarabayashi, N., Kimura, M., Sugiura, Y., Tamai, S., Matsubara, O., Hatsuse, K., and Mochizuki, H. (2004). The correlation between cytoplasmic overexpression of epidermal growth factor receptor and tumor aggressiveness: poor prognosis in patients with pancreatic ductal adenocarcinoma. Pancreas *29*, e1-8.

Van Cutsem, E., van de Velde, H., Karasek, P., Oettle, H., Vervenne, W. L., Szawlowski, A., Schoffski, P., Post, S., Verslype, C., Neumann, H.*, et al.* (2004). Phase III trial of gemcitabine plus tipifarnib compared with gemcitabine plus placebo in advanced pancreatic cancer. J Clin Oncol *22*, 1430-1438.

Von Hoff, D. D., Ervin, T., Arena, F. P., Chiorean, E. G., Infante, J., Moore, M., Seay, T., Tjulandin, S. A., Ma, W. W., Saleh, M. N.*, et al.* (2013). Increased survival in pancreatic cancer with nab-paclitaxel plus gemcitabine. N Engl J Med *369*, 1691-1703.

Voskoglou-Nomikos, T., Pater, J. L., and Seymour, L. (2003). Clinical predictive value of the in vitro cell line, human xenograft, and mouse allograft preclinical cancer models. Clin Cancer Res *9*, 4227-4239.

Waddell, N., Pajic, M., Patch, A. M., Chang, D. K., Kassahn, K. S., Bailey, P., Johns, A. L., Miller, D., Nones, K., Quek, K.*, et al.* (2015). Whole genomes redefine the mutational landscape of pancreatic cancer. Nature *518*, 495-501.

Wagner, M., Redaelli, C., Lietz, M., Seiler, C. A., Friess, H., and Buchler, M. W. (2004). Curative resection is the single most important factor determining outcome in patients with pancreatic adenocarcinoma. Br J Surg *91*, 586-594.

Wang, H., Daouti, S., Li, W. H., Wen, Y., Rizzo, C., Higgins, B., Packman, K., Rosen, N., Boylan, J. F., Heimbrook, D., and Niu, H. (2011). Identification of the MEK1(F129L) activating mutation as a potential mechanism of acquired resistance to MEK inhibition in human cancers carrying the B-RafV600E mutation. Cancer Res *71*, 5535-5545.

Wang, Z., Li, Y., Kong, D., Banerjee, S., Ahmad, A., Azmi, A. S., Ali, S., Abbruzzese, J. L., Gallick, G. E., and Sarkar, F. H. (2009). Acquisition of epithelial-mesenchymal transition phenotype of gemcitabine-resistant pancreatic cancer cells is linked with activation of the notch signaling pathway. Cancer Res *69*, 2400-2407.

Wee, S., Jagani, Z., Xiang, K. X., Loo, A., Dorsch, M., Yao, Y. M., Sellers, W. R., Lengauer, C., and Stegmeier, F. (2009). PI3K pathway activation mediates resistance to MEK inhibitors in KRAS mutant cancers. Cancer Res *69*, 4286-4293.

Wellbrock, C., Karasarides, M., and Marais, R. (2004). The RAF proteins take centre stage. Nat Rev Mol Cell Biol *5*, 875-885.

Wickenden, J. A., Jin, H., Johnson, M., Gillings, A. S., Newson, C., Austin, M., Chell, S. D., Balmanno, K., Pritchard, C. A., and Cook, S. J. (2008). Colorectal cancer cells with the BRAF(V600E) mutation are addicted to the ERK1/2 pathway for growth factor-independent survival and repression of BIM. Oncogene *27*, 7150-7161.

Winslow, T. (2010). Anatomy diagram shows the pancreas, liver, bile duct, stomach, gallbladder, duodenum, spleen, colon, and small intestine. Pancreatic Cancer - Cancer Stat Facts. Surveillance, Epidemiology, and End Results - National Cancer Institute. Retrieved 13.04.2014, from https://seer.cancer.gov/statfacts/html/pancreas.html.

Willis, S., Day, C. L., Hinds, M. G., and Huang, D. C. (2003). The Bcl-2-regulated apoptotic pathway. J Cell Sci *116*, 4053-4056.

Wu, J., Harrison, J. K., Vincent, L. A., Haystead, C., Haystead, T. A., Michel, H., Hunt, D. F., Lynch, K. R., and Sturgill, T. W. (1993). Molecular structure of a protein-tyrosine/threonine kinase activating p42 mitogen-activated protein (MAP) kinase: MAP kinase kinase. Proc Natl Acad Sci U S A *90*, 173-177.

Wu, J., Jiao, Y., Dal Molin, M., Maitra, A., de Wilde, R. F., Wood, L. D., Eshleman, J. R., Goggins, M. G., Wolfgang, C. L., Canto, M. I.*, et al.* (2011). Whole-exome sequencing of neoplastic cysts of the pancreas reveals recurrent mutations in components of ubiquitin-dependent pathways. Proc Natl Acad Sci U S A *108*, 21188-21193.

Yeh, J. J., and Der, C. J. (2007). Targeting signal transduction in pancreatic cancer treatment. Expert Opin Ther Targets *11*, 673-694.

Yeh, T. C., Marsh, V., Bernat, B. A., Ballard, J., Colwell, H., Evans, R. J., Parry, J., Smith, D., Brandhuber, B. J., Gross, S.*, et al.* (2007). Biological characterization of ARRY-142886 (AZD6244), a potent, highly selective mitogen-activated protein kinase kinase 1/2 inhibitor. Clin Cancer Res *13*, 1576-1583.

Yin, T., Wang, C., Liu, T., Zhao, G., Zha, Y., and Yang, M. (2007). Expression of snail in pancreatic cancer promotes metastasis and chemoresistance. J Surg Res *141*, 196-203.

Ying, H., Kimmelman, A. C., Lyssiotis, C. A., Hua, S., Chu, G. C., Fletcher-Sananikone, E., Locasale, J. W., Son, J., Zhang, H., Coloff, J. L.*, et al.* (2012). Oncogenic Kras maintains pancreatic tumors through regulation of anabolic glucose metabolism. Cell *149*, 656-670.

Yoon, S., and Seger, R. (2006). The extracellular signal-regulated kinase: multiple substrates regulate diverse cellular functions. Growth Factors *24*, 21-44.

Yu, C., Wang, S., Dent, P., and Grant, S. (2001). Sequence-dependent potentiation of paclitaxel-mediated apoptosis in human leukemia cells by inhibitors of the mitogen-activated protein kinase kinase/mitogen-activated protein kinase pathway. Mol Pharmacol *60*, 143-154.

Zeitouni, D., Pylayeva-Gupta, Y., Der, C. J., and Bryant, K. L. (2016). KRAS Mutant Pancreatic Cancer: No Lone Path to an Effective Treatment. Cancers (Basel) *8*.

Zeng, J. Y., Sharma, S., Zhou, Y. Q., Yao, H. P., Hu, X., Zhang, R., and Wang, M. H. (2014). Synergistic activities of MET/RON inhibitor BMS-777607 and mTOR inhibitor AZD8055 to polyploid cells derived from pancreatic cancer and cancer stem cells. Mol Cancer Ther *13*, 37-48.

Zhang, Z., Wang, Y., Vikis, H. G., Johnson, L., Liu, G., Li, J., Anderson, M. W., Sills, R. C., Hong, H. L., Devereux, T. R.*, et al.* (2001). Wildtype Kras2 can inhibit lung carcinogenesis in mice. Nat Genet *29*, 25-33.

Zheng, X., Carstens, J. L., Kim, J., Scheible, M., Kaye, J., Sugimoto, H., Wu, C. C., LeBleu, V. S., and Kalluri, R. (2015). Epithelial-to-mesenchymal transition is dispensable for metastasis but induces chemoresistance in pancreatic cancer. Nature *527*, 525-530.

Zhou, Q., Law, A. C., Rajagopal, J., Anderson, W. J., Gray, P. A., and Melton, D. A. (2007). A multipotent progenitor domain guides pancreatic organogenesis. Dev Cell *13*, 103-114.

Zmajkovicova, K., Jesenberger, V., Catalanotti, F., Baumgartner, C., Reyes, G., and Baccarini, M. (2013). MEK1 is required for PTEN membrane recruitment, AKT regulation, and the maintenance of peripheral tolerance. Mol Cell *50*, 43-55.

Zoncu, R., Efeyan, A., and Sabatini, D. M. (2011). mTOR: from growth signal integration to cancer, diabetes and ageing. Nat Rev Mol Cell Biol *12*, 21-35.

7. Appendix

7.1 Abbreviations

A	adenine
ABC	avidin-biotin complex
ADM	acinar-ductal metaplasia
ADP	adenosine diphosphate
AFL	atypical flat lesion
AKT	v-akt murine thymoma viral oncogene homolog
ATP	adenosine triphosphate
aU	arbitrary units
BC	before Christ
BCA	bicinchoninic acid
Bcl-2	B-cell lymphoma 2
BIM	Bcl-2-interacting mediator of cell death
bp	base pairs
BRCA2	breast cancer 2
BrdU	5-bromo-2'-deoxyuridine
BSA	bovine serum albumin
C	cytosine
CDK	cyclin-dependent kinase
cDNA	complementary desoxyribonucleic acid
cm	centimeter
CO_2	carbon dioxide
Cre	causes recombination or cyclization recombinase
°C	degree Celsius
d	days
ddH_2O	double distilled water
DAB	3,3'-diaminobenzidine
DEPTOR	Dep domain-containing mTOR-interacting protein
DMEM	Dulbecco's Modified Eagle Medium
DMSO	dimethylsulfoxide
DNA	desoxyribonucleic acid

DPC4	deleted in pancreatic carcinoma 4 (also called SMAD4)
E	embryonic day
ECL	enhanced chemiluminescence
EDTA	ethylenediaminetetraacetic acid
EGF	epidermal growth factor
EGFR	epidermal growth factor receptor
ELISA	Enzyme Linked Immunosorbent Assay
EMT	epithelial-to-mesenchymal transition
ERBB2	human epidermal growth factor receptor 2 (HER2/Neu)
ERBB3	Erb-B2 receptor tyrosine kinase 3 (also known as human epidermal growth factor receptor 3 (HER3))
ERK1/2	extracellular signal-regulated kinase 1/2
et al.	*et alii*
EtOH	ethanol
FCS	fetal calf serum
FFPE	formalin-fixed, paraffin-embedded
Flp/FRT	*Flippase*/*Flp* recombination target
5-FU	5-fluorouracil
g	gram
G	guanine
GAP	GTPase activating protein
GAPDH	Glyceraldehyde-3-Phosphate Dehydrogenase
GDP	guanine diphosphate
GEF	guanine nucleotide exchange factor
GEMM	genetically engineered mouse model
Glis3	GLI-similar 3
GTP	guanine triphosphate
h	hours
H_2O	water
H_2SO_4	sulfuric acid
H&E	haematoxylin & eosin
HCl	hydrochloric acid
Hes1	Hairy/enhancer of split 1
Hlxb9	Homeobox hb9 (also called Motor neuron and pancreas homeobox 1 (Mnx1)
Hras	Harvey rat sarcoma viral oncogene homolog

HRP	horseradish peroxidase
HSP90	heat shock protein 90
IC_{50}	half-maximal inhibitory concentration
IGF1Rß	Insulin-like growth factor-1 receptor ß
IHC	immunohistochemical staining
i.p.	intraperitoneal
IPMN	intraductal papillary mucinous neoplasm
IRß	Insulin receptor ß
kDa	kilodalton
kg	kilogram
Kras	V-Ki-Ras2; Kirsten rat sarcoma viral oncogene homolog
KSR	kinase suppressor of RAS
LOH	loss of heterozygositiy
LoxP	locus of crossing over, bacteriophage P1
LSL	*LoxP-Stop-LoxP*
M	Molar (mol/l)
m	mouse/ murine
mA	milliampere
MAPK	mitogen activated protein kinase
MAPKK	mitogen activated protein kinase kinase
MAPKKK	mitogen activated protein kinase kinase kinase
MCN	mucinous cystic neoplasm
MEK1/2	MAPK and extracellular signal-regulated kinase kinase 1/2
mg	milligram
Mg	magnesium
ml	milliliter
MLB	Magnesium-containing lysis buffer
mLST8	mammalian lethal with SEC13 protein 8
mm	millimeter
mm^3	cubic millimeter
mM	millimolar (mmol/l)
mPanIN	mouse pancreatic intraepithelial neoplasia
MPC	multipotent progenitor cell
MR	magnetic resonance
MRI	magnetic resonance imaging
MS	median survival

mTOR	mammalian target of rapamycin
mTORC	mammalian target of rapamycin complex
MTT	3-[4,5-Dimethylthiazol-2-yl]-2,5-diphenyltetrazolium bromide
µg	microgram
µl	microliter
µm	micrometer
µM	micromolar (µmol/l)
n	number
N	normality
NaCl	sodium chloride
NDLB	non-denaturing lysis buffer
nm	nanometer
nM	nanomolar (nmol/l)
NP-40	nonyl phenoxypolyethoxylethanol
Nras	neuroblastoma RAS viral (v-ras) oncogene homolog
ns	statistically not significant
O_2	oxygen
p	phosphorylated
PAGE	polyacrylamide gel electrophoresis
PanIN	pancreatic intraepithelial neoplasia
PAK1	p21-activated kinase-1
PARP	Poly (ADP-ribose) polymerase
PBS	phosphate buffered saline
PBT	phospho-tyrosine binding
PCNA	proliferating cell nuclear antigen
PCR	polymerase chain reaction
PDAC	pancreatic ductal adenocarcinoma
PDEC	primary pancreatic duct epithelial cell
PDK1	3-phosphoinositide-dependent protein kinase 1
PDVF	polyvinylidene difluoride
Pdx1	pancreas duodenum homeobox 1
pH	*potentia Hydrogenii*
PI3K	phosphoinositide-3-kinase
pM	picomolar
p.o.	peroral
Prox1	prospero homeobox 1

PTEN	phosphatase and tensin homolog deleted on chromosome 10
Ptf1a	pancreas transcription factor subunit alpha
p70S6Kinase	ribosomal protein S6 kinase
qRT-PCR	quantitative real-time-PCR
RAF	rapidly accelerated fibrosarcoma (also called MAPKKK)
RalGDS	Ral guanine nucleotide dissociation stimulator
RAPTOR	regulatory-associated protein of mTOR
RBD	Ras binding domain
RNA	ribonucleic acid
RPLP0	ribosomal protein, large, P0
rpm	revolutions per minute
RPMI	Roswell Park Memorial Institute
RT	room temperature
RTK	receptor tyrosine kinase
SDS	sodium dodecyl sulfate
SHC	Src homology 2 domain containing
SOS	Son-of-sevenless
Sox9	SRY (sex determining region Y)-box 9
SS II	SuperScript™ II
STK11/LKB1	Serine/threonine kinase 11 / liver kinase B1
Stsp.	staurosporine
S6	ribosomal protein S6
T	Tesla
T	thymine
TBS	tris buffered saline
TBS-T	tris buffered saline-Tween® 20
Tcf2	transcription factor-2 (also called hepatocyte nuclear factor 1-ß (HNF-1β) or variant hepatic nuclear factor 1 (vHNF1))
TE	echo time
TEMED	N,N,N',N'-tetramethylethylenediamine
TGF-α	transforming growth factor α
TGF-ß	transforming growth factor ß
TP53	Tumor Protein P53
TR	repetition time
Tris	tris(hydroxymethyl)-aminomethane
TSE	turbo spin-echo (TSE) sequence

TUNEL	TdT-mediated dUTP-biotin nick end labeling
V	volt
W	watt
WT	wild-type
%	percent
% (v/v)	percent by volume

7.2 List of Figures

7.3 List of Tables

Acknowledgement - Danksagung

An dieser Stelle möchte ich mich bei all jenen bedanken, die direkt oder indirekt zum Entstehen meiner Dissertation beigetragen und mich im Verlauf dieser unterstützt haben.

Prof. Dr. Jens Siveke danke ich ganz herzlich für die Möglichkeit und finanzielle Unterstützung der Anfertigung meiner Dissertation in seiner Arbeitsgruppe, die Teilnahme an zahlreichen nationalen und internationalen Konferenzen, die sehr motivierende, verständnisvolle und diskussionsfreudige Betreuung sowie die fortwährende Unterstützung auch nach meinem Ausscheiden aus dem Labor und der präklinischen Forschung bis zum endgültigen Abschluss meiner Dissertation.

Mein besonderer Dank gilt Dr. Marija Trajkovic-Arsic für ihre intensive wissenschaftliche und engagierte Betreuung des praktischen Teils der Arbeit, ihre Diskussionsbereitschaft sowie ihre fachliche Kompetenz und Unterstützung, die entscheidend zum Erfolg und Abschluss dieser Arbeit beigetragen haben.

Vielen Dank an die Mitglieder meines Thesis Advisory Committees Prof. Dr. Angelika Schnieke, Prof. Dr. med. Roland Schmid, Prof. Dr. rer. nat. Marc Schmidt-Supprian und PD Dr. med. Rickmer Braren für ihre Zeit und Mühe und die sehr hilfreichen Diskussionsbeiträge und Versuchsvorschläge. Bei Prof. Dr. Angelika Schnieke möchte ich mich außerdem für die Erstellung des Zweitgutachtens zu dieser Arbeit bedanken und bei Prof. Dr. med. Roland Schmid für die zahlreichen Wanderausflüge.

Mein großer Dank geht an die International Max Planck Research School for Molecular and Cellular Life Sciences (IMPRS-LS), in deren Rahmen ich diese Doktorarbeit machen durfte. Ganz lieben Dank an das Coordination Office Dr. Hans-Jörg Schäffer, Dr. Ingrid Wolf und Maximiliane Reif für ihre fortwährende Unterstützung, große Einsatzbereitschaft sowie die super organisierten und sehr interessanten IMPRS Workshops und Seminare.

Dank gilt auch der Arbeitsgruppe von PD Dr. med. Rickmer Braren für die freundliche Kooperation und die Nutzung des MRTs. Vor allem möchte ich Irina Heid dafür danken, dass sie mir immer mit Rat und Tat zur Seite stand und mir all meine (MRT-)Fragen jederzeit geduldig beantwortet hat. Iryna Skuratovska danke ich für ihre Bereitschaft und Hilfe zum Schneiden meiner Parraffinblöcke am Mikrotom.

Herzlichen Dank auch an Juliane Blumenberg und Tamara Kley für die Unterhaltung und Unterstützung beim nächtelangen Scannen sowie an Stefan Ambos und Christina Lesti für ihre zeitweilige Mithilfe und Unterstützung nicht nur beim Scannen, sondern auch in der Zellkultur und bei Western Blots.

Ganz besonders möchte ich Florian Neff, Thomas Briel und Tobias Leibfritz für ihre Freundschaft und gegenseitige Unterstützung sowie die zahlreichen Diskussionen zu unseren Projekten danken. Außerdem werde ich unsere genialen Freitagsparties und unsere (Rotkäppchen)Sekt-Abende nie vergessen =).

Zudem möchte ich mich bei allen weiteren und ehemaligen Mitarbeitern unserer Arbeitsgruppe für die angenehme Arbeitsatmosphäre und Hilfestellungen im Labor bedanken, vor allem bei Carina, Barbara, Vicky, Clara, Roxanne, Mathilde, Katharina, Silke, Alex und Marcel.

Und natürlich nicht zu vergessen meine IMPRS-Freunde, insbesondere Denise Orozco und Katrin Strecker, und alle Mitarbeiter des Adolf-Butenandt-Institutes vom Lehrstuhl für Biochemie der LMU München für die Einladungen zu unseren legendären Laborparties - ich sag nur Erdbeer-Margarita =).

Mein Dank gilt auch meiner Familie und besonders meiner Omi für ihre Liebe und wunderbare Fürsorge. Danke Omi, dass du immer für mich da gewesen bist und mir dadurch viel Kraft, Zuspruch und Mut während meiner gesamten Promotionszeit gegeben hast.

Abschließend gebührt mein ganz besonderer Dank meinen deutschlandweiten Freunden und ehemaligen Novartis-Kollegen Sarah Matheisl, Franziska Förtsch, Julia Dallwitz, Julia Kleber, Mandy Schröder, Juliane Macheleidt, Maria Kontou, Gerd-Marten Kuscher und Christian Bernklau-Hedler für ihre Freundschaft, ihre moralische Unterstützung und offenen Ohren während der letzten Jahre, sowie die willkommene Abwechslung und die unvergesslichen Reisen nach Asterdam, Belfast, Ibiza, Neuseeland, Vendig und Paris.

Danke, dass ihr immer und vor allem bis heute an mich geglaubt habt =).

Declaration of Authorship

Hiermit versichere ich, dass ich die vorliegende Dissertation in allen Teilen selbstständig verfasst und keine anderen Quellen und Hilfsmittel, als die angegebenen, verwendet habe. Alle Stellen, die dem Wortlaut oder dem Sinn nach anderen Werken entnommen sind, wurden durch Angabe der Quellen kenntlich gemacht.
Die Dissertation wurde in dieser oder ähnlicher Form keiner anderen Prüfungsbehörde vorgelegt und ist bisher nicht veröffentlicht.

München, den 21.09.2018

_____

Nicole Teichmann